# Spatially Adaptive MultiWavelet Representations on Unstructured Grids with Applications to Multidimensional Computational Modeling

by

Julio E. Castrillón Candás

Ingeniero en Electrónica y Comunicaciones, ITESM-CEM, Atizapán, México (1992)
S.M., Massachusetts Institute of Technology (1996)

Submitted to the Department of Electrical Engineering and Computer Science
in partial fulfillment of the requirements for the degree of

Doctor of Philosophy in Electrical Engineering and Computer Science

at the

MASSACHUSETTS INSTITUTE OF TECHNOLOGY

June 2001





Author .....
Department of Electrical Engineering and Computer Science
May, 2001

Certified by .....
Kevin S. Amaratunga
Assistant Professor
Thesis Supervisor

Accepted by .....
Arthur C. Smith
Chairman, Department Committee on Graduate Students

# Spatially Adaptive MultiWavelet Representations on Unstructured Grids with Applications to Multidimensional Computational Modeling

by

Julio E. Castrillón Candás

Submitted to the Department of Electrical Engineering and Computer Science
on May, 2001, in partial fulfillment of the
requirements for the degree of
Doctor of Philosophy in Electrical Engineering and Computer Science

## Abstract

In this thesis, we develop wavelet surface wavelet representations for complex surfaces, with the goal of demonstrating their potential for 3D scientific and engineering computing applications. Surface wavelets were originally developed for representing geometric objects in a multiresolution format in computer graphics. However, we further extend the construction of surface wavelets and prove the existence of a large class of multiwavelets in $R^n$ with vanishing moments around corners that are well suited for *complex geometries*. These wavelets share all of the major advantages of conventional wavelets, in that they provide an analysis tool for studying data, functions and operators at different scales. However, unlike conventional wavelets, which are restricted to uniform grids, surface wavelets have the power to perform signal processing operations on *complex meshes*, such as those encountered in finite element modeling. This motivates the study of surface wavelets as an efficient representation for the modeling and simulation of physical processes. We show how surface wavelets can be applied to partial differential equations, cast in the integral form. We analyze and implement the wavelet approach for a model 3D potential problem using a surface wavelet basis with linear interpolating properties. We show both theoretically and experimentally that an $O(h_n^2)$ convergence rate, $h_n$ being the mesh size, can be obtained by retaining only $O((logN)^{\frac{7}{2}}N)$ entries in the discrete operator matrix, where $N$ is the number of unknowns. Moreover our theoretical proof of accuracy vs compression is applicable to a large class of Calderón-Zygmund integral operators. In principle, this convergence analysis may be extended to higher order wavelets with greater vanishing moment. This results in higher convergence and greater compression.

Thesis Supervisor: Kevin S. Amaratunga
Title: Assistant Professor

# Acknowledgments

I have been fortunate for completing my education at MIT. I thank my advisor Kevin Amaratunga for his mentoring and guidance. I am also grateful to Bernie Lesieutre, Jacob White and Jerome Connor for their diligence in following my work and as teachers. I acknowledge the support given to me from the National Science Foundation for funding my research.

I am also thankful for the faculty, student and friends during my long stay at school.

Foremost, I am blessed with a loving and supportive family. My parents Samuel Castrillón and María Teresa Candás. My brother Samuel Castrillón Candás and sister María Evelyn Talei Castrillón Candás.

*Me da dau doka ka vinakata na vanua*

# List of Symbols

See [22] for many of these definitions.

**1.** Multiindex notation for $D^{\alpha}u(x)$: Let $\alpha = (\alpha_1, \ldots, \alpha_2)$, where $\alpha_i \in Z^+$ and let

$$|\alpha| = \alpha_1 + \ldots + \alpha_2,$$

then

$$D^{\alpha}u(x) = \frac{\partial^{|\alpha|}u(x)}{\partial x_1^{\alpha_1} \ldots \partial x_n^{\alpha_n}}.$$

**2.** $L^p_{loc}(U) = \{u : U \to R \,|\, v \in L^p(V)$ for each $V$ compactly contained in $U\}$.

**3.** $C_0^k(U)$: Compactly $C^k(U)$.

**4.** $C^k(U)$: $\{u : U \to R \,|\, u$ is $k$-times continuously differentiable $\}$

**5.** *Weak derative*: Suppose $u, v \in L^1_{loc}$, and $\alpha$ is a multiindex. We say that $v$ is the $\alpha^{th}$-weak partial derivative of $u$, written

$$D^{\alpha}u = v,$$

provided

$$\int_U uD^{\alpha}\phi dx = (-1)^{|\alpha|} \int_U v\phi dx$$

for all test functions $\phi \in C_0^{\infty}(U)$.

**6.** $W^{k,p}(U)$: The Sobolev space consists of all locally summable functions $u : U \to R$ such that for each multiindex $\alpha$ with $|\alpha| \leq k, D^{\alpha}u$ exists in the weak sense and belongs to $L^P(U)$.

**7.** $H_0^k(U)$: Compactly supported Sobolev space $W^{k,p}(U)$ with $p = 2$.

# Contents

# List of Figures

# List of Tables

# Chapter 1

# Introduction

During the past two decades, wavelet representations have emerged as a powerful new tool for signal processing and mathematical analysis. The power of wavelets lies in their ability to dissect data, functions and operators according to the scale of the features that are present. This allows us to develop fast algorithms to extract information of interest and represent it in a compact form.

The origin of wavelets dates back to the beginning of the 20th century with the development of the first orthogonal wavelet by Haar. The field further developed independently in areas such as mathematics (Calderón-Zygmund operator theory), physics (Coherent state and renormalization group theory) and electrical engineering (Subband coding theory and filterbanks).

Many of these ideas merged in the 80's with the development of *Wavelets* by researchers such as Morlet, Arens, Fourgeau and Giard [30] , Morlet [29], and Grossman and Morlet [27]. Most notably the multiresolution framework by Meyer and Mallat, which with together with filter bank theory led to the discrete wavelet transform.

However, it was not until the development of compactly supported orthogonal and biorthogonal wavelets by Ingrid Daubechies [21] that wavelets extended substantially to other domains. In particular, wavelet theory has revolutionized *Signal and Image processing.* Such authors as P.P. Vaidyanathan and Martin Vetterli have extensively written about this field.

More recently M-band wavelets [46, 48] and Multiwavelets [1, 25] extend the con-

cept of wavelets to vector wavelets. Furthermore, W. Sweldens develops a new framework, called *Lifting*, to construct wavelets over finite irregular grids [40, 41]. As pointed out in this thesis this concept permits a generalization of Multiwavelet to irregular grids. Although independently Dahmen, Carnicer and Peña developed a similar wavelet construction tool termed *Stable Completion* [10], which may be though as a generalization of *Lifting*, however, we shall apply *Lifting* extensively in this thesis.

Wavelets have already been shown to be conceptually attractive for problems in computational mechanics, where one is often interested in studying local features such as shocks, stress concentrations and other discontinuities (see e.g. [5, 6, 7, 47]). In fact, a considerable body of literature now exists on the application of wavelet techniques to the solution of partial differential equations (PDEs), in particular in the field of integral equations [16, 17, 18, 19, 20, 1, 2, 8, 10, 11, 12, 24, 34, 35, 36, 37, 38].

Much of the current research in wavelets for the numerical solution of integral operators dwells on Multiwavelet constructions. Traditional wavelets suffer from the drawback that they do not form a basis for finite domains. This problem has led to the development of Multiwavelets by Alpert [1]. However, such constructions are limited to tensor products of 1D Multiwavelets. In contrast, Petersdorff and Schwab [34, 35, 36] develop a 2D Multiwavelet scheme to solve boundary element problems over arbitrary surfaces in 3D. This method consists of mapping flat 2D polynomial multiwavelets patches onto the 3D geometry. However, these wavelets are ill suited for geometries with corners, where the compression is low, and up to our knowledge, there exists no practical implementation of Petersdoff scheme for linear or higher order wavelets.

Alternate work by Alpert *et al* [2] consists of forming sparse representations by sampling the kernel of the integral equation. This method consists of mapping a finite set of points in 1D to a discrete orthonormal pseudo wavelet basis with vanishing moments in a discrete sense. This basis construction is then applied to solve integral operators. The kernel is first sampled at $n$ discrete points with a quadrature scheme. A sparse representation is achieved by applying the discrete wavelet mapping to the quadrature matrix. This sparse form representation retains the full accuracy of

quadrature method but only requires $\mathcal{O}(n\,log^2(n))$ computations. This method is applicable to a large class of integral equations. However, applications are limited to 1D problems.

To quote Wolfgang Dahmen:"It is fair to say that wavelet analysis as it stands has by far not yet reached a steady state in this field. As promising as many of the underlying concepts are, it would be naive to expect their immediate practical success in complex, real-life applications governed by PDEs." [14]

## 1.1 Motivation

One may naturally ask, "How successful are wavelet techniques compared to finite element techniques?". Responses to this question are often mixed. Both techniques use similar bases, which are designed to represent functions that are piecewise polynomial. Wavelets are also intrinsically capable of representing functions at multiple resolutions (cf. adaptive finite element methods). However, previous work on wavelet techniques for PDEs has typically relied on traditional wavelet constructions, such as the one by Daubechies [21]. Such wavelets are best suited for problems that are discretized on uniform grids, a constraint that can be rather restrictive when it comes to modeling 3D problems with complex geometry. Some attempts have been made to address the problem of complex geometry using Multiwavelets, but with mixed results. For example although a fully discrete Multiwavelet boundary element method for 3D computational problems exists [36, 35], it is very difficult to implement, moreover, to our knowledge, no implantation of linear or higher order Multiwavelets exists. By contrast, we note that finite elements are very well suited for complex meshes.

In this thesis we combine the flexibility of finite element basis functions with the localization and decorrelation property of wavelets. We will investigate a generalization of the wavelet concept that permits the application of wavelet techniques to 3D problems on complex domains in computational mechanics. The generalized wavelets are a fairly recent development in the literature, known as second-generation wavelets [41]. They have been used primarily by the computer graphics community to gener-

ate multiresolution descriptions of complex geometric shapes [42]. Here, we develop the main ideas behind these generalized wavelet representations, their extensions to higher order polynomials and dimensions, and applications to PDEs. Moreover, we show that the second generation framework permit a generalization of Multiwavelets to irregular grids. The contributions of these thesis include

- The construction of a class of interpolating irregular Multiwavelets in $R^n$ which combine the fast transform, decorrelation and localization properties of wavelets with the flexibility of finite elements on irregular meshes. These constructions may represent polynomials of arbitrary polynomial order. Moreover, we explicitly construct irregular Multiwavelets over curves and surfaces with vanishing moments around corners. In essence these novel constructions allow practical multiresolution decompositions over irregular meshes.

- Application of interpolating irregular Multiwavelets to solve Calderón-Zygmund integral operators. We derive theoretical estimates of convergence under compression in $R^3$, more explicitly, we show that we may achieve the asymptotic convergence of the full stiffness matrix with only $\mathcal{O}(N(logN)^{7/2})$ entries.

- Implementation of a 3D linear surface Multiwavelet with one vanishing moment to solve a second kind integral equation over an irregular mesh.

- Implementation of a 2D linear surface Multiwavelet which vanishes global linear functions around corners to solve a second kind integral equation.

The basis constructions in this thesis are similar to a new development by *Tausch* and *White* [33]. This alternate multiscale basis is constructed from piecewise polynomials and may also be applied to integral equations of the first kind in 3D over complex geometries. Such approach is similar to the polynomial functions constructed in this thesis. However, this alternate approach does not lead to refinable functions. We shall elaborate more in the discussion session in Chapter 7.

## 1.2 Thesis Outline

In Chapter 2, we introduce wavelets and Multiwavelets as a tool for multiscale analysis. This chapter covers the basic theory of wavelets, Multiwavelets and their properties.

Chapter 3 introduces the basic concepts of lifting and Surface Wavelet constructions introduced by Sweldens. We introduce the basic concepts of *Lifting* and illustrate linear wavelet constructions. Although Sweldens [42, 43] only covers the construction of the primary scaling functions, we further develop the construction of the dual scaling functions. Moreover we investigate the stability of both the primary and dual basis, and under a normalization show that the $l^2$ norm of the projection coefficients of any function belonging to $H^3(S)$ is bounded both by above and below by non zero constants.

Chapter 4 deals with the generalization of Linear Surface Wavelets to higher order polynomial bases. We prove the existence and construction of a wide class of interpolating Multiwavelets. With this construction theorem we build examples of quadratic Multiwavelets on irregular domains in 1D and 2D. In many practical computational modeling problems the presence of corners may seriously degrade the performance of compression algorithms. However, we further show that the construction theorem allows the construction of Surface Multiwavelets which produce vanishing moments around corners, thus conserving the compression properties of the wavelets at any section of the mesh.

Chapter 5 demonstrates the application of Multiwavelets to Calderón-Zygmund Integral Operators in three space. We obtain estimates for the decay of the kernel expansion coefficients in the Surfacewavelet basis and develop a compression criterion such that asymptotic convergence, under compression, is of the same order as without compression. We show that it is sufficient to compute $\mathcal{O}(N(logN)^{7/2})$ of the entries of the stiffness matrix to achieve quadratic asymptotic convergence.

In Chapter 6 we apply linear surface wavelets with one vanishing moment to the 3D Poisson PDE with a Petrov Galerkin formulation of the second kind integral

equation. We also implement a Galerkin formulation of the Poisson PDE in 2D using wavelets with three vanishing moments around corners. Experimental results reveal we only have to compute $\mathcal{O}(N(log_q N)^p)$ of the entries of the stiffness matrix to achieve quadratic asymptotic convergence.

In Chapter 7 we summarize the thesis, contributions, its strength and weakness, and give directions for further research. We effectively have a wealth of problems to solve with Multiwavelets. In particular, we have not explored the finite element variational or weak formulation.

# Chapter 2

# Elementary Theory of Wavelets

This chapter provides the necessary background in the theory of wavelets. The focus is on orthogonal, biorthogonal wavelets and MultiWavelets.

## 2.1 Basic concepts

Wavelet theory has been used extensively in many areas of mathematics and engineering. As the name implies, they indeed look like small waves. These functions are highly connected with *signal representation*, that is, arbitrary signals may be constructed from wavelets.

Suppose we have some signal and are given a "box" function, as shown in Fig 2-1 (a). This box function is called the *scaling* function in the Wavelet literature and is denoted by $\phi(t)$. On every unit interval, we may place a "box" whose height is the average of the waveform on this interval. This results in a staircase representation of the original signal, with unit resolution, as shown in Fig 2-1 (b). Thus, we have approximated the signal at some resolution, just as an image is represented with a certain number of pixels on a computer screen. It is only necessary to remember the height of the boxes to construct our approximation.

Let us reduce the width of the box function by one half. Now, we may fit twice as many boxes in the same unit interval, thus the signal is represented at twice the resolution, as show in Fig 2-1 (c) . We continue this process by making the boxes

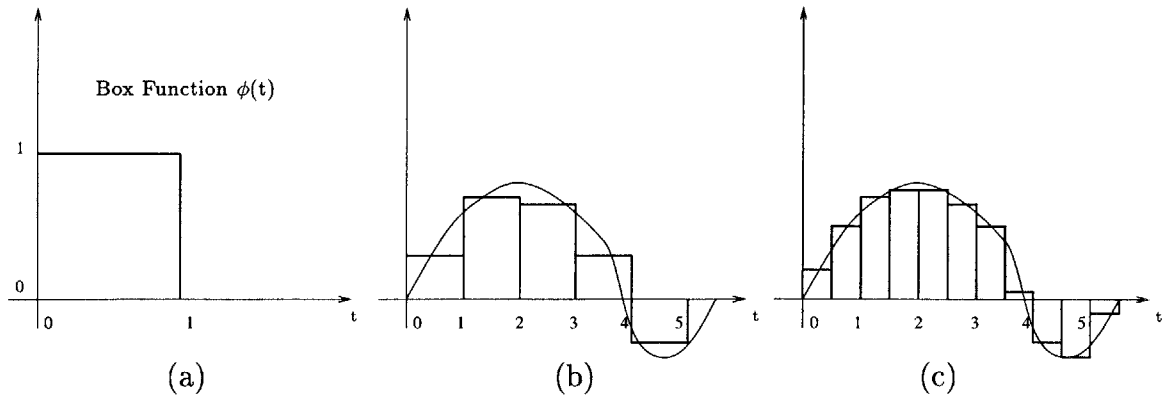


Figure 2-1: (a) Box function. (b) Coarse approximation. (c) Finer approximation

thinner and thinner. Eventually, the staircase approximation will be indistinguishable from the original waveform. However, for all practical applications, the signal is of finite length and may be represented at some high, but finite resolution. This implies we only need a finite amount of memory to represent the signal.

The relation between the scaling functions at different resolutions is of special significance. Suppose we take the box function and add the *wavelet* function denoted by $\psi(t)$, as shown in Fig 2-2. We obtain the same box function, but reduced in width by one half. This is exactly the scaling function at the next resolution level, scaled in height by two. This implies that we may represent a signal at one level of resolution with a combination of scaling and wavelet functions at a coarser resolution. The wavelet function may be thought of as the detail we need to add to move from one level of resolution to the next higher one.

Now, suppose we know something about our signal. Suppose it is very flat in some regions, but very detailed in some short intervals. Trying to represent the entire signal at some fixed high resolution with scaling functions is a waste of memory. It is much more efficient to represent some regions at low resolutions and some at higher resolutions. This is where wavelets are useful. We may represent the entire signal at some coarse resolution and then, add the details where they are necessary, to increase

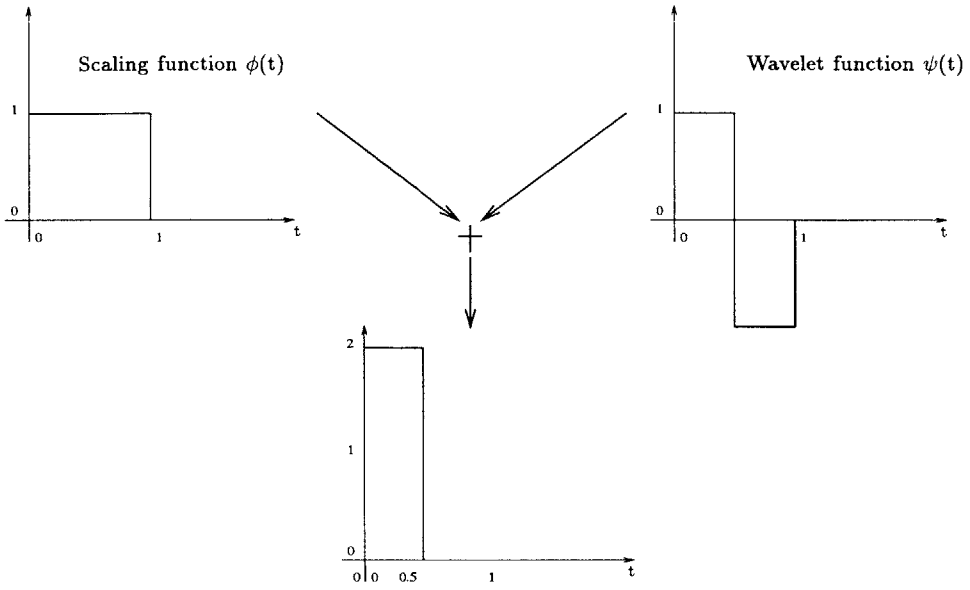


Figure 2-2: Scaling function and Wavelet function are added together to form the scaling function at a higher resolution

the resolution locally. This results in a multi resolution representation of a signal. Example applications of multiresolution representation include the compression of audio and video signals.

The scaling function and wavelet described in this section are the basic building blocks for the *Haar* basis, which is one of the most simple orthogonal wavelet decompositions. In the following sections we will introduce the general description of orthogonal and biorthogonal wavelets.

## 2.2 Orthogonal Wavelets

### 2.2.1 Time Domain Representation

We now introduce a more formal description of wavelet theory and extend the *Haar* wavelets discussed in the introduction to a larger class of orthogonal wavelets.

Suppose we have the following sequence of embedded subspaces,

$$\{0\} \subset \cdots \subset V_{-2} \subset V_{-1} \subset V_0 \subset V_1 \subset V_2 \subset \cdots \subset L^2(R),$$

which possess the following properties:

1. $\bigcup_{j\epsilon Z} V_j$ is dense in $L^2(R)$. ($Z$ denotes the set of integers.)

2. $\bigcap_{j\epsilon Z} V_j = \{0\}$ .

3. The embedded subspaces are related by a scaling law

$$g(t) \in V_j \Longleftrightarrow g(2t) \in V_{j+1} .$$

4. Each subspace is spanned by integer translates of a single function, $g(t)$, such that

$$g(t) \in V_0 \Longleftrightarrow g(t+1) \in V_0 .$$

Condition 4 suggests that we can find a function, $\phi(t) \in V_0$, whose integer translates form a basis [1] for $V_0$. It follows from Condition 3 that the functions $\phi(2t-k)$ must span $V_1$. Now since since $V_0 \subset V_1$, this implies that any function in $V_0$ is also in $V_1$, in particular, we may write a two-scale difference equation of the form

$$\phi(t) = \sum_k a_k \phi(2t-k) . \tag{2.1}$$

Here $\{a_k;\ k \in Z,\ a_k \in C\}$ is a sequence of constant coefficients. This equation is known as the *dilation* or *refinement* equation and forms the basis for the multiresolution properties of wavelet theory. The *filter* coefficients $a_k$ are of importance since they are closely linked to the properties of the multiresolution, in particular, the shape of $\phi(t)$.

The filter coefficients $a_k$ may be real or complex valued and an infinite or finite sequence. However, for many practical applications the filter coefficients are chosen to be real and finite. This family of finite impulse response filters will give rise to compactly supported scaling functions, which are are important to the study of

[1] The bases we deal with are *Reisz stable* bases. See Section 3.2.2 for the definition of a Reisz stable basis.

signals with local features. In addition, we may choose $a_k$ such that the basis functions $\{\phi(t-k);\, k\}$ form an orthonormal set.

We may now extend the refinement equation to all spaces $V_j$. Conditions 3 and 4 state that the collection of scaling functions $\{\phi(2^j t - k);\, k\}$ form a basis for the function space $V_j$. However, we are mostly interested in stable *Reisz* basis for all $j$. To satisfy this condition we must rescale the scaling functions at every single resolution. It follows then from the translation and scaling argument that we may define a function

$$\phi_{j,k}(t) = 2^{j/2}\phi(2^j t - k), \quad k \in Z \ , \tag{2.2}$$

which forms a Reisz basis for the subspace $V_j$, and

$$\phi_{j,0}(t) = \sum_k a_k \phi_{j+1,k}(2^j t - k) \ .$$

We have now set up a framework for multiresolution signal representation. Given a function $f(t) \in L^2(R)$ we may generate a sequence of successive approximations to $f(t)$ by projecting it on to the subspaces $V_j$. Define $P_j$ as the orthogonal projection of $f(t)$ onto $V_j$, thus

$$P_j f(t) = \sum_k c_k^j \phi_{j,k}(t) \ . \tag{2.3}$$

Since $\{\phi_{j,k}(t)\}$ forms an orthonormal set, the coefficients $c_k^j$ are given by

$$c_k^j = \int_{-\infty}^{\infty} f(t)\phi_{j,k}(t)dt \ . \tag{2.4}$$

In general the orthogonality of the scaling function $\phi(t)$ may directly be related to the filter coefficients $a_k$

$$\sum_k a_k a_{k-2l} = 2\delta_l.$$

This last relation follows from the refinement equation and is known as Condition O

[44]. Moreover, we normalize the coefficients such that

$$\sum_k a_k = 2 \ .$$

We have constructed a series of multiresolution function spaces, able to represent a function $f(t) \in L^2$ at any resolution $j$. The next logical step is to represent $f(t)$ at a higher resolution $j+1$. However, in wavelet theory, instead of representing $f(t)$ as a projection on to the subspace $V_{j+1}$ we are mostly interested in the difference between $V_j, V_{j+1}$. In other words: what do I have to add to $P_j f(t)$ to get to $P_{j+1} f(t)$? We use the notation $W_j$ to denote this detail space and we use $Q_j f(t)$ to denote the projection of $f(t)$ on to $W_j$. For orthogonal wavelets, the spaces $W_j$ and $V_j$ are orthogonal, and $W_j$ is said to be the orthogonal complement of $V_j$ in $V_{j+1}$. This is written as

$$V_{j+1} = V_j \bigoplus W_j; \qquad W_j \perp V_j \ . \tag{2.5}$$

where $\bigoplus$ is the direct sum. Equivalently, the projections are related by

$$P_{j+1} f(t) = P_j f(t) + Q_j f(t); \qquad P_j f(t) \perp Q_j f(t) \ . \tag{2.6}$$

Now, the collection of functions $\{\phi(2t-k);\ k \in Z\}$ forms a basis for $V_1$ then necessarily

$$\psi(t) = \sum_k b_k \phi(2t-k) \tag{2.7}$$

where $b_k$ is a sequence of real numbers. If we choose

$$b_k = (-1)^k \ a_{N-1-k} \tag{2.8}$$

then the collection of functions $\{\psi(t-k);\ k \in Z\}$ forms an orthonormal basis for $W_0$. This can be easily derived as

$$\begin{aligned}
\int \psi(t)\phi(t-k) &= \int \sum_{l=0}^{N} b_l \phi(2t-l) \sum_{k=0}^{N} a_k \phi(2t-k) \\
&= \int \sum_{k=0}^{N} (-1)^n a_{N-l} \phi(2t-l) \sum_{k=0}^{N} a_k \phi(2t-k) \\
&= \int \sum_{l=0}^{N} (-1)^n a_{N-l} a_l \\
&= 0 \quad \text{(where N is odd).}
\end{aligned}$$

The function $\psi(t)$ is referred to as a *wavelet.* Following the same pattern we may define a wavelet basis for $W_j$ for all $j$. Define

$$\psi_{j,k}(t) = 2^{j/2}\psi(2^j t - k);\ k \in Z,$$

then the collection of $\{\psi_{j,k}(t);\ k \in Z\}$ forms an orthonormal basis for $W_j$. In particular,

$$\begin{aligned}
\langle \phi_{j,k}(.), \phi_{j,l}(.) \rangle &= \delta_{k-l}\ , \\
\langle \phi_{j,k}(.), \psi_{j,l}(.) \rangle &= 0\ , \\
\langle \psi_{j,k}(.), \psi_{m,l}(.) \rangle &= \delta_{j-m}\ \delta_{k-l}\ .
\end{aligned} \tag{2.9}$$

Notice that since these bases are orthonormal, therefore they are automatically *Reisz* stable bases (cf. Parsevals thm). Moreover, they form a *tight frame* (see [44]).

Denote $Q_j$ as the orthogonal projection of $f(t)$ on $W_j$, thus

$$Q_j f(t) = \sum_k d_k^j \psi_{j,k}(t) \tag{2.10}$$

with

$$d_k^j = \int_{-\infty}^{\infty} f(t)\psi_{j,k}(t)dt\ . \tag{2.11}$$

We may now represent a function $f(t)$ as a linear combination of the projections on

to the detail spaces $W_j$, a complete wavelet decomposition may be written as

$$f(t) = \sum_{j=-\infty}^{\infty} Q_j f(t) = \sum_j \sum_k d_k^j \psi_{j,k}(t) \ . \tag{2.12}$$

### 2.2.2 Fourier Domain Representation

The Fourier domain representation of orthogonal wavelets is at least as instructive to consider as the time domain representation. In particular, the design process for regularly spaced wavelets, before the discovery of *lifting* (see Chapter 3), is usually done in the Fourier domain. For sake of notation, let the Continuous-Time Fourier Transform (CTFT) of $f(t)$ be defined

$$F(j\Omega) = \int_{-\infty}^{\infty} f(t) e^{-j\Omega t} dt \ . \tag{2.13}$$

and the inverse CTFT is given by

$$f(t) = \frac{1}{2\pi} \int_{-\infty}^{\infty} F(j\Omega) e^{j\Omega t} d\Omega \ . \tag{2.14}$$

We now take the Fourier transform of the *Refinement* Equation, Equation 2.1. We obtain

$$\Phi(j\Omega) = \frac{1}{2} A\left(e^{j\Omega/2}\right) \Phi\left(j\Omega/2\right) \ , \tag{2.15}$$

where

$$A\left(e^{j\omega}\right) = \sum_{n=0}^{N-1} a_n e^{-j\omega n} \ . \tag{2.16}$$

Note that $A\left(e^{j\omega}\right)$ is the Discrete-Time Fourier Transform (DTFT) of the filter $a_n$. Similarly, by taking the Fourier transform of equation (2.7), we arrive at the Fourier representation for the wavelet:

$$\Psi(j\Omega) = \frac{1}{2} B\left(e^{j\Omega/2}\right) \Phi\left(j\Omega/2\right) \ , \tag{2.17}$$

where

$$B\left(e^{j\omega}\right) = \sum_{n=0}^{N-1} b[n]e^{-j\omega n} = e^{-j(\omega+\pi)(N-1)}\ A^*\left(e^{j(\omega+\pi)}\right)\ . \tag{2.18}$$

The orthogonality condition (Condition O) in the Fourier domain can be derived from the time domain orthogonality condition, equation (2.9), by using Parseval's theorem. The result is

$$\frac{1}{4}\left[\left|A\left(e^{j\omega}\right)\right|^2 + \left|A\left(e^{j(\omega+\pi)}\right)\right|^2\right] = 1\ . \tag{2.19}$$

### 2.2.3 Daubechies Wavelets and the Acuracy Condition

Another important characteristic of wavelets is the ability to represent polynomials up to a certain degree. This *accuracy* condition[2] is an important property of Daubechies Wavelets [21] which is referred to as Condition A.

Condition A is closely related to the *vanishing moments* of the wavelets i.e.

$$\int_{-\infty}^{\infty} \psi(t)\ t^k dt = 0\ ; \qquad k = 0, 1, \cdots, N/2 - 1\ . \tag{2.20}$$

Forcing the wavelets to have vanishing moments at all the levels of resolution implies that the scaling function spaces may represent polynomials. This is simple to see. Define $P_n^{2^j}$ as the space of piecewise polynomials of degree $n = N/2 - 1$ with length $2^j$ and split $L^2 = V_m \bigoplus \sum_{l \geq m} W_l$. The vanishing moment property states that $P_n^{2^j}$ is orthogonal to $W_j$, furthermore, $P_n^{2^j} \subset P_n^{2^{(j+1)}}$ for all $j$, thus $P_n^{2^m}$ is orthogonal to $W_j$, for $j = m, m+1, \ldots$. This necessarily implies that $P_n^{2^m} \subset V_m$.

The vanishing moment condition is translated to the filter as

$$\sum_k (-1)^k a_k\ k^l = 0\ ; \qquad k = 0, 1, \cdots, N/2 - 1\ . \tag{2.21}$$

However, it is in the $z$ and discrete Fourier domain where we clearly see the accuracy condition. Taking the Fourier transform of the filter $a_k$ gives us the condition

[2]Formally known as a Strang-Fix condition.

$$A(e^{j\omega}) = \left(\frac{1+e^{-j\omega}}{2}\right)^{N/2} R(e^{j\omega}) \ , \tag{2.22}$$

where $R(e^{j\omega})$ is chosen to satisfy Condition O. In the z-transform domain, this means that $A(z)$ has a zero of order $N/2$ at $z = -1$.

Daubechies wavelets are the most famous example which satisfy Condition A. The ability to represent polynomials makes it well suited for applications involving image compression and PDEs. However, the regular grid restriction on Daubechies wavelets is still a handicap for solving PDEs for complex meshes.

## 2.3 Biorthogonal Wavelets

Biorthogonal wavelets maybe viewed as a generalization of the orthogonal wavelets setting. With biorthogonal wavelets, there are *two* sequences of embedded subspaces

$$\{0\} \cdots V_{-2} \subset V_{-1} \subset V_0 \subset V_1 \subset V_2 \cdots L^2(R) \ ,$$
$$\{0\} \cdots \tilde{V}_{-2} \subset \tilde{V}_{-1} \subset \tilde{V}_0 \subset \tilde{V}_1 \subset \tilde{V}_2 \cdots L^2(R).$$

These two set of multiresolution subspaces are *biorthogonal* (dual) to each other. As expected, we now have two scaling functions. The primary scaling function $\phi_j(t)$ which belongs to $V_j$ and the dual scaling function $\tilde{\phi}_j(t)$ which belongs to $\tilde{V}_j$.

Define a series of nested *primary* multiresolution subspaces $V_j \subset L_2(R)$, where $j \in \mathcal{Z}$, which satisfies the following conditions:

**(a).** $V_j = \text{clos span}\{\phi_{j,k} \mid k \in \mathcal{Z}\}$, where the span of the *scaling* functions $\phi_{j,m} = 2^{j/2}\phi(2^j t - k)$ forms a *Reisz* basis (see [44])

**(b).** $V_j \subset V_{j+1}$

**(c).** $\cup_{j=-\infty}^{\infty} V_j$ is dense in $L_2$

**(d)** Let $W_j = \text{clos span}\{\psi_{j,k} \mid k \in \mathcal{Z}\}$ be a series of subspaces, such that $V_{j+1} = V_j \oplus W_j$, where the *wavelet* function $\psi_{j,k} = 2^{j/2}\psi(2^j t - k)$. This condition forms the basis for the multi resolution property of wavelets. We may project a function onto $V_{j+1}$ and then decompose it into $V_j$ and $W_j$ through the Biorthogonal Discrete Wavelet Transform.

Similarly, we define a series of *dual* subspaces $\tilde{V}_j \subset L_2$, with the following conditions:

**(e)**. $\tilde{V}_j = \text{clos span}\{\tilde{\phi}_{j,k} \mid k \in \mathcal{Z}\}$, where the span of $\tilde{\phi}_{j,m} = 2^{j/2}\tilde{\phi}(2^j t - k)$ forms a *Reisz* basis

**(f)**. $\tilde{V}_j \subset \tilde{V}_{j+1}$

**(g)**. $\cup_{j=-\infty}^{\infty} \tilde{V}_j$ is dense in $L_2$

**(h)**. $\tilde{V}_{j+1} = \tilde{V}_j \oplus \tilde{W}_j$, where $\tilde{W}_j = \text{clos span}\{\tilde{\psi}_{j,k} \mid k \in \mathcal{Z}\}$ and $\tilde{\psi}_{j,k} = 2^{j/2}\tilde{\psi}(2^j t - k)$

Now, $V_j$ and $W_j$ are not necessarily orthogonal, although their intersection is zero, but they satisfy the following condition:

$$V_j \perp \tilde{W}_j, \; W_j \perp \tilde{V}_j \tag{2.23}$$

The basis functions of $V_j$ and $W_j$ satisfy the following *biorthogonality* condition:

$$\langle \phi(t-k), \tilde{\phi}(t-l) \rangle = \delta_{k-l}, \;\; \langle \psi(t-k), \tilde{\psi}(t-l) \rangle = \delta_{k-l}. \tag{2.24}$$

Now, Conditions **(a)** to **(h)** imply

$$\phi(t) = \sum_k a_k \phi(2t-k) \qquad \tilde{\phi}(t) = \sum_k \tilde{a}_k \tilde{\phi}(2t-k) \tag{2.25}$$

$$\psi(t) = \sum_k b_k \phi(2t-k) \qquad \tilde{\phi}(t) = \sum_k \tilde{b}_k \tilde{\phi}(2t-k). \tag{2.26}$$

for some real coefficients $a_k, \tilde{a}_k, b_k$ and $\tilde{b}_k$. In contrast to the orthogonal wavelets we now have two scaling relations and two wavelet relations. Furthermore $\{a_k, b_k, \tilde{a}_k, \tilde{b}_k\}$ satisfy

$$b_k = (-1)^k a_{N-1-k} \quad \text{and} \quad \tilde{b}_k = (-1)^k \tilde{a}_{N-1-k}$$

and condition (2.24) implies

$$\sum_k a_l \tilde{a}_{l-2k} = 2\delta_k.$$

### 2.3.1 Fourier Domain Representation

Taking the Fourier transform of equations (2.25) and (2.26) results in the following frequency domain scaling relations:

$$\Phi(j\Omega) = \frac{1}{2} A\left(e^{j\Omega/2}\right) \Phi\left(j\Omega/2\right), \qquad \tilde{\Phi}(j\Omega) = \frac{1}{2} \tilde{A}\left(e^{j\Omega/2}\right) \tilde{\Phi}\left(j\Omega/2\right), \tag{2.27}$$

$$\Psi(j\Omega) = \frac{1}{2} B\left(e^{j\Omega/2}\right) \Phi\left(j\Omega/2\right), \qquad \tilde{\Psi}(j\Omega) = \frac{1}{2} \tilde{B}\left(e^{j\Omega/2}\right) \tilde{\Phi}\left(j\Omega/2\right), \tag{2.28}$$

where

$$B\left(e^{j\omega}\right) = e^{-j(\omega+\pi)(N-1)}\ A^*\left(e^{j(\omega+\pi)}\right) \quad \text{and} \quad \tilde{B}\left(e^{j\omega}\right) = e^{-j(\omega+\pi)(\tilde{N}-1)}\ \tilde{A}^*\left(e^{j(\omega+\pi)}\right) . \tag{2.29}$$

Furthermore, condition (2.24), leads to the following biorthogonality condition in the Fourier domain:

$$\frac{1}{4}\left[A(e^{j\omega})\tilde{A}^*(e^{j\omega}) + A(e^{j(\omega+\pi)})\tilde{A}^*(e^{j(\omega+\pi)})\right] = 1 . \tag{2.30}$$

## 2.4 Orthogonal Discrete Wavelet Transforms

One of the key properties of the wavelet theory is the existence of the Discrete Wavelet Transform (DWT). This computational procedure allows us to quickly move between a single scale representation to a multiscale representation. In fact, this transformation is of $\mathcal{O}(N)$. In contrast to such popular methods as the Fast Fourier Transform which is $\mathcal{O}(Nlog_2N)$. We shall now derive the DWT. Note that

$$P_j f(t) = P_{j-1} f(t) + Q_{j-1} f(t) \tag{2.31}$$

and then taking the inner product with $\phi_{j-1,n}(t)$ and $\psi_{j-1,n}(t)$, from equations (2.1) and (2.7), we obtain

$$\langle \phi_{j,k}(t), \phi_{j-1,n}(t) \rangle \ = \ \frac{1}{\sqrt{2}}\, a_{k-2n} , \tag{2.32}$$

$$\langle \phi_{j,k}(t), \psi_{j-1,n}(t) \rangle = \frac{1}{\sqrt{2}} b_{k-2n} . \tag{2.33}$$

The DWT may then be written as

$$c_n^{j-1} = \frac{1}{\sqrt{2}} \sum_{k=2n}^{2n+N-1} c_k^j \, a_{k-2n} , \tag{2.34}$$

$$d_n^{j-1} = \frac{1}{\sqrt{2}} \sum_{k=2n}^{2n+N-1} c_k^j \, b_{k-2n} . \tag{2.35}$$

Equations 2.34 and 2.35 may be also written in filter form as shown in Figure 2-3. The DWT may be thought of as low pass filtering with the dilation equation coefficients followed by downsample and also high pass filtering with the wavelet equation coefficients. As Figure 2-3 shows, we may further decompose the coarse coefficients into different frequency bands. Thus, applying recursively the DWT to the coefficients of $f(t)$, which belong in $V_m$, gives us a decomposition of the form $V_0 \bigoplus \sum_{0 \geq j \geq m-1} W_j$. This effectively leads to a *logarithmic* frequency decomposition of the original signal $f(t)$.

To obtain the inverse DWT we simply take the inner product of Equation 2.31 with $\phi_{m,n}(t)$ and apply Equations (2.1) and (2.7), thus

$$\begin{aligned} c_n^j = & \frac{1}{\sqrt{2}} \sum_{k=\lceil (n-N+1)/2 \rceil}^{\lfloor n/2 \rfloor} c_k^{j-1} \, a_{n-2k} + \\ & \frac{1}{\sqrt{2}} \sum_{k=\lceil (n-N+1)/2 \rceil}^{\lfloor n/2 \rfloor} d_k^{j-1} \, b_{n-2k} . \end{aligned} \tag{2.36}$$

We are, however, not restricted to signals in $R^1$. We may extend the DWT to a two dimensional domain by taking tensor products of one dimensional wavelets. In Figure 2-4 we show an example of applying the wavelet transform to images. We first apply the DWT to the rows of the original image to obtain two downsampled images. We now apply the DWT to the columns. As shown in Figure 2-4 we now have four images; Each image corresponds to one of four subands. In fact, it has been shown

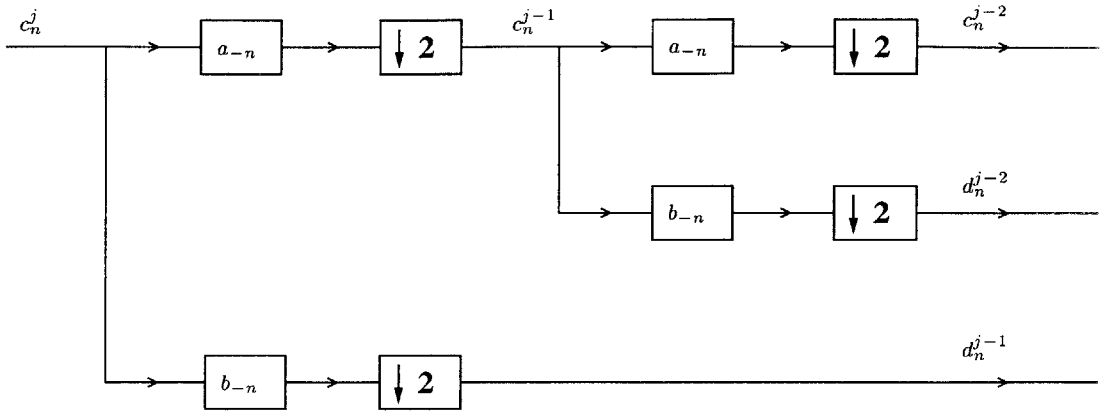


Figure 2-3: Signal flow graph for a two stage implementation of the Discrete Wavelet Transform.

that the entropy of high pass subands is substantially reduced.

In Figure 2-5 the four images are reconstructed to get the original image back. Note that due to the entropy reduction of the wavelet transform it is possible to remove substantial amounts of data and still recover an image of very high quality. In practice, several applications of the DWT leads to a thirty to one compression with very high quality.

The low frequency component is easily recognized as being a subsampled version of the original image.

### 2.4.1 Biorthogonal Discrete Wavelet Transform

A change of basis from the primary scaling function subspace, at some fixed resolution, into a series of nested subspaces, at lower resolutions, may be easily accomplished by the biorthogonal discrete wavelet transform (BDWT). This transformation is of order $\mathcal{O}(n)$.

Let $P_j : L^2 \to V_j$ and $Q_j : L^2 \to W_j$ be projection operators such that

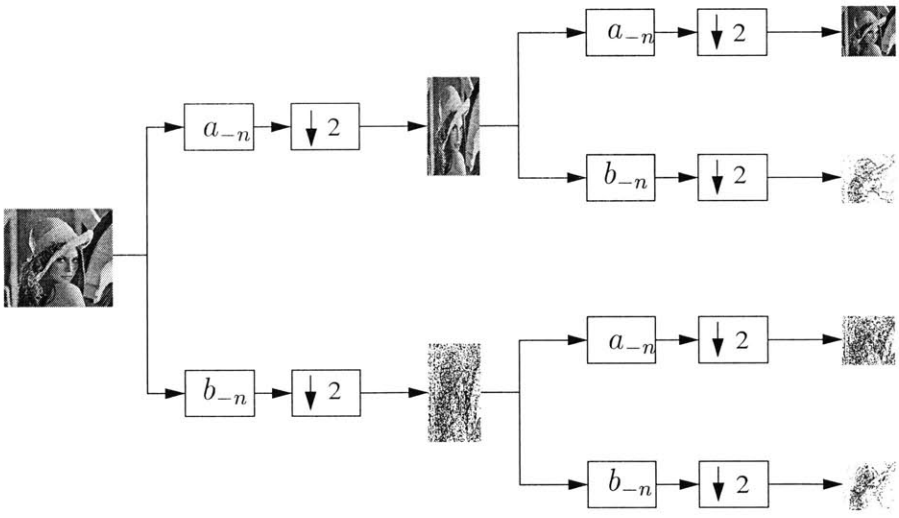


Figure 2-4: Two-dimensional Discrete Wavelet Transform.

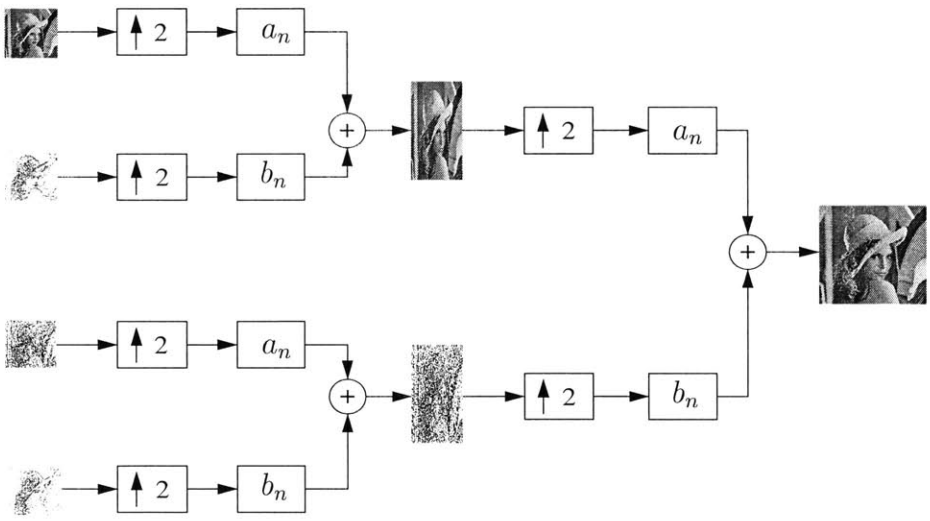


Figure 2-5: Two-dimensional inverse Discrete Wavelet Transform.

$$P_j f = \sum_k c_{j,k}\phi_{j,k} \quad \text{and} \quad Q_j f = \sum_k d_{j,k}\psi_{j,k},$$

where $c_{j,k} =< f, \tilde{\phi}_{j,k} >$, $d_{j,k} =< f, \tilde{\psi}_{j,k} >$ and $f \in L^2$. Similarly, let us define the dual operators $\tilde{P}_j : L^2 \to \tilde{V}_j$ and $\tilde{Q}_j : L^2 \to \tilde{W}_j$, such that

$$\tilde{P}_j f = \sum_k \tilde{c}_{j,k}\tilde{\phi}_{j,k} \quad \text{and} \quad \tilde{Q}_j f = \sum_k \tilde{d}_{j,k}\tilde{\psi}_{j,k},$$

where $\tilde{c}_{j,k} =< f, \phi_{j,k} >$ and $\tilde{d}_{j,k} =< f, \psi_{j,k} >$. By combining (2.24) to (2.26) with condictions **(a)** and **(b)** in Section 2.3, we obtain the BWDT:

$$c_{j,l} = \frac{1}{\sqrt{2}} \sum_k \tilde{a}_{k-2l} c_{j+1,k}, \qquad d_{j,l} = \frac{1}{\sqrt{2}} \sum_k \tilde{b}_{k-2l} c_{j+1,k},$$

and it's inverse:

$$c_{j+1,l} = \frac{1}{\sqrt{2}} \sum_k a_{k-2l} c_{j,k} + \frac{1}{\sqrt{2}} \sum_k b_{k-2l} d_{j,k}.$$

We obtain in a similar fashion the dual Briothogonal DWT

$$\tilde{c}_{j,l} = \frac{1}{\sqrt{2}} \sum_k a_{k-2l} \tilde{c}_{j+1,l}, \qquad \tilde{d}_{j,l} = \frac{1}{\sqrt{2}} \sum_k b_{k-2l} \tilde{c}_{j+1,k},$$

and it's inverse:

$$\tilde{c}_{j+1,l} = \frac{1}{\sqrt{2}} \sum_k \tilde{a}_{k-2l} \tilde{c}_{j,k} + \frac{1}{\sqrt{2}} \sum_k \tilde{b}_{k-2l} \tilde{d}_{j,k}.$$

The BWDT establishes the connection of wavelet functions spaces to discrete linear systems.

## 2.5 Spatial Decorrelation

One of the key properties of wavelets is the decorrelation of sets of data. The perpendicular relation of Equation (2.23) implies that the statistical correlation between $V_j$ and $\tilde{W}_j$ is exactly zero. This is also true for $\tilde{V}_j$ and $W_j$.

Let us start with a scaling function space $V_j$, which has some overlap with $\tilde{V}_j$, as shown in Figure 2-6. By applying the Biorthogonal DWT, we may efficiently map $V_j$ onto $V_{j-1}$ and $W_{j-1}$. By Equation (2.23), $V_{j-1}$ and $\tilde{W}_{j-1}$ are completely decorrelated, which implies that the intersection of $W_{j-1}$ and $\tilde{W}_{j-1}$ is decorrelated from $V_{j-1}$. We may further map $V_{j-1}$ onto $V_{j-2}$ and $W_{j-2}$. Equation (2.23) implies $W_{j-1} \cap \tilde{W}_{j-1}$ is decorrelated from $W_{j-2} \cap \tilde{W}_{j-2}$. By continuing this process, we obtain the following multiresolution decomposition:

$$V_j = W_{j-1} \oplus ... W_0 \oplus V_0,$$

where the intersections $U_i = W_i \cap \tilde{W}_i$, for $i = 1..j-1$, are completely decorrelated from each other. The previous analysis implies that if we want "good" decorrelation of data then $W_i \cap \tilde{W}_i$ must be as large as possible. In general, they should have the same vanishing moments. This decomposition appears very frequently in the wavelet literature and forms a basic framework for compression and entropy reduction schemes.

## 2.6 MultiWavelets

An underlying limitation of wavelets is that they do not naturally form a basis for functions on a finite interval. This problem was mitigated by the construction of a class of wavelets defined over a finite domain. In [1] Alpert introduces the concept of an orthogonal *Multiwavelet* basis. It is further generalized to the biorthogonal setting [25, 45]

In a multiwavelet basis, one has $r > 1$ scaling functions $\phi_q(x)$ $(q = 0, 1..., r-1)$ and a similar number of wavelets $w_q(x)$. The scaling functions then satisfy a matrix

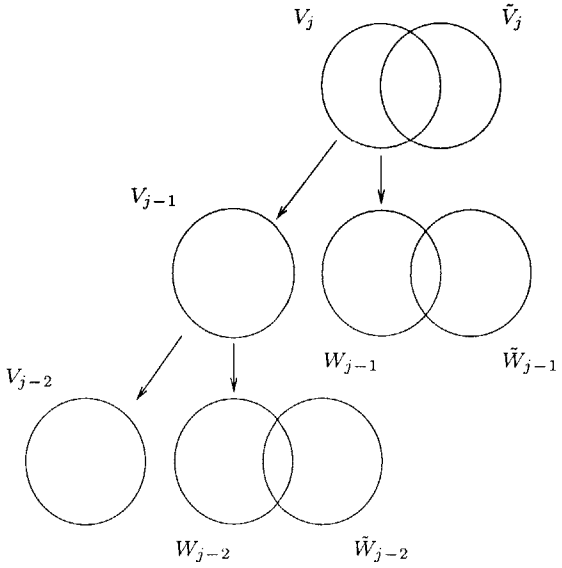


Figure 2-6: $V_j$ is decomposed into $W_{j-1} \oplus ... \oplus W_0 \oplus V_0$ by use of the Biorthogonal DWT. The intersections of $W_i$ and $\tilde{W}_i$ , for $i = j - 1...0$, are completely decorrelated from each other, which gives rise to a highly decorrelated function basis.

refinement equation:

$$\begin{bmatrix} \phi_0(x) \\ \vdots \\ \phi_{r-1}(x) \end{bmatrix} = \sum_k \begin{bmatrix} h_{00}[k] & \cdots & h_{0,r-1}[k] \\ \vdots & & \vdots \\ h_{r-1,0}[k] & \cdots & h_{r-1,r-1}[k] \end{bmatrix} \begin{bmatrix} \phi_0(2x-k) \\ \vdots \\ \phi_{r-1}(2x-k) \end{bmatrix}$$

Likewise , the wavelets are given by a matrix wavelet equation. This form of basis allows for greater complexity and adaptability of the wavelet scheme. However it is still limited to regular grids. In this thesis we generalize the concept of multiwavelets to irregular grids by dropping the requirements of shift and scale invariance, and respectively replacing the notations $\phi_q(x-k')$, $\phi_q(2x-k)$ and $h_{q,q'}[k]$ with $\phi^j_{q,k'}(x)$, $\phi^{j+1}_{q,k}(x)$ and $h^j_{q,q'}[k,k']$.

A simple example is given in Figure 2-7. These wavelets form a biorthogonal set i.e.

$$\langle \phi_q(x), \tilde{\phi}_{q'}(x-k) \rangle = \delta_{q-q'}\delta_k \quad \langle w_q(x), \tilde{w}_{q'}(x-k) \rangle = \delta_{q-q'}\delta_k$$

$$\langle \phi_q(x), \tilde{w}_{q'}(x-k) \rangle = 0 \quad \langle w_q(x), \tilde{\phi}_{q'}(x-k) \rangle = 0$$

and that they satisfy the following scaling laws

$$\begin{bmatrix} \phi_0(x) \\ \phi_1(x) \end{bmatrix} = \begin{bmatrix} 1 & 1/2 \\ 0 & 1/2 \end{bmatrix} \begin{bmatrix} \phi_0(2x) \\ \phi_1(2x) \end{bmatrix} + \begin{bmatrix} 1/2 & 0 \\ 1/2 & 1 \end{bmatrix} \begin{bmatrix} \phi_0(2x-1) \\ \phi_1(2x-1) \end{bmatrix}$$

$$\begin{bmatrix} \tilde{\phi}_0(x) \\ \tilde{\phi}_1(x) \end{bmatrix} = \begin{bmatrix} 3/2 & 1/2 \\ -1/2 & 0 \end{bmatrix} \begin{bmatrix} \tilde{\phi}_0(2x) \\ \tilde{\phi}_1(2x) \end{bmatrix} + \begin{bmatrix} 0 & -1/2 \\ 1 & 3/2 \end{bmatrix} \begin{bmatrix} \tilde{\phi}_0(2x-1) \\ \tilde{\phi}_1(2x-1) \end{bmatrix}$$

$$\begin{bmatrix} w_0(x) \\ w_1(x) \end{bmatrix} = \begin{bmatrix} 1 & -1 \\ 1 & -2 \end{bmatrix} \begin{bmatrix} \phi_0(2x) \\ \phi_1(2x) \end{bmatrix} + \begin{bmatrix} -1 & 1 \\ 2 & -1 \end{bmatrix} \begin{bmatrix} \phi_0(2x-1) \\ \phi_1(2x-1) \end{bmatrix}$$

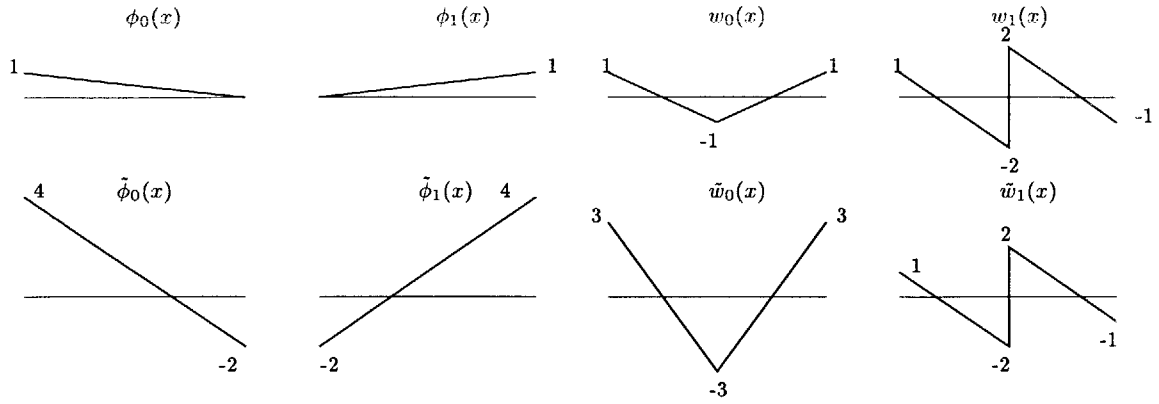


Figure 2-7: Example of piecewise linear multiwavelets (top row) and their duals (bottom row).

$$\begin{bmatrix} \tilde{w}_0(x) \\ \tilde{w}_1(x) \end{bmatrix} = \begin{bmatrix} 1/2 & -1/2 \\ 0 & -1/2 \end{bmatrix} \begin{bmatrix} \tilde{\phi}_0(2x) \\ \tilde{\phi}_1(2x) \end{bmatrix} + \begin{bmatrix} -1/2 & 1/2 \\ 1/2 & 0 \end{bmatrix} \begin{bmatrix} \tilde{\phi}_0(2x-1) \\ \tilde{\phi}_1(2x-1) \end{bmatrix}.$$

# Chapter 3

# Linear Surface Wavelets

In this chapter we discuss the extension of wavelets to irregular geometries. The *lifting scheme*, by Sweldens [40], is introduced as a tool to construct linear surface wavelets over complex meshes. Moreover we construct the dual scaling functions and wavelets, and prove stability properties of the basis. Many of these results are located in [4].

## 3.1 Wavelets for Complex Surfaces

### 3.1.1 Traditional wavelet construction

Traditional wavelet constructions are characterized by the operations of scaling and shifting of a single function. A typical example of such a construction starts with the hat function and represents it as a combination of scaled and shifted versions of itself as illustrated in Figure 3-1. Mathematically, this example can be expressed as a two-scale difference equation

$$\phi(x) = \sum_{k=-1}^{1} h_k^0 \phi(2x - k)$$

with $h_k^0 = \left\{\frac{1}{2}, 1, \frac{1}{2}\right\}$. The function $\phi(x)$ in this case is the hat function on the interval $[-1, 1]$ and in wavelet terminology it is referred to as a scaling function. Note that the

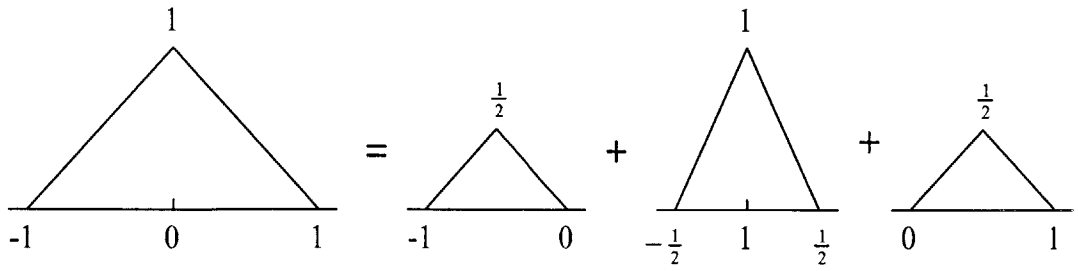


Figure 3-1: Representation of the hat function as a combination of scaled and shifted versions of itself.

scaling function in this example has linear interpolating properties. Scaling functions with other properties, such as orthogonality and higher order, can be designed with an appropriate choice of $h_k^0$ (see e.g. [44].)

Wavelets are constructed from scaling functions, using a different combination of the scaled and shifted versions of $\phi(x)$

$$\psi(x) = \sum_k h_k^1 \phi(2x - k) \tag{3.1}$$

The theory of wavelets and filter banks tells us how to design admissible filters, $h_k^0$ and $h_k^1$, using Fourier transform techniques [44]. The admissibility conditions are referred to as biorthogonality or perfect reconstruction conditions. The term biorthogonality implies the existence of dual functions, which we denote by $\tilde{\phi}(x)$ and $\tilde{w}(x)$. If we denote the corresponding dual filters by $f_k^0$ and $f_k^1$, then the admissibility conditions can be stated as:

| $k$ | -2 | -1 | 0 | 1 | 2 | 3 |
|---|---|---|---|---|---|---|
| $h_k^0$ | | $\frac{1}{2}$ | 1 | $\frac{1}{2}$ | | |
| $h_k^1$ | | $-\frac{1}{4}$ | $-\frac{1}{2}$ | $\frac{3}{2}$ | $-\frac{1}{2}$ | $-\frac{1}{4}$ |
| $f_k^0$ | $-\frac{1}{4}$ | $\frac{1}{2}$ | $\frac{3}{2}$ | $\frac{1}{2}$ | $-\frac{1}{4}$ | |
| $f_k^1$ | | | $-\frac{1}{2}$ | 1 | $-\frac{1}{2}$ | |

Table 3.1: Admissible set of filters for hat function

$$F_0(z^{-1})H_0(z) + F_1(z^{-1})H_1(z) = 4 \tag{3.2}$$

$$F_0(-z^{-1})H_0(z) + F_1(-z^{-1})H_1(z) = 0 \tag{3.3}$$

Here, we have used the notation $H_0(z)$to denote the $z$-transform[1] of $h_k^0$

$$H_0(z) = \sum_k h_k^0 z^{-k} \tag{3.4}$$

The design proceeds by choosing $H_1(z) = z^{-l}F_0(-z^{-1})$, $F_1(z^{-1}) = z^l H_0(-z)$, where $l$ is odd, and then looking for $P(z) = F_0(z^{-1})H_0(z)$ such that

$$P(z) + P(-z) = 4$$

We thus find that an admissible set of filters for the hat function example is shown in Table 3.1.

Now that the design process is complete, one can construct a basis for functions

[1]The Fourier transform can be easily obtained from Eq. (3.4) by replacing $z$ with $e^{i\omega}$.

| $k$ | -2 | -1 | 0 | 1 | 2 |
|---|---|---|---|---|---|
| $h_k^{0,old}$ | | $\frac{1}{2}$ | 1 | $\frac{1}{2}$ | |
| $h_k^{1,old}$ | | | | 2 | |
| $f_k^{0,old}$ | | | 2 | | |
| $f_k^{1,old}$ | | | $-\frac{1}{2}$ | 1 | $-\frac{1}{2}$ |

Table 3.2: Old admissible set of filters for hat function

in $L^2(R)$ by taking the following set of scaled and shifted functions

$$\left\{\phi(x-k), \psi(2^j x - k) \mid j,k \in Z, j \geq 0\right\}$$

This brief introduction illustrates a key point about traditional wavelets: they are naturally associated with uniform grids. This can be easily seen from the fact that the functions $\psi(2^j x - k)$ are located at the dyadic points $x = 2^{-j}k$. Furthermore, we note that the Fourier transform techniques for designing the discrete filters are only applicable to uniform grids.

An alternative methodology for designing wavelets called the lifting scheme was recently described by Sweldens [40]. The main idea behind lifting is that one can use very simple operations to transform an initial set of admissible filters into a more complex set of admissible filters. For instance, if we were given the admissible filters in Table 3.2, we could obtain new admissible filters by letting

$$H_0(z) = H_0^{old}(z) \tag{3.5}$$

$$H_1(z) = H_1^{old}(z) - S(z^2)H_0(z) \tag{3.6}$$

$$F_0(z^{-1}) = F_0^{old}(z^{-1}) + S(z^2)F_1(z^{-1}) \tag{3.7}$$

$$F_1(z^{-1}) = F_1^{old}(z^{-1}) \tag{3.8}$$

The choice $S(z) = \frac{1}{2}(1 + z^{-1})$ would then give us the more complex filters shown in Table 1. Note, however, that the admissibility conditions, Eqs. (3.2) and (3.3), will be satisfied regardless of the actual choice for $S(z)$. Here, the only filters to change were $h_k^1$ and $f_k^0$, however, a similar procedure can be used to update the filters $h_k^0$ and $f_k^1$. We may thus produce filters of any desired order by alternately lifting one pair of filters and then the other pair.

### 3.1.2 Second-generation wavelets

The lifting scheme can also be stated in the spatial domain. This allows the generalization of the wavelet concept to irregular grids. The generalized wavelets are typically referred to as second-generation wavelets [40]. Thus, Eqs. (3.5)-(3.8) can be shown to be equivalent to the following operations on the scaling functions and wavelets:

$$\phi(x) = \phi^{old}(x) \tag{3.9}$$

$$\psi(x) = \psi^{old}(x) - \sum_k s_k \, \phi(x - k) \tag{3.10}$$

$$\tilde{\phi}(x) = \tilde{\phi}^{old}(x) + \sum_k s_k \, \tilde{\psi}(x + k) \tag{3.11}$$

$$\tilde{\psi}(x) = \sum_k f_k^{1,old} \tilde{\phi}(2x - k) \tag{3.12}$$

One can then state the biorthogonality conditions in terms of the following $L^2$ inner products:

$$\langle \phi(.), \, \tilde{\phi}(. - k) \rangle = \delta_{0,k} \tag{3.13}$$

$$\langle \phi(.), \, \tilde{\psi}(. - k) \rangle = 0 \tag{3.14}$$

$$\langle \psi(.),\, \tilde{\phi}(.-k) \rangle = 0 \tag{3.15}$$

$$\langle \psi(.),\, \tilde{\psi}(.-k) \rangle = \delta_{0,k} \tag{3.16}$$

Again, it is quite straightforward to verify that these conditions remain valid when an initially biorthogonal set, $\left\{\phi^{old}, \psi^{old}, \tilde{\phi}^{old}, \tilde{\psi}^{old}\right\}$, is lifted using Eqs. (3.9)-(3.12). For the filters given in Table 3.2, the initial set of functions is particularly simple. $\phi^{old}$ is the hat function on $[-1, 1]$, $\psi^{old}$ is a hat function on $[0, 1]$, $\tilde{\phi}^{old}$ is the Dirac delta function, $\delta(x)$, and $\tilde{\psi}^{old}$ is a combination of Dirac functions at 0, $\frac{1}{2}$ and 1. These functions do not lead to a good wavelet basis, but they do provide a useful starting point since the biorthogonality conditions can be verified using the property that $\langle f(.),\, \delta(.) \rangle = f(0)$. The lifting construction allows us to improve the properties of the wavelet basis by adding *vanishing moments* to the wavelet. In our example, we may add two vanishing moments to $w$ by choosing $s_0$ and $s_1$ in Eq. (3.10), such that

$$\int \psi(x) x^m dx = 0$$

for $m = 0, 1$. This gives us $s_0 = s_1 = 1/2$. The resulting wavelet is shown in Figure 3-2.

We are now in a position to generalize the wavelet construction to non-uniform grids. To do this, we need to relax the constraint that the wavelet basis functions are all shifted and scaled versions of the same function. Figure 3-3 illustrates how a hat function on a non-uniform grid can be represented as a combination of hat functions on a finer version of the grid. In this example, the grid was refined by the subdivision of each interval into two intervals of equal size (the points $x_{m-1}$ and $x_m$ are the midpoints). Note that the functions on the finer grid are not scaled and shifted versions of the function on the coarser grid, although they are similar in shape.

We introduce the notation $\phi_{j,k}(x)$ to denote the scaling function on the coarser grid. Here, the subscript $k$ refers to the spatial position, $x_k$, at which the scaling function is located. The subscript $j$ refers to the resolution of the coarser grid; the

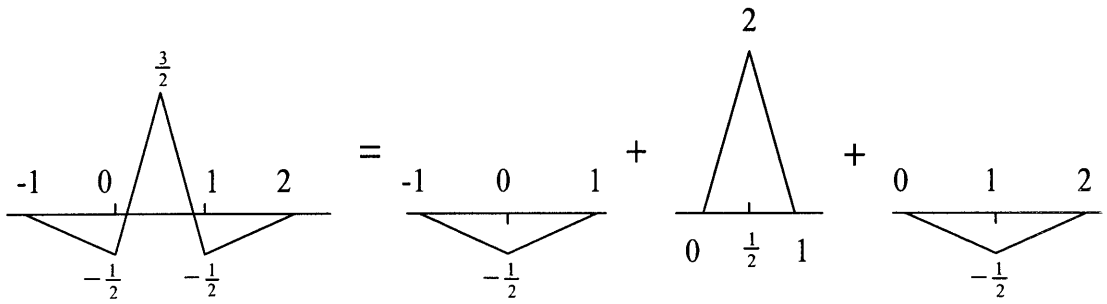


Figure 3-2: Construction of wavelet by lifting.

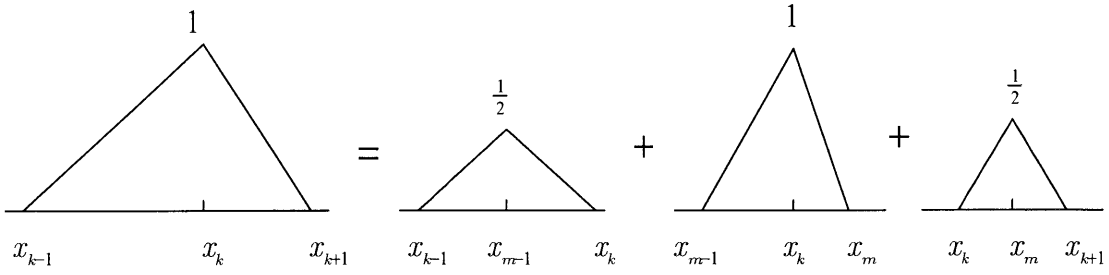


Figure 3-3: Generalization of scaling function to a non-uniform grid.

finer grid then has resolution $j+1$. One may think of the function $\phi_{j,k}(x)$ as a generalized version of $\phi(2^j x - k)$. With this in mind, we write the generalized two-scale difference equation as

$$\phi_{j,k}(x) = \sum_l h^0_{j,k,l} \phi_{j+1,l}(x) \tag{3.17}$$

In Equation 3.17, the filter $h^0_{j,k,l}$ is no longer constrained to be invariant with respect to space and scale. However, the filter coefficients can be constant in special cases, such as the case of equal subdivision shown in Figure 3-3.

The construction for the wavelet can be generalized in a similar fashion. The generalized version of Eq. (3.10) is given by

$$\psi_{j,m}(x) = \psi^{old}_{j,m}(x) - \sum_k s_{j,k,m} \phi_{j,k}(x).$$

Note that the wavelet is spatially located at one of the subdivision points. Although the coefficients $s_{j,k,m}$ are now dependent on $j$ and $m$, they can still be determined using the vanishing moment criterion described earlier.

### 3.1.3 Wavelets on surfaces in three-dimensions

The second-generation wavelet construction can be applied to more complex meshes in three dimensions (Schroder and Sweldens [42]). In fact, the hat function example has a direct analogy in the three-dimensional case. Suppose that Figure 3-4 represents a portion of a triangular (polyhedral) surface mesh $S \subset R^3$ , which we will refer to as the $j$th resolution mesh. The nodes of the $j$th resolution mesh are identified by a set of indices, $K(j)$, which includes the indices $\{k, k'_i | i = 1, ..., 6\}$. The $(j+1)$th resolution mesh is obtained by introducing new nodes, identified by a set of indices, $M(j)$, which subdivide the mesh at its edges. The nodes labeled $\{m_i | i = 1, ..., 6\}$ are examples of such subdivision points. The complete set of nodes in the $j+1$th resolution mesh is then given by $K(j+1) = K(j) \cup M(j)$. In practice we shall have a maximum resolution level $n$ and denote each triangular patch, at resolution $n$, as

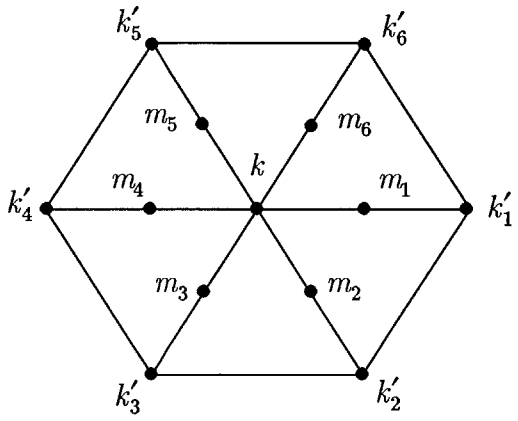


Figure 3-4: Refinement of the surface grid by subdivision of the edges.

$Q_k^n$, where $k$ is the index of that triangle. Thus our mesh becomes $S = \bigcup_k Q_k^i$ for any resolution level $i$. We shall assume that any further conceptual refinements are of the form $Q_k^{n+i} \subset Q_l^n$ for some $l$ and $i = 1, 2, \ldots,$.

We use the notation $\vec{x}_k$ to refer to the position vector of the node whose index is $k$. The hat scaling function can then be defined as the function, $\phi_{j,k}(\vec{x})$, that varies linearly from the value 1 at the vertex $\vec{x}_k$ to the value 0 at the vertices $\vec{x}_{k'_i}$ ($i$ = 1, ..., 6). As in the one-dimensional case, the scaling function on the $j$th resolution mesh can be expressed as a combination of scaling functions on the $j+1$th resolution mesh:

$$\phi_{j,k}(\vec{x}) = \phi_{j+1,k}(\vec{x}) + \sum_{m \in n(j,k)} h^0_{j,k,m} \phi_{j+1,m}(\vec{x}). \tag{3.18}$$

The hat function fits this equation with

$$h^0_{j,k,m} = \begin{cases} ||\vec{x}_{m_i} - \vec{x}_{k'_i}||/||\vec{x}_k - \vec{x}_{k'_i}|| & ; \quad m \in n(j,k) \\ 0 & ; \quad m \notin n(j,k) \end{cases}$$

Here, $n(j,k) = \{m_i | i = 1, ..., 6, m_i \in M(j)\}$ i.e. the set of subdivision points neighboring node $k$ at the $j$th level. Note that the filter $h^0_{j,k,m}$ becomes considerably simpler if the edges are subdivided at their midpoints. In this case, all the nonzero coefficients in the filter are $\frac{1}{2}$. One can construct higher order scaling functions by expanding the neighborhood $n(j,k)$ beyond the immediate neighbors. In doing so, it is usually convenient to restrict the neighborhood to subdivision points only i.e. $n(j,k) \subset M(j)$. This ensures that $\phi_{j,k}(\vec{x})$ has interpolating properties, which helps to simplify the calculations in many practical applications [42].

The wavelet can then be defined as

$$\psi_{j,m}(\vec{x}) = \phi_{j+1,m}(\vec{x}) - \sum_{k \in A(j,m)} h^1_{j,k,m} \phi_{j,k}(\vec{x}) \tag{3.19}$$

where $A(j,m)$ is a neighborhood of node $m$. The simplest choice for $A(j,m)$ is to use the two immediate neighbors, i.e. the parent nodes of the subdivision point. This allows us to construct a wavelet with up to two vanishing moments. As a matter of convenience, one can instead choose to work with a zero integral constraint and a symmetry constraint on the filter. (This is based on the observation that the filter $s_k$ turned out to be symmetric in the case of a regular one-dimensional grid.) The wavelet filter is then given by

$$h^1_{j,k,m} = I_{j+1,m}/2I_{j,k}$$

where $I_{j,k}$ is the integral of the scaling function, $\phi_{j,k}(\vec{x})$, over the surface. In practice such integrals are computed for the scaling functions on the finest resolution grid that we will use. The integrals over the coarser resolution grids can be obtained using a recursion of the form

$$
\begin{aligned}
I_{j,k} &= \int_S \phi_{j,k}(\vec{x})\, dS \\
&= I_{j+1,k} + \sum_{m \in n(j,k)} h^0_{j,k,m}\, I_{j+1,m}.
\end{aligned}
$$

Figure 3-5 illustrates examples of a scaling function and a wavelet constructed in accordance with the preceding recipe. Now that the filters, $h^0_{j,k,m}$ and $h^1_{j,k,m}$, have been determined, the dual scaling function and the dual wavelet may be defined such that the biorthogonality conditions are satisfied:

$$
\tilde{\phi}_{j,k}(\vec{x}) = \tilde{\phi}_{j+1,k}(\vec{x}) + \sum_{m \in a(j,k)} h^1_{j,k,m}\, \tilde{\psi}_{j,m}(\vec{x}) \tag{3.20}
$$

$$
\tilde{\psi}_{j,m}(\vec{x}) = \tilde{\phi}_{j+1,m}(\vec{x}) - \sum_{k \in N(j,m)} h^0_{j,k,m}\, \tilde{\phi}_{j+1,k}(\vec{x}) \tag{3.21}
$$

Here, the neighborhood sets are the adjoints of the neighborhood sets defined for the primary functions i.e. $a(j,k) = \{m | k \in A(j,m)\}$and $N(j,m) = \{k | m \in n(j,k)\}$.

### 3.1.4 Representation of functions

Ideas from approximation theory have historically played an important role in the evolution of wavelet techniques. Most of the ideas that apply to the representation of univariate functions using traditional wavelets can be extended to the representation of functions on three-dimensional surfaces using second-generation wavelets. Let $S$ be such a surface and let $\vec{x}$ be a point on $S$. We may then approximate the function $f(\vec{x})$ by an expansion of the form

$$
f(\vec{x}) = \sum_{k \in K(j)} \lambda_{j,k} \phi_{j,k}(\vec{x}). \tag{3.22}
$$

The coefficients, $\lambda_{j,k}$, are formally given by the inner products $\langle f(\vec{x}), \tilde{\phi}_{j,k}(\vec{x}) \rangle$. This follows from the biorthogonality condition, Eq. (3.13). When the scaling functions

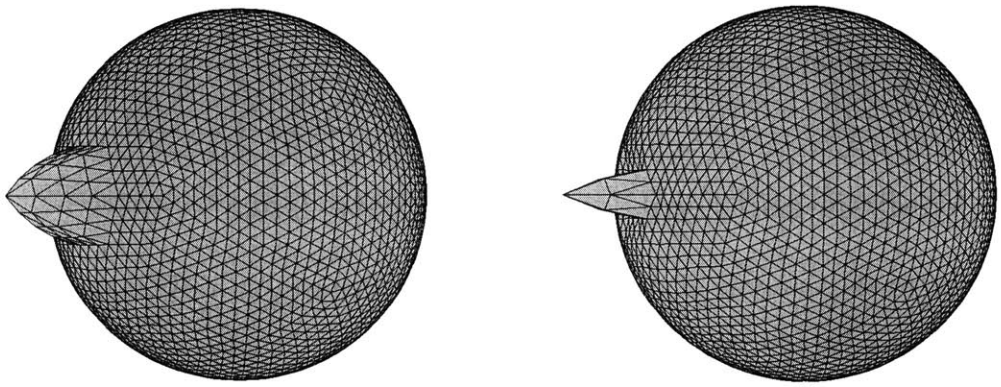

Figure 3-5: Examples of surface wavelet basis functions. (a) Scaling function and (b) wavelet.

are designed to be interpolating functions, the calculation of the coefficients can be greatly simplified, since putting $\vec{x} = \vec{x}_k$ in Eq. (3.22) gives $\lambda_{j,k} = f(\vec{x}_k)$. The error in approximating $f(\vec{x})$ is dependent on the both the order of the scaling functions and the characteristic size, $h_j$, of the $j$th resolution mesh. For example, when $\phi_{j,k}(\vec{x})$ are the generalized hat functions considered earlier, the error would be $O(h_j^2)$. This is the order of the lowest order terms in a Taylor series expansion of $f(\vec{x})$ that cannot be exactly represented by the scaling functions.

The accuracy of the function approximation can be improved by adding in wavelets, $w_{j,m}(\vec{x})$, which are located at the mesh subdivision points, thus

$$f(\vec{x}) = \sum_{k \in K(j)} \lambda_{j,k} \phi_{j,k}(\vec{x}) + \sum_{m \in M(j)} \gamma_{j,m} w_{j,m}(\vec{x}).$$

The correct choice for the coefficient, $\gamma_{j,m}$, is the inner product $\langle f(\vec{x}), \tilde{w}_{j,m}(\vec{x}) \rangle$, which again follows from biorthogonality. With this choice, the improved approxi-

mation for $f(\vec{x})$ will be identical to the resolution $j+1$ approximation in terms of the finer level scaling functions, $\phi_{j+1,k}(\vec{x})$. Of course, the main advantage of using wavelets is that often many of the $\gamma_{j,m}$ are very small, which means that the corresponding wavelet, $w_{j,m}(\vec{x})$, can be dropped from the expansion altogether. This can happen, for example, if $f(\vec{x})$ is mostly smooth, with a few local features. By adding in wavelets locally, one can develop efficient adaptive function representations that are suitable for simulation and visualization.

### 3.1.5 Analysis and Synthesis of Discrete Data

We now turn to the analysis of discrete data that is defined on a 3D mesh, such as the output or error produced by a finite element program. One can think of this as a problem in signal processing. However, standard signal processing techniques based on Fourier analysis lack the flexibility to handle signals sampled over geometry of complex shape. Surface wavelet representations provide a powerful tool for addressing this problem.

Wavelet analysis of a discrete signal can be performed using the discrete wavelet transform (DWT)[2] . This consists of a set of filtering and subsampling operations, which is typically iterated several times. Suppose that data is available on the $(j+1)^{th}$ resolution mesh and that it is denoted by $\lambda_{j+1,k}$. Then the DWT for the surface wavelet representation can be expressed as a highpass filtering and subsampling operation

$$\gamma_{j,m} = \lambda_{j+1,m} - \sum_{k \in N(j,m)} h^0_{j,k,m}\, \lambda_{j+1,k} \quad ; \quad m \in M(j) \tag{3.23}$$

which extracts detail information from the data by differencing, and a lowpass filtering and subsampling operation

[2]Also known as the Mallat pyramid algorithm.

$$\lambda_{j,k} = \lambda_{j+1,k} + \sum_{m \in a(j,k)} h^1_{j,k,m}\, \gamma_{j,m} \quad ; \quad k \in K(j) \tag{3.24}$$

which reduces the resolution of the data from level $j+1$ to level $j$ by effectively computing a local average. Here, subsampling is implied by the fact that the data is being mapped from a finer mesh to a coarser mesh. Note that the $\gamma_{j,m}$ coefficients must be computed first, since they are needed to compute the $\lambda_{j,k}$ coefficients. The filters $h^0_{j,k,m}$ and $h^1_{j,k,m}$ are the same filters that were used to construct the scaling functions and wavelets. In fact, Eq. (3.23) and (3.24) can be directly derived from Eq. (3.21) and (3.20) if $\lambda_{j,k}$ and $\gamma_{j,m}$ are defined as the inner products $\langle f(\vec{x}), \tilde{\phi}_{j,k}(\vec{x})\rangle$ and $\langle f(\vec{x}), \tilde{w}_{j,m}(\vec{x})\rangle$. The dual DWT can be similarly derived from Eq. (3.18) and (3.19).

One may iterate Eq. (3.23) and (3.24), starting with $j = n-1$, where $n$ denotes the finest resolution, and continuing until $j = 0$. The initial data, $\lambda_{n,k}$ $(k \in K(n))$, is the signal we wish to analyze, such as the output from a finite element program. The signal may already be in discrete form; if not, it can legitimately be sampled as $\lambda_{n,k} = f(\vec{x}_k)$ because of the interpolating property. After $n$ iterations, one has a complete set of wavelet coefficients

$$\{\lambda_{0,k}, \gamma_{j,m} | k \in K(0),\, m \in M(j),\, 0 \le j < n\}\,.$$

These coefficients can then be studied to identify features of interest in the signal. For example, a few large values of $\gamma_{j,m}$ in the same spatial proximity occurring over the complete range of scales, $0 \le j < n$, may indicate the presence of a sudden jump or some other discontinuity in the signal. One can similarly look for other features based on the space-scale distribution of the wavelet coefficients. This multiresolution signal processing capability will be exploited in Chapter 5 section to realize a class of high performance algorithms for modeling 3D problems.

It is now a simple matter to synthesis $\{\lambda_{j,k}\}$, and $\{\gamma_{j,m}\}$, where $(k \in K(j))$ and $m \in M(j)$, to obtain $\{\lambda_{j,k+1}\}$. By reversing equations 3.23 and 3.24 we obtain

$$\forall k \in K(j),\ \lambda_{j+1,k} = \lambda_{j,k} - \sum_{m \in a(j,k)} h^0_{j,k,m} \gamma_{j,m}, \tag{3.25}$$

$$\forall m \in M(j),\ \lambda_{j+1,m} = \gamma_{j,m} + \sum_{k \in N(j,m)} h^1_{j,k,m} \lambda_{j+1,k}. \tag{3.26}$$

## 3.2 Dual Wavelet Constructions and Basis Stability

We now deal with the construction of the dual wavelets and analyze the stability of the primary and dual spaces wavelet functions for a $S \subset R^3$. This dual wavelet construction is based on the idea of recursive wavelets by Donoho applied to the second generation setting [47]. It allows us to construct a dual wavelet basis at an arbitrary level of resolution $n$ and then solve for the wavelets. After a rescaling of the wavelets we then show that this basis is *stable* in some norm sense.

### 3.2.1 Dual Wavelet Construction

In this section we descibe a method to obtain the dual scaling fuctions. The first step is to calculate the filter coefficients $\{h_{j,k,l}, h_{j,m,l}, \tilde{h}_{j,k,l}, \tilde{h}_{j,k,m}\}$ by use the lifting scheme. This will give us the primary scaling functions, wavelets and all the filter coefficients. The second step is to obtain the *dual* scaling functions and wavelets. They are traditionally obtained by applying the *cascade* algorithm to the dual filter coefficients. However, in this section we follow a different approach based on the *recursive* wavelet idea by Donoho. An explicit expression for the dual scaling function may be obtained by fixing the highest level of resolution to an arbitrarily large $n$ and solving for $\tilde{\phi}_{n,k}(\vec{x})$ such that $\tilde{V}_n$ is biorthogonal to $V_n$. Once the dual space $\tilde{V}_n$ is obtained, the spaces $\tilde{W}_j$ and $\tilde{V}_j$ are automatically obtained for $j = 0...n-1$ from the refinement equations (3.20) - (3.21).

The first step is to use the lifting scheme to obtain the wavelet filters described. The filters will then satisfy the following conditions

$$\sum_{l\in K(j+1)} h^0_{j,k_1,l}\tilde{h}^0_{j,k_2,l} = \delta\left[k_1 - k_2\right] \qquad k_1, k_2 \in K(j)$$
$$\sum_{l\in K(j+1)} h^0_{j,k,l}\tilde{h}^1_{j,m,l} = 0$$
$$\sum_{l\in K(j+1)} h^1_{j,m_1,l}\tilde{h}^1_{j,m_2,l} = \delta\left[m_1 - m_2\right] \quad m_1, m_2 \in M(j)$$
$$\sum_{l\in K(j+1)} h^1_{j,k,l}\tilde{h}^0_{j,m,l} = 0,$$

where $h^0_{j,k,k} = 1$ $(k \in K(j))$, $h^1_{j,m,m} = 1$ $(m \in M(j))$,

$$\tilde{h}^0_{j,k,l} = \begin{cases} \delta_{k,l} & l \in K(j) \\ h^1_{j,k,m} & m \in M(j) \end{cases}, \text{ and } \quad \tilde{h}^1_{j,m,l} = \begin{cases} \delta_{m,l} & l \in M(j) \\ -h^0_{j,m,l} & l \in K(j) \end{cases}.$$

The second step is to obtain the dual scaling functions. These may be computed by the application of the *cascade* algorithm [44] (section 4.1.2). This would be the prefered way to go. However, since the mesh is inherently irregular, a convergence analysis of the *cascade algorithm* for the dual filters would be in general difficult to perform. Albeit, we do prove convergence, in Chapter 4, for the primary filters. We thus reply on an alternative construction method, which is discribed as follows:

For scaling functions in $V_n$, divide the support of the primary scaling function (Figure 3-4) into $Q^n_p$, $p = 1 \ldots q$, triangles. Define the dual scaling functions as piecewise linear polynomials over every single triangle $Q^n_p$. Thus $\tilde{\phi}_{n,k} = a_0^{k,p} + a_1^{k,p}x_1 + a_2^{k,p}x_2$whenever $(x_1, x_2) \in Q^n_p$. Given that the characteristic mesh size $h_n \neq 0$ and the following conditions

$$\int_{Q^p_k} \tilde{\phi}_{n,k}\phi_{n,k}dS = \tfrac{1}{q}, \forall p = 1...q$$
$$\int_{Q^p_k} \tilde{\phi}_{n,k}\phi_{n,l}dS = 0, \forall l \neq k$$

then we can uniquely solve for the coefficients $\left\{a_0^{k,p}, a_1^{k,p}, a_2^{k,p}\right\}$. Furthermore, $sup(\tilde{\phi}_{n,k}) \leq \frac{C}{h_n^2}$. We now have constructed a dual function space $\tilde{V}_n$ which is biorthogonal to $V_n$.

The next step is to apply the refinement and wavelet equations (3.20)-(3.21) to $\tilde{V}_n$ to obtain the dual spaces $\tilde{V}_j$ and $\tilde{W}_j$ for $j = 0 \ldots n-1$ (Notice that we assume that all these coefficients are bounded, which will be the case for the linear surface wavelets).

Although we may construct the dual scaling functions at any arbitrary position the downside of constructing the dual wavelets in this form is that as $n \to \infty$, the coarse level scaling functions in $V_0$ might not converge to a function in $L^2(S)$, possibly not even in a weak sense. This implies that as we go to higher resolutions the entire basis has to be recalculated. Moreover, it will make it difficult to numerically integrate functions with the dual scaling functions as $n$ is increased.

In practice, we may still use the recursive biorthogonal decomposition by either resorting to Galerkin formulations, thus avoiding the dual functions altogether, or employing the interpolating property of the primary spaces. These two approaches will be shown in Chapter 5.

### 3.2.2 Stability and Normalization of the Wavelet Basis

A wavelet basis is stable if the energy of the wavelet expansion coefficients is finite for finite energy functions. Let $f(\vec{x})$ be a function in $L^2(S)$ with the expansion

$$f(\vec{x}) = \sum_{k \in K(n_0)} \lambda_{n_0,k}\, \phi_{n_0,k}(\vec{x}) + \sum_{j=n_0}^{\infty} \sum_{m \in M(j)} \gamma_{j,m}\, \psi_{j,m}(\vec{x}) \tag{3.27}$$

Then the basis is said to be stable if it satisfies the Riesz criterion

$$A\|f(\vec{x})\|^2 \leq \sum_{k \in K(n_0)} (\lambda_{n_0,k})^2 + \sum_{j=n_0}^{\infty} \sum_{m \in M(j)} (\gamma_{j,m})^2 \leq B\|f(\vec{x})\|^2 \tag{3.28}$$

where $A$ and $B$ are constants, which are independent of $n_0$, with $B \geq A > 0$.

The normalization of the wavelet basis is an important consideration in satisfying the Riesz criterion. In the preceding sections, we assumed for convenience that the primary scaling functions, $\phi_{j,k}(\vec{x})$, were normalized to have a maximum height of unity. We note, however, that we are free to re-normalize the primary basis functions and the dual basis functions in a reciprocal fashion, without affecting the biorthog-

onality and vanishing moment conditions (see Section 3.1.2). The correct normalization for $\psi_{j,m}(\vec{x})$, for example, can be determined by considering the case where $f(\vec{x}) = \psi_{j,m}(\vec{x})$. Eq. (3.28) then gives

$$A\|\psi_{j,m}(\vec{x})\|^2 \leq 1 \leq B\|\psi_{j,m}(\vec{x})\|^2 \tag{3.29}$$

from which we obtain

$$\frac{1}{B} \leq \int_S \left|\psi_{j,m}(\vec{x})\right|^2 dS(\vec{x}) \leq \frac{1}{A} \tag{3.30}$$

A similar condition can be obtained for the scaling functions. To satisfy these conditions, we re-normalize $\phi_{j,k}(\vec{x})$ and $\psi_{j,m}(\vec{x})$ by a factor of $1/h_j$, where $h_j$ is the characteristic size of the $j$th resolution mesh. Correspondingly, the dual basis functions are normalized by a factor of $h_j$. We now have $\bar{\phi}_{j,k}(\vec{x})=\frac{\phi_{j,k}(\vec{x})}{h_j}$ and similarly $\bar{\tilde{\phi}}_{j,k}(\vec{x})=h_j\tilde{\phi}_{j,k}(\vec{x})$ where the characteristic mesh size is chosen such that, for every element $i$ at the $j$th resolution, the corresponding element size, $h_{j,i}$, satisfies the condition $C_1 h_j \leq h_{j,i} \leq C_2 h_j$ where $C_2 \geq C_1 > 0$. Under this rescaling the new filter coefficients satisfy the biorthogonal conditions

$$\begin{aligned}
&\sum_{l\in K(j+1)} \bar{h}^0_{j,k_1,l}\bar{\tilde{h}}^0_{j,k_2,l} = \delta\left[k_1 - k_2\right] \qquad k_1, k_2 \in K(j)\\
&\sum_{\in K(j+1)l} \bar{h}^0_{j,k,l}\bar{\tilde{h}}^1_{j,m,l} = 0\\
&\sum_{l\in K(j+1)} \bar{h}^1_{j,m_1,l}\bar{\tilde{h}}^1_{j,m_2,l} = \delta\left[m_1 - m_2\right] \quad m_1, m_2 \in M(j)\\
&\sum_{l\in K(j+1)} \bar{h}^1_{j,k,l}\bar{\tilde{h}}^0_{j,m,l} = 0,
\end{aligned}$$

In addition $\bar{\phi}_{j,k}, \bar{\tilde{\phi}}_{j,k} \in L^2(S)$ and

$$sup(\bar{\phi}_{j,k}) \sim \mathcal{O}\left(\frac{1}{h_j}\right), sup(\bar{\tilde{\phi}}_{j,k}) \sim \mathcal{O}\left(\frac{1}{h_j}\right)$$

for all $k$. Under this rescaling we analyze the behavior of the projection coefficients, for arbitrary $n$. More precisely, we show that if $f \in H^3_0(S)$, then the projection

coefficients onto the primary and dual spaces belong to $l_2$ i.e. the sum of the squares of the projection coefficients is bounded.

**Lemma 3.2.1** *Let $\vec{x} \in S$, $f \in H_0^3(S)$ and $\lambda_{n_0,k}$ be the projection coefficients of $f$ with respect to $\{\bar{\phi}_{n_0,k}\}$. Then $A\|f\|^2 \leq \sum(\lambda_{n_0,k})^2 \leq B\|f\|^2$ for arbitrary $n_0$, where $A/B < \infty$.*

*Proof* The upper bound may easily proved for all $n_0$ with the Schwartz inequality. Thus

$$\sum_k (\lambda_k^j)^2 = \sum_k (\int f(\vec{x})\bar{\bar{\phi}}_{j,k}(\vec{x})\, dS)^2$$

$$\sum_k (\lambda_k^j)^2 \leq \sum_k \int f(\vec{x})^2 dS \int \frac{1}{h_j^2}\, dS$$

$$\leq C \sum_k \int f(\vec{x})^2\, dS$$

$$\leq B\|f\|^2 .$$

Notice that B will depend on the overlap between the supports of the scaling functions, thus in practice it will be small. Now, for any finite $n_0$

$$A\|f\|^2 \leq \sum_{k \in K(n_0)} (\lambda_{n_0,k})^2.$$

However, more importantly, we analyze the behavior of the bounds as $n_0 \to \infty$. First notice that if $f \in H_0^3(S)$, then $f \in C_0^1(S)$, and $\sup|f| < \infty$. For sufficiently large $n_0$

$$\sum_k (\sum_l f(\vec{x}_l)\phi_{n_0,l}(\vec{x})\bar{\bar{\phi}}_{n_0,k}(\vec{x}))^2 \to \sum_k (\int f(\vec{x})\bar{\bar{\phi}}_{n_0,k}(\vec{x})\, dS)^2 = \sum_k (\lambda_k^j)^2$$

since $\sum_l f(\vec{x}_l)\phi_{n_0,l}(\vec{x}) \to f$ due to the interpolating property of $\bar{\phi}_{n_0,k}(\vec{x})$. Now, $\|f\|^2 \leq C\sum_k f(\vec{x}_k)^2 h_j^2$ for $C > 0$, then the result follows.

□

**Lemma 3.2.2** *Let $f \in H_0^3(S)$ and $\tilde{\lambda}_{n_0,k}$ be the projection coefficients of $f$ with respect to $\{\tilde{\bar{\phi}}_{n_0,k}\}$. Then $A\|f\|^2 \leq \sum (\tilde{\lambda}_{n_0,k})^2 \leq B\|f\|^2$ for sufficiently large $n_0$, where $A/B < \infty$.*

*Proof* The upper bound is proven by the Schwartz inequality argument. Now, for sufficiently large $n_0$

$$\sum_k (\int \sum_l f(\vec{x}_l)\bar{\phi}_{n_0,l}(\vec{x})\bar{\phi}_{n_0,k}(\vec{x})h_j\, dS)^2 \to \sum_k (\int f(\vec{x})\bar{\phi}_{n_0,k}(\vec{x})\, dS)^2 = \sum_k (\tilde{\lambda}_{j,n_0})^2$$

Now, since $C\|f\|^2 \leq \sum_k f(\vec{x}_k)^2 h_j^2$, $C \neq 0$, and

$$C_1 \sum_k (\int \sum_l f(\vec{x}_l)\bar{\phi}_{n_0,l}(\vec{x})\bar{\phi}_{n_0,k}(\vec{x})h_j\, dS)^2 \geq \sum_k f(\vec{x}_k)^2 h_j^2$$

then the result follows.

□

We may now derive stability properties of the basis.

**Theorem 3.2.1** *Suppose $f \in H_0^3(S)$ and let $\gamma_{j,m}$ be the projection coefficients of $f$ with respect to $\{\bar{\psi}_{n_0,m}\}$, then $A\|f\|^2 \leq \sum (\lambda_{n_0,k})^2 + \sum_{j=n_0}^{\infty} \sum_{m \in M(j)} (\gamma_{j,m})^2 \leq B\|f\|^2$, where $B/A < \infty$.*

*Proof* $f \in H_0^3(S)$ implies $f \in C_0^1(U)$. By a Taylor series expansion of $f \in C^1$ and vanishing moments of the wavelets

$$\sum_{j \geq n_0}^{\infty} \sum_{m \in M(j)} (\gamma_{j,m})^2 = \sum_{j \geq n_0}^{\infty} \sum_{m \in M(j)} (\int f(x)\tilde{\bar{\psi}}_{j,k}\, dS)^2 \leq C \sum_{j \geq n_0}^{\infty} \sum_{m \in M(j)} h_j^4 < \infty.$$

Notice that it is sufficient for the wavelet to vanish constant functions to satisfy the previous bound. Lemma 3.2.1 implies

$$\|f\|^2 \leq \sum_{k \in K(n_0)} (\lambda_{n_0,k})^2 + \sum_{j=n_0}^{\infty} \sum_{m \in M(j)} (\gamma_{j,m})^2 \leq B\|f\|^2.$$

□

**Theorem 3.2.2** *Suppose* $f \in H_0^3(S)$ *and let* $\tilde{\gamma}_{j,m}$ *be the projection coefficients of* $f$ *with respect to* $\{\bar{\tilde{\psi}}_{n_0,m}\}$, *for* $j = n...\infty$ *then* $A\|f\|^2 \leq \sum(\tilde{\lambda}_{n_0,k})^2 + \sum_{j=n}^{\infty}\sum_{m\in M(j)}(\tilde{\gamma}_{j,m})^2 \leq B\|f\|^2$, *where* $B/A < \infty$.

*Proof* Similar argument as for Theorem 3.2.1.

□

# Chapter 4

# Spatially Adaptive MultiWavelets

Second generation wavelets have been recently introduced by Sweldens [41]. First and second generation wavelets have the same properties of fast transform, localizability and decorrelation. However, second generation wavelets are characterized by a set of *spatial variant* filters that allows the construction of wavelets over unstructured grids. We shall first expand on the lifting theory from Chapter 3 to a more general setting and prove a construction theorem on a wide class of interpolating wavelet functions over irregular grids and finally provide some examples of these constructions.

## 4.1 Second Generation Wavelets and The Lifting Scheme

Most of the details of this section may be found in [41] and [42]. Suppose we have an initial mesh over some domain $S$ in $R^n$. Denote by $\vec{x}_{0,k}$ the vertex nodes, where $k = 1...N_0$ and $N_0$ is the number of initial vertices on the surface. Further refinements to the mesh may be applied by adding more vertices on $S$. Let $K(j)$ be the index set at each level $j$ of refinement. Let $X_j = \{\vec{x}_{j,k} \in S | k \in K(j)\}$ be the set of vertex values defined over the index set $K(j)$. The vertices are constrained such that $X_j \subset X_{j+1}$ an $\vec{x}_{j,k} = \vec{x}_{j+1,k}$. The index sets are also constrained such that $K_j \subset K_{j+1}$ and the difference between the index sets from one level to another is

given by $M(j) = K(j+1)/\ K(j)$. Furthermore, let $\{S_{j,v}\}$ be a partitioning of the domain $S$ at resolution level $j$ with index $v \in K(j)$.

Second generation biorthogonal wavelet subspaces are defined similarly to classical wavelets. Let $V_j \subset L^2(S)$ be a series of nested subspaces such that

**(a).** $V_j = \text{clos span}\{\phi_{j,k} | k \in K(j)\}$, where the basis elements $\phi_{j,k}$ form a *Riesz* basis.

**(b).** $V_j \subset V_{j+1}$.

**(c).** $\cup_{j=0}^{\infty} V_j$ is dense in $L^2(S)$.

**(d).** $V_{j+1} = V_j + W_j$, where $W_j = \text{clos span}\{\psi_{j,m} \mid m \in M(j)\}$.

Similarly, the *dual* subspaces $\tilde{V}_j \subset L^2(S)$, are defined as follows

**(e).** $\tilde{V}_j = \text{clos span}\{\tilde{\phi}_{j,k} | k \in K(j)\}$, where the basis elements $\tilde{\phi}_{j,k}$ forms a *Riesz* basis.

**(f).** $\tilde{V}_j \subset \tilde{V}_{j+1}$.

**(g).** $\cup_{j=0}^{\infty} \tilde{V}_j$ is dense in $L^2(S)$.

**(h).** $\tilde{V}_{j+1} = \tilde{V}_j + \tilde{W}_j$, where $\tilde{W}_j = \text{clos span}\{\tilde{\psi}_{j,m} \mid m \in M(j)\}$.

The subspaces $V_j, W_j, \tilde{V}_j$ and $\tilde{W}_j$ satisfy

$$V_j \perp \tilde{W}_j, W_j \perp \tilde{V}_j. \tag{4.1}$$

In addition, the basis functions $\phi_{j,k}, \tilde{\phi}_{j,k}, \psi_{j,m}$ and $\tilde{\psi}_{j,m}$ satisfy

$$\langle \phi_{j,k}, \tilde{\phi}_{j,l} \rangle = \delta_{k-l}, \quad \langle \psi_{j,m}, \tilde{\psi}_{j,l} \rangle = \delta_{m-l} \tag{4.2}$$

and the following *Refinement* equations

$$\begin{aligned} \phi_{j,k} &= \sum_{l \in K(j+1)} h^0_{j,k,l} \phi_{j+1,l}, \quad k \in K(j) \\ \tilde{\phi}_{j,k} &= \sum_{l \in K(j+1)} \tilde{h}^0_{j,k,l} \tilde{\phi}_{j+1,l}, \quad k \in K(j) \\ \psi_{j,m} &= \sum_{l \in K(j+1)} h^1_{j,m,l} \phi_{j+1,l}, \quad m \in M(j) \end{aligned} \tag{4.3}$$

$$\tilde{\psi}_{j,m} = \sum_{l \in K(j+1)} \tilde{h}^1_{j,m,l} \tilde{\phi}_{j+1,l}, \quad m \in M(j).$$

Notice that these equations are equivalent to the *scaling* and *wavelet* relations of first generation wavelets. The difference is that the filters are not shift invariant and scale invariant in general. We shall also use the operator notation introduced by Sweldens, where $\phi_j = H_j \phi_{j+1}$ means

$$\phi_{j,k} = \sum_{l \in K(j+1)} h^0_{j,k,l} \phi_{j+1,l},$$

and similarly for $\tilde{H}, G$ and $\tilde{G}$. Where, $\tilde{H}$ comes from $\tilde{h}^0_{j,k,l}$, $G$ from $h^1_{j,m,l}$ and $\tilde{G}$ from $\tilde{h}^1_{j,m,l}$.

The fast biorthogonal wavelet transform is given by

$$\begin{aligned} \lambda_{j,k} &= \sum_{l \in K(j+1)} \tilde{h}^0_{j,k,l} \lambda_{j+1,l} \\ \gamma_{j,m} &= \sum_{l \in K(j+1)} \tilde{h}^1_{j,m,l} \lambda_{j+1,l}, \end{aligned}$$

where $\lambda_{j,k} = \langle f, \tilde{\phi}_{j,k} \rangle$, $\gamma_{j,k} = \langle f, \tilde{\psi}_{j,k} \rangle$ and $f$ a function in $L^2(S)$. The inverse fast biorthogonal wavelet transform is given by

$$\lambda_{j+1,l} = \sum_{k \in K(j)} h^0_{j,k,l} \lambda_{j,k} + \sum_{m \in M(j)} h^1_{j,m,l} \gamma_{j,m}.$$

Second generation wavelets have the same properties as classical wavelets: fast transform, localizability, decorrelation and polynomial approximation, among others. In fact, classical wavelets are a subset of the larger class of second generation wavelets. However, second generation wavelets are constructed from the lifting scheme.

### 4.1.1 The Lifting Scheme

First generation wavelets are usually designed using the Fourier transform. However, due to the irregularity of unstructured grids, this transform is not adequate for the

design of second generation wavelets. The lifting scheme was built as a tool for the design of second generation wavelets [41].

Suppose we have a biorthogonal set of wavelet filters $\{h^{0,old}_{j,k,l}, h^{1,old}_{j,m,l}, \tilde{h}^{0,old}_{j,k,l}, \tilde{h}^{1,old}_{j,m,l}\}$ and corresponding scaling and wavelet functions $\{\phi^{old}_{j,k}, \psi^{old}_{j,m}, \tilde{\phi}^{old}_{j,k}, \tilde{\psi}^{old}_{j,m}\}$. A new set of filters $\{h^0_{j,k,l}, h^1_{j,m,l}, \tilde{h}^0_{j,k,l}, \tilde{h}^1_{j,m,l}\}$ may be readily lifted (constructed)

$$\begin{aligned} h^0_{j,k,l} &= h^{0,old}_{j,k,l}, \qquad & h^1_{j,m,l} &= h^{1,old}_{j,m,l} - \sum_{k\in K(j)} s_{j,k,m} h^0_{j,k,l} \\ \tilde{h}^1_{j,m,l} &= \tilde{h}^{1,old}_{j,m,l}, \qquad & \tilde{h}^0_{j,k,l} &= \tilde{h}^{0,old}_{j,k,l} + \sum_{m\in M(j)} s_{j,k,m} \tilde{h}^1_{j,m,l}, \end{aligned} \tag{4.4}$$

which are biorthogonal for any choice $s_{j,k,m}$ [41]. The refinement and wavelet equations now take the form

$$\begin{aligned} \phi_{j,l} &= \phi^{old}_{j,l}, & \psi_{j,m} &= \sum_{l\in K(j+1)} h^{1,old}_{j,m,l} \phi_{j+1,l} - \sum_{k\in K(j)} s_{j,k,m} \phi_{j,k} \\ \tilde{\psi}_{j,l} &= \sum_{l\in K(j+1)} \tilde{h}^{1,old}_{j,m,l} \tilde{\phi}_{j+1,l}, & \tilde{\phi}_{j,k} &= \sum_{l\in K(j+1)} \tilde{h}^{0,old}_{j,k,l} \tilde{\phi}_{j+1,l} + \sum_{m\in M(j)} s_{j,k,m} \tilde{\psi}_{j,m}. \end{aligned} \tag{4.5}$$

A large class of wavelets may be designed by use of the lifting scheme. The procedure is to start from a simple wavelet and then "lift" it. The variables $s_{j,k,m}$ may be chosen to satisfy desired criteria e.g. vanishing moments. After lifting, the wavelet transform may be written as a two step procedure:

$$\begin{aligned} \gamma_{j,m} &= \sum_{l\in K(j+1)} \tilde{h}^{1,old}_{j,m,l} \lambda_{j+1,l}, \quad \forall m \in M(j) \\ \lambda_{j,k} &= \sum_{l\in K(j+1)} \tilde{h}^{0,old}_{j,k,l} \lambda_{j+1,l} + \sum_{m\in M(j)} s_{j,k,m} \gamma_{j,m}, \quad \forall k \in K(j). \end{aligned}$$

Note that there is an equivalent notion of lifting for the dual wavelet. We simply interchange the duals with the primals and apply the lifting procedure.

In this section, second generation wavelets have been introduced in its most general form. We shall now concentrate on the class of interpolating wavelets.

### 4.1.2 Interpolating Wavelets

An interpolating function $\phi_{j,k}$, satisfies the following condition

$$\phi_{j,k}(\vec{x}_{j,k'}) = \delta_{k-k'}, \forall k, k' \in K(j).$$

Define $n(j,k)$ and $N(j,m)$ as local neighborhoods to the indices $k$ and $m$ respectively as follows:

- $n(j,k) \subset M(j)$ is the set of indices of the new values $\lambda_{j+1,m}$ $(m \in n(j,k))$ that are formed by the old value $\lambda_{j,k}$.
- $N(j,m) \subset K(j)$, is the set of indices of the old values $\lambda_{j,k}$ $(k \in N(j,m))$ that are used in the construction of a new value $\lambda_{j+1,m}$.

Notice that $n(j,k)$ and $N(j,m)$ are related as $n(j,k) = \{m \,|\, k \in N(j,m)\}$. The linear operator $H_j$ and its adjoint $H_j^*$ may now be written as $H_j : n(j,k) \to k$ and $H_j^* : N(j,m) \to m$. Define the sequences $\vec{\lambda}_j = \{\lambda_{j,k} \,|\, k \in K(j)\}$. The subdivision scheme now takes the form

$$\lambda_{j+1,m} = \sum_{k \in N(j,m)} h^0_{j,k,m} \lambda_{j,k}, \tag{4.6}$$

or in operator notation

$$\vec{\lambda}_{j+1} = H_j^* \vec{\lambda}_j$$

with an initial condition of $\lambda_{j_0,k_0} = 1$ for $k_0 = k$ and $\lambda_{j_0,k_0} = 0$ for $k_0 \neq k$, where $k, k_0 \in K(j_0)$. Define

$$f^{(j)}_{j_0,k_0} = \sum_{k \in \mathcal{K}(j)} \lambda_{j,k} \chi_{S_{j,k}},$$

taking (4.6) ad infinitum, and assuming the algorithm converges, we obtain

$$\lim_{j \to \infty} f^{(j)}_{j_0,k_0} = \phi_{j_0,k_0} \quad j \geq j_0, \tag{4.7}$$

which is interpolating. The previous scheme is also known as the *cascade algorithm.* Assuming that (4.7) converges for all $j_0$ and $k_0$, then $\phi_{j_0,k_0}$ satisfies the following refinement equation

$$\phi_{j,k} = \sum_{l \in K(j+1)} h_{j,k,l}\phi_{j+1,l} = \phi_{j+1,k} + \sum_{m \in n(j,k)} h_{j,k,m}\phi_{j+1,m}, \ \forall j \text{ and } \forall k \in K(j)$$

We now turn our attention to the wavelet construction. At every single node $m \in M(j)$, choose $\psi^{old}_{j,m} = \phi_{j+1,m}$. We now define the local neighborhoods $A(j,m)$ and $a(j,k)$ such that

- $A(j,m) \subset K(j)$, is the set of indices of the scaling functions at level $j+1$ that $\psi_{j,m}$ will depend upon.
- $a(j,k) \subset M(j)$, is equal to $\{m \mid k \in A(j,m)\}$.

By applying the lifting scheme, we "lift" the old wavelet with scaling functions at the resolution level $j+1$. The new wavelet now takes the form

$$\psi_{j,m} = \phi_{j+1,m} - \sum_{k \in A(j,m)} s_{j,k,m}\phi_{j,k},$$

where, in general, $A(j,m)$ is some finite set neighborhood. This implies that the wavelet will have compact support. The variables $s_{j,k,m}$ may be chosen such that the new wavelets meet with desired performance criteria.

The next step is to look at the duals. As for the primary case, the *cascade* algorithm also applies to the dual scaling function filters. However, we iterate over the filters $\tilde{h}^0_{j,k,l}$. In this case, if the cascade algoithm converges then

$$\tilde{\phi}_{j,k} = \sum_{l \in K(j+1)} \tilde{h}^0_{j,k,l}\tilde{\phi}_{j+1,l} = \tilde{\phi}_{j+1,k} + \sum_{m \in a(j,k)} s_{j,k,m}\tilde{\psi}_{j,m},$$

and the wavelet equation is equal to

$$\tilde{\psi}_{j,m} = \tilde{\phi}_{j+1.m} - \sum_{k \in N(j,m)} h^0_{j,k,m} \tilde{\phi}_{j+1,k}.$$

From the primary and dual refinement and wavelet equations, the wavelet transform and its inverse, may be computed as a two step procedure [42, 43]:

*Analysis*

$$\begin{aligned} \forall m \in M(j), \ \gamma_{j,m} &= \lambda_{j+1,m} - \sum_{k \in N(j,m)} h^0_{j,k,m} \lambda_{j+1,k}. \\ \forall k \in K(j), \ \lambda_{j,k} &= \lambda_{j+1,k} + \sum_{m \in a(j,k)} s_{j,k,m} \gamma_{j,m}. \end{aligned}$$

*Synthesis*

$$\begin{aligned} \forall k \in K(j), \ \lambda_{j+1,k} &= \lambda_{j,k} - \sum_{m \in a(j,k)} s_{j,k,m} \gamma_{j,m}, \\ \forall m \in M(j), \ \lambda_{j+1,m} &= \gamma_{j,m} + \sum_{k \in N(j,m)} h^0_{j,k,m} \lambda_{j+1,k}. \end{aligned}$$

See section 12 in [41] for more details.

## 4.2 Construction of Interpolating Wavelets over Unstructured Grids

In this section we build interpolating scaling functions that may represent a set of linearly independent functions. If these functions are chosen to be polynomials, then we obtain multiresolution finite elements [49]. However, the main difference is that we also construct the wavelets which bridge across the different multiresolution scales.

For many numerical applications it is useful to have an analytical form for the scaling function. This may be achieved if we restrict all interpolated values at the nodes $\vec{x}_{j,m}$ over some partition (surface element) $S_{j,v}$ to lie on $\sum_{i=0}^{M-1} a_i P_i(x)$ for some unique set of coefficients $\{a_0, a_1, \ldots, a_{M-1}\}$ where $\{P_i(x)\}$ is a set of linearly

independent functions.

We shall first show that the cascade algorithm, for the primary scaling functions, converges for a class of interpolating scaling functions.

**Lemma 4.2.1** *Suppose that* $\{P_0, P_1, \ldots, P_{M-1}\}$ *forms a set of continous, bounded linearly independent functions over* $S_{j,v}$. *If* $y(\vec{x}) = \sum_{i=0}^{M-1} a_i P_i(\vec{x})$ *for some unique set of coefficients* $\{a_0, a_1, \ldots, a_{M-1}\}$ *then there exists a set of coefficients* $\tilde{s}_{j,k,m} (k \in N(j,m))$ *such that*

$$y(\vec{x}_{j,m}) \equiv \sum_{k \in N(j,m)} \tilde{s}_{j,k,m} y(\vec{x}_{j,k}), \ \ \forall m \in \mathcal{M}(j).$$

*Proof* Starting from the lazy wavelet [43]( $\tilde{\phi}_{j,k}^{old} = \delta(\vec{x} - \vec{x}_{j,k})$ and $\tilde{\psi}_{j,m}^{old} = \delta(\vec{x} - \vec{x}_{j,m})$) and lifting the dual wavelet, so that $\int_S P_i(\vec{x}) \ \tilde{\psi}_{j,m}(\vec{x}) \ dS = 0$ for all $i = 0 \ldots M-1$, we obtain

$$\int_S P_i(\vec{x}) \ \tilde{\psi}_{j,m}^{old}(\vec{x}) \ dS = \sum_{k \in N(j,m)} \tilde{s}_{j,k,m} \int_S P_i(\vec{x}) \ \tilde{\phi}_{j,k}^{old}(\vec{x}) \ dS,$$

for all $\{P_0, P_1, \ldots, P_{M-1}\}$, where $N(j,m) = \{k_0, k_1, \ldots, k_{M-1}\}$. This can be written in matrix form

$$\begin{bmatrix} P_0(\vec{x}_{j,m}) \\ P_1(\vec{x}_{j,m}) \\ \vdots \\ P_{M-1}(\vec{x}_{j,m}) \end{bmatrix} = \begin{bmatrix} P_0(\vec{x}_{j,k_0}) & P_0(\vec{x}_{j,k_1}) & \ldots & P_0(\vec{x}_{j,k_{M-1}}) \\ P_1(\vec{x}_{j,k_0}) & P_1(\vec{x}_{j,k_1}) & \ldots & P_1(\vec{x}_{j,k_{M-1}}) \\ \vdots & \vdots & \ddots & \vdots \\ P_{M-1}(\vec{x}_{j,k_0}) & P_{M-1}(\vec{x}_{j,k_1}) & \ldots & P_{M-1}(\vec{x}_{j,k_{M-1}}) \end{bmatrix} \begin{bmatrix} \tilde{s}_{j,k_0,m} \\ \tilde{s}_{j,k_1,m} \\ \vdots \\ s_{j,k_{M-1},m} \end{bmatrix}$$

The result follows. (Note that in the case of polynomials, this matrix is a Vandermode matrix which is always invertible.)

□

Thus any new nodal quantities formed by the family of filters $\tilde{S}_j^*$ lie on some space of linearly independent functions. We use this fact to prove the convergence of the cascade algorithm.

For many numerical applications it is useful to have an analytical form of the scaling function. This may be achieved if we restrict all interpolated nodes $\vec{x}_{j,m}$ over some partition $S_{j,v}$ to lie on $\sum_{i=0}^{M-1} a_i P_i(x)$ for some unique set of coefficients $\{a_0, a_1, \ldots, a_{M-1}\}$.

**Theorem 4.2.1** *Suppose that for all the nodes $\vec{x}_{z,m}$ in $S_{j,v}$, $z > j$, all the neighboring nodes $\vec{x}_{z,k}$, such that $k \in N(z,m)$, are contained in $S_{j,v}$. Further assume that the number of elements of $N(z,m)$ is equal to some positive integer $M$ and the collection of nodes $\{\vec{x}_{j,k}\}$ in $S_{j,v}$ forms a dense subset in $S_{j,v}$. Then there exists an interpolating scaling function, which is given by*

$$\phi_{j,k}(\vec{x}) = \sum_{i=0}^{M-1} a_i P_i(\vec{x}) \quad a.e.$$

*over $S_{j,v}$ for some set of unique coefficients $\{a_0, a_1, \ldots, a_{M-1}\}$, such that*

$$\sum_{i=0}^{M-1} a_i P_i(\vec{x}_{j,k'}) = \begin{cases} 1 & k' = k \\ 0 & k' \neq k \end{cases} \qquad k' \in \mathcal{K}(j).$$

*In addition*

$$\int_S P_i(\vec{x}) \tilde{\psi}_{j,k}(\vec{x})\, dS(\vec{x}) = 0.$$

*Moreover, the support of $\phi_{j,k}$ is equal to union of all the neighboring partitions of the node $k$.*

*Proof* It is sufficient to analyze the convergence properties of the cascade algorithm, i.e. the sequence

$$H^*_{j+i} H^*_{j+i-1} H^*_{j+i-2} \ldots H^*_j \delta_k$$

as $i \to \infty$, where

$$h^0_{j,k,l} = \begin{cases} \delta_{k-l} & l \in \mathcal{K}(j) \\ \tilde{s}_{j,k,l} & l \in n(j,k) \end{cases}.$$

Suppose that $\lambda_{z,k'} = y(\vec{x}_{z,k'})$, $k' \in N(z,m)$, and $\vec{\lambda}_z = \{\lambda_{z,k'} \mid k' \in K(z)\}$. By Lemma (4.2.1) $\vec{\lambda}_{z+1} = H_z^* \vec{\lambda}_z$ satisfies $\lambda_{z+1,m} = y(\vec{x}_{z,m})$. Now, let $\lambda_{j,k} = \delta_k$ and choose $\{a_0, a_1, \ldots, a_{M-1}\}$ such that

$$y(\vec{x}_{j,k''}) = \begin{cases} 1 & k'' = k \\ 0 & k'' \neq k \end{cases},$$

for $k'' \in K(j)$. The result follows.

□

The coefficients of the refinement equation are given by

$$h^0_{j,k,l} = \begin{cases} \delta_{k-l} & l \in \mathcal{K}(j) \\ \sum_{i=0}^{M-1} a_i P_i(\vec{x}_{j,l}) & l \in n(j,k), \vec{x}_{j,l} \in S_{j,v} \end{cases}.$$

With Theorem 4.2.1 we may construct interpolating scaling functions that represent polynomials over the domain $S$. Moreover, the domain $S$ does not have to be connected since the scaling functions are constructed directly over the partition $S_{j,k}$.

Suppose we restrict $S = R$, partition the real line into $S_{j,k} = (2^{-j}(k-1), 2^{-j}k)$ and let $P_0(x) = 1, P_1(x) = x$ and $P_2(x) = x^2$. By Theorem (4.2.1), all scaling functions $\phi_{j,k}$ are equal to a polynomial $a_0 + a_1 x + a_2 x^2$ over the segment $S_{j,v}$. In Figure 4-1 a) and b) the scaling functions over the nodes 0 and 1 are shown. Notice that we have two different forms of scaling functions at the even and odd nodes. The shift invariance property of classical wavelets is no longer satisfied. However, scaling functions at any resolution level can be constructed from scaling functions at a finer level,from the refinement equation, as shown in Figure 4-2.

The scaling functions constructed in Figure 4-1 are an example of a Multiwavelet representation. Since we have two basic shapes of the scaling function we separate them in even and odd components. Let $\phi_{even} = \phi_{0,2i}$ and $\phi_{odd} = \phi_{0,2i+1}$ for all $i$, where $i$ is an integer. It is simple to see that the two scaling functions satisfy

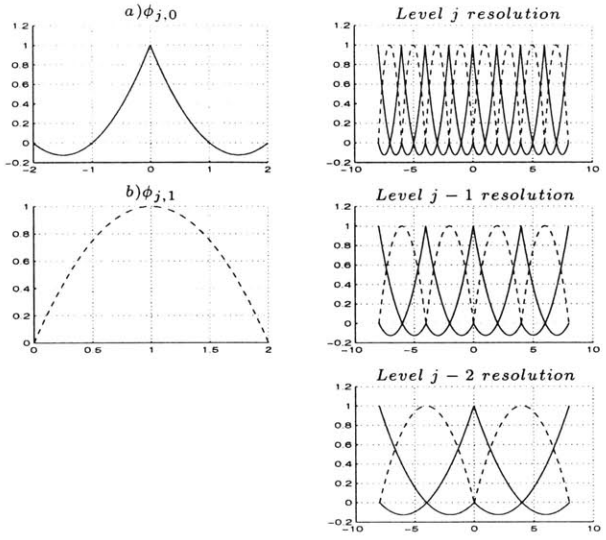


Figure 4-1: Quadratic interpolating scaling functions over the real line at different scales of resolution.

$$\begin{bmatrix} \phi_{even}(x) \\ \phi_{odd}(x) \end{bmatrix} = \begin{bmatrix} 1 & 3/8 \\ 0 & 3/4 \end{bmatrix} \begin{bmatrix} \phi_{even}(2x) \\ \phi_{odd}(2x) \end{bmatrix} + \begin{bmatrix} 0 & -1/8 \\ 1 & 3/4 \end{bmatrix} \begin{bmatrix} \phi_{even}(2x-4) \\ \phi_{odd}(2x-4) \end{bmatrix}$$
$$+ \begin{bmatrix} 1 & 3/8 \\ 0 & 0 \end{bmatrix} \begin{bmatrix} \phi_{even}(2x+4) \\ \phi_{odd}(2x+4) \end{bmatrix} + \begin{bmatrix} 1 & -1/8 \\ 0 & 0 \end{bmatrix} \begin{bmatrix} \phi_{even}(2x+8) \\ \phi_{odd}(2x+8) \end{bmatrix}.$$

The next step is to construct vanishing moments on the wavelet. This condition is satisfied by forcing

$$\int P_i(\vec{x})\psi_{j,m}(\vec{x})\ dS = 0.$$

With the use of the lifting scheme this condition reduces to solving the coefficients $s_{j,k,m}$ such that

$$\int P_i(\vec{x})\phi_{j+1,m}(\vec{x})\ dS = \sum_{k \in A(j,m)} s_{j,k,m} \int P_i(\vec{x})\phi_{j,k}(\vec{x})\ dS. \tag{4.8}$$

This completes the construction of the primal basis. Note that we may construct the dual scaling functions with the same procedure described in Chapter 3. However, we

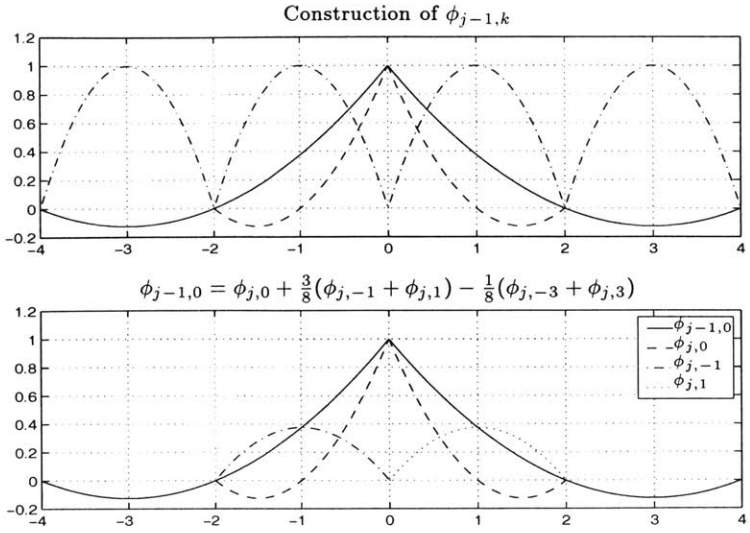


Figure 4-2: The function $\phi_{j,k}$ may be easily reconstructed from scaling functions from a finer level of resolution. In this example, the refinement equation $\phi_{j-1,0} = \phi_{j,0} + \frac{3}{8}(\phi_{j,-1} + \phi_{j,1}) - \frac{1}{8}(\phi_{j,-3} + \phi_{j,3})$ is satisfied. The filter coefficients are determined by the values of $\phi_{j-1,0}$ at $x = +/-1$ and $x = +/-3$.

leave the stability analysis as future work.

### 4.2.1 Basis Properties

**Theorem 4.2.2** *The basis elements of* $V_j + \sum_{i=j}^{n-1} W_i$ *form a linearly independent set.*

*Proof* Choose an element $v \in V_n$. Due to the interpolating property of $\{\phi_{n,k}\}$, there exists a unique set of coefficients $\{s_i\}$ such that $v = \sum_k s_k \phi_{n,k}$. Now, let

$$Y = \begin{bmatrix} H_{j-n}H_{j-n-1}\ldots H_{j-1} \\ G_{j-n}H_{j-n-1}\ldots H_{j-1} \\ \vdots \\ G_{j-2}H_{j-1} \\ G_{j-1} \end{bmatrix}$$

and apply this matrix to every single basis element in $V_n$. Thus, any element of $V_j + \sum_{i=j}^{n-1} W_i$ is a linear combination of basis elements of $V_n$. Linear independence

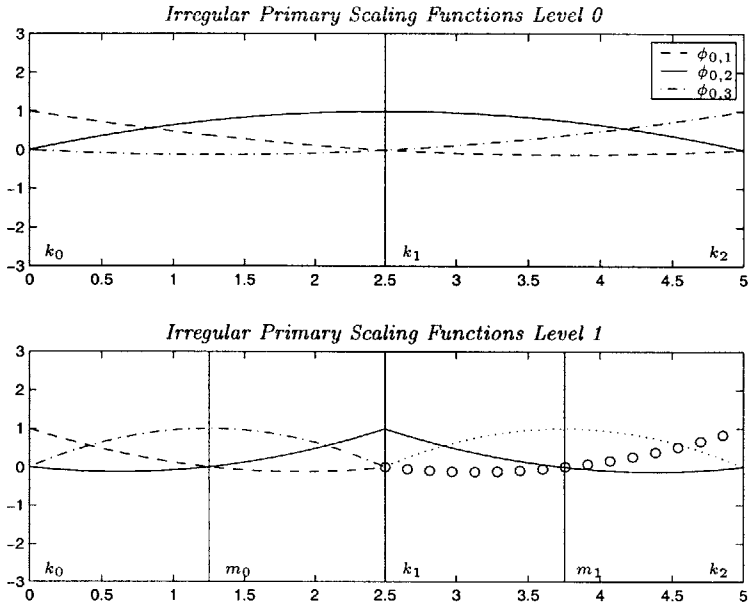


Figure 4-3: Scaling functions at level 0 and 1 over the finite interval S=[0, 5]. The scaling functions $\{\phi_{0,1}, \phi_{0,2}, \phi_{0,3}\}$ are located at the nodes $\{k_0, k_1, k_2\}$ respectively and $\{\phi_{1,1}, \ldots, \phi_{1,5}\}$ at $\mathcal{K}(0) = \{k_0, k_1, k_2, m_0, m_1\}$.

follows from the full rank property of Y.

□

**Corollary 4.2.1** *The basis elements of* $\tilde{V}_j + \sum_{i=j}^{n-1} \tilde{W}_i$ *form a linearly independent set.*

*Proof* The proof follows from the biorthogonal relation between the basis elements of $V_n$ and $\tilde{V}_n$. □

### 4.2.2 Construction of 1-D Wavelets

We may now construct scaling functions and wavelets over more complex geometries. Suppose that S= [0, 5], $P_0 = 1, P_1 = x$, $P_2 = x^2$. We group the nodes at level 0 and 1 as $\mathcal{K}(0) = \{k_0, k_1, k_2\}$, $\mathcal{M}(0) = \{m_0, m_1\}$ with $\mathcal{K}(1) = \mathcal{K}(0) \cup \mathcal{M}(0) = \{k_0, k_1, k_2, m_0, m_1\}$ , as shown in Figure 4-3. As in the previous example we construct piecewise quadratic scaling functions, however, in this case, we have a finite domain. Theorem 4.2.1 allows the construction of scaling functions adapted to the local domain, thus

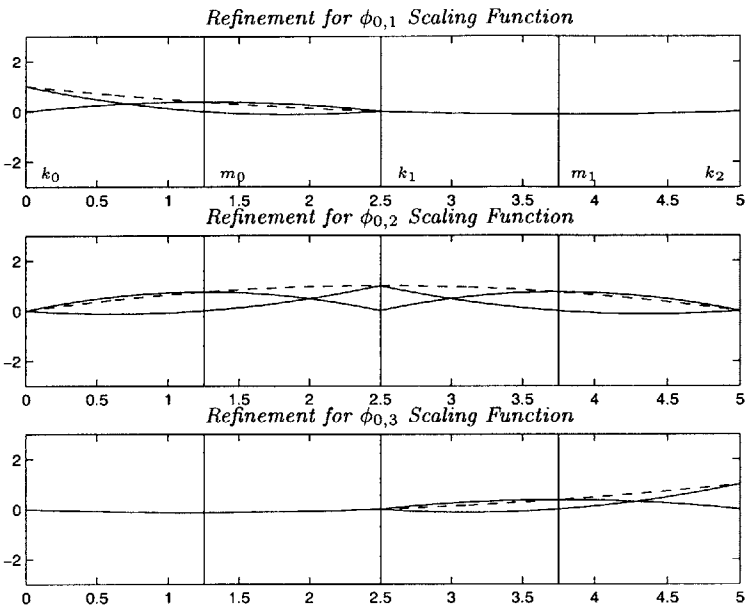


Figure 4-4: In this figure we construct all linear scaling functions $\{k_0, k_1, k_2\}$ at level 0 from linear combinations of scaling functions at level 1.

the boundary scaling functions $\phi_{0,1}$ and $\phi_{0,3}$ are inherently different from the middle scaling function $\phi_{0,1}$, However, the refinement equation is still satisfied. Figure 4-4 shows the relation of the scaling functions at level 0 and 1. All three scaling functions $\phi_{0,1}, \phi_{0,2}$ and $\phi_{0,3}$ are constructed from a linear combination of $\phi_{1,1}, \ldots, \phi_{1,5}$.

With the lifting scheme we may now build the two wavelets located at the nodes $\{m_0, m_1\}$ as shown in Figure 4-5. In this case we impose vanishing moments up to quadratics. As a check, we integrate the wavelets against polynomials $\{1, x, x^2\}$, indeed confirming the vanishing moment property of the wavelet. This will be significant for computational modeling problems, where the number of vanishing moments is directly related to the rates of decay of the coefficients of the stiffness matrix, which leads to a sparse system representation. This will investigated further in chapters 5 and 6.

We now demonstrate the adaptability of the wavelet constructions. If the nodes at level $\mathcal{K}(0)$ and $\mathcal{M}(0)$ are shifted, the adaptive property of Theorem 4.2.1 still allows the reconstruction of wavelets and scaling functions. However, as seen in Figures

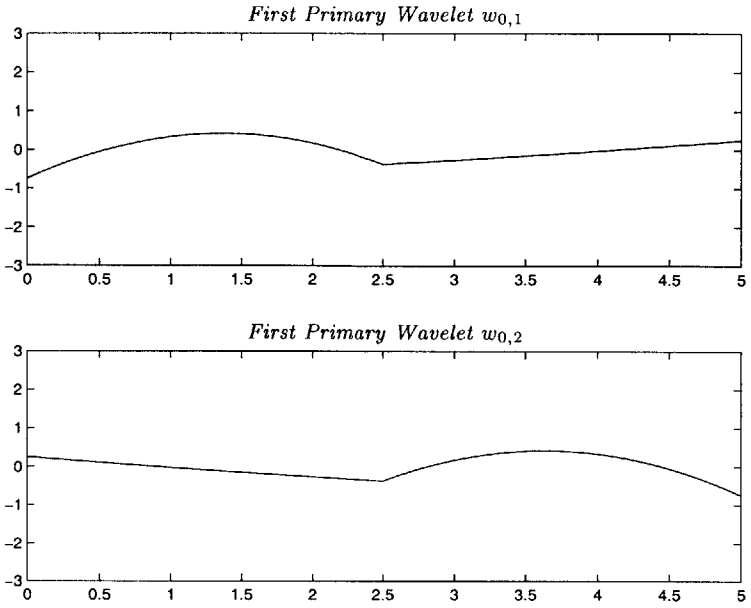


Figure 4-5: Wavelets located at the nodes $m_0$ and $m_1$. The two wavelets satisfy the vanishing moment condition up to quadratics.

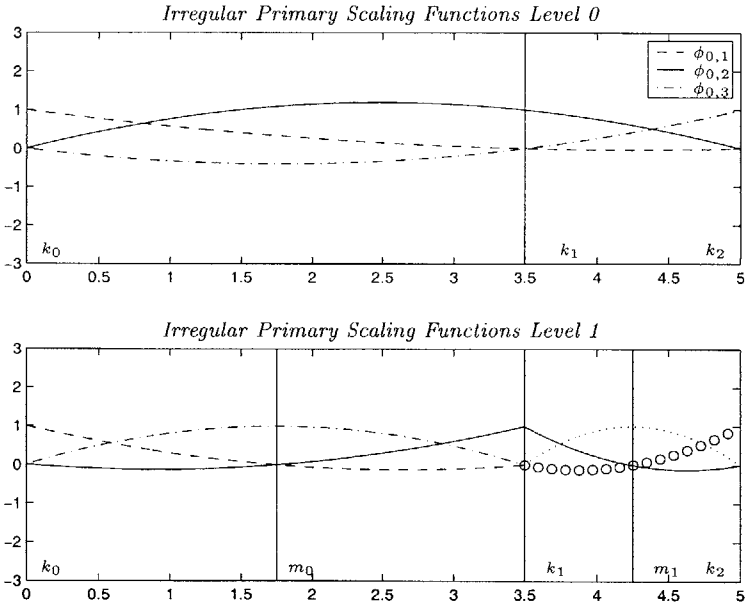


Figure 4-6: Scaling functions at level 0 and 1. In this example the nodes $\{k_1, m_0, m_1\}$ are shifted, breaking the regularity of the scaling functions at level 0. As shown, the new scaling functions depend on the local properties of the domain.

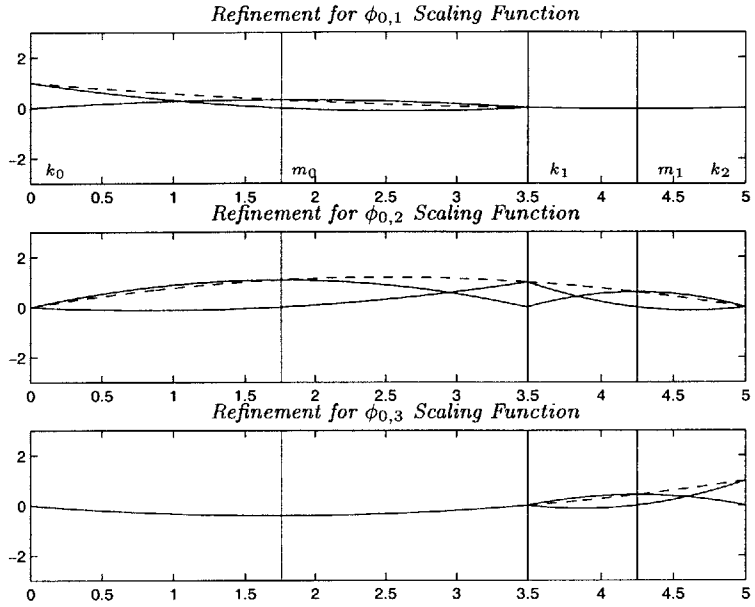


Figure 4-7: After the nodes $\{k_1, m_0, m_1\}$ are shifted, the refinement equation is still satisfied.

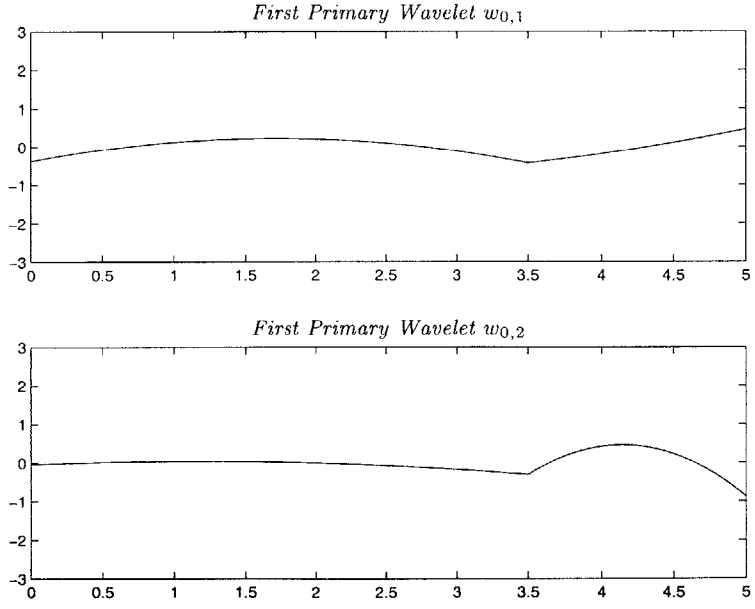


Figure 4-8: Wavelets created at the shifted nodes $\{m_0, m_1\}$. The vanishing moment of the wavelets is still satisfied.

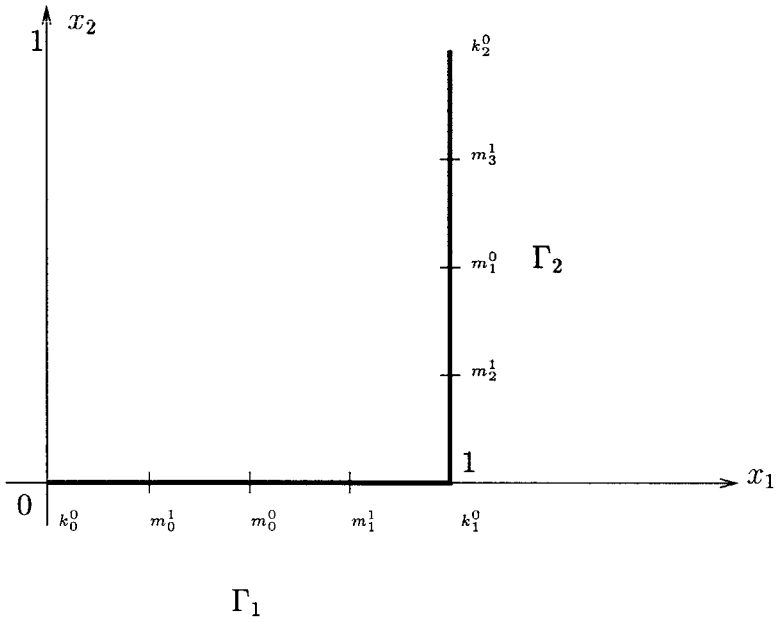


Figure 4-9: Wavelet construction around corners. $\mathcal{K}(0) = \{k_0^0, k_1^0, k_2^0\}$, $\mathcal{M}(0) = \{m_0^0, m_1^0\}$, $\mathcal{M}(1) = \{m_0^1, m_1^1, m_2^1, m_3^1\}$

4-6, 4-7 and Figures 4-8, the refinement equation for the scaling functions and the vanishing moment property for the wavelet are still satisfied.

### 4.2.3 2D constructions with corners

We may now extend scaling functions built in 1-D to curvilinear domains in $R^2$. One solution might be to map scaling functions and wavelets from $R^1$ to $R^2$. However, when 1D wavelets with $M$ vanishing moments are mapped onto a curve in $R^2$, one cannot expect to obtain the $M^{th}$ order of vanishing moments with respect to the global 2D cartesian coordinates. We may mitigate this problem by restricting the domain to be smooth, but in many practical computational problems we have to deal with corners. The solution is to construct wavelets on the curve but impose vanishing moments in the global 2D coordinates.

Divide the domain $S \subset R^2$ into two intervals $\Gamma_1$ and $\Gamma_2$ with a corner at $k_1^0$, as shown in Figure 4-9. Further choose $P_0 = 1$, $P_1 = x_1$, and $P_2 = x_2$, where $(x_1, x_2) \in S$. Now, the neighborhood set $N(j, m)$ depends on the location of the

node. Around the corner we need to lift three dual scaling functions to kill three moments $\{1, x_1, x_2\}$, thus $N(0, m_0^0) = N(0, m_1^0) = \{k_0^0, k_1^0, k_2^0\}$. Similarly for $m_1^1$ and $m_2^1$, $N(1, m_1^1) = N(1, m_2^1) = \{m_0^0, k_1^0, m_1^0\}$. However, for $m_0^1$ and $m_3^1$ only two moments ($\{1, x_1\}$ or $\{1, x_2\}$) need to vanish, thus $N(1, m_0^1) = \{k_0^0, m_0^0\}$ and $N(1, m_3^1) = \{k_2^0, m_1^0\}$. Following the same pattern ad infinitum we have for the scaling functions at level 0

$$\begin{aligned}
\phi_{0,k_0^0} &= 1 - x_1 \quad && \text{on } \Gamma_1, \\
\phi_{0,k_0^0} &= 0 && \text{on } \Gamma_2, \\
\phi_{0,k_1^0} &= x_1 - x_2 && \text{on } \Gamma_1, \\
\phi_{0,k_1^0} &= x_1 - x_2 && \text{on } \Gamma_2, \\
\phi_{0,k_2^0} &= 0 && \text{on } \Gamma_1, \\
\phi_{0,k_2^0} &= x_2 && \text{on } \Gamma_2.
\end{aligned}$$

The refinement equation coefficients are given by

$$\begin{aligned}
h_{0,k_0^0,m_0^0} &= \tfrac{1}{2}, \quad h_{0,k_0^0,m_1^0} = 0, \quad h_{0,k_1^0,m_0^0} = \tfrac{1}{2}, \\
h_{0,k_1^0,m_1^0} &= \tfrac{1}{2}, \quad h_{0,k_2^0,m_0^0} = 0, \quad h_{0,k_2^0,m_1^0} = \tfrac{1}{2}.
\end{aligned}$$

The refinement equations are of the form

$$\begin{aligned}
\phi_{0,k_0^0} &= \phi_{1,k_0^0} + \frac{1}{2}\phi_{1,m_0^0} \\
\phi_{0,k_1^0} &= \phi_{1,k_1^0} + \frac{1}{2}\phi_{1,m_0^0} + \frac{1}{2}\phi_{1,m_1^0} \\
\phi_{0,k_2^0} &= \phi_{1,k_2^0} + \frac{1}{2}\phi_{1,m_1^0}.
\end{aligned}$$

The dual wavelets at level 0 are

$$\begin{aligned}
\tilde{\psi}_{0,m_0^0} &= \tilde{\phi}_{1,m_0^0} - \frac{1}{2}\tilde{\phi}_{1,k_0^0} - \frac{1}{2}\tilde{\phi}_{1,k_1^0} \\
\tilde{\psi}_{0,m_1^0} &= \tilde{\phi}_{1,m_1^0} - \frac{1}{2}\tilde{\phi}_{1,k_1^0} - \frac{1}{2}\tilde{\phi}_{1,k_2^0},
\end{aligned} \tag{4.9}$$

It is not hard to show that the dual wavelets at level 0 vanish moments in $\{1, x_1, x_2\}$. For example:

$$\int_S x_1 \tilde{\psi}_{0,m_0^0} = \int_S (\phi_{0,k_1^0} + \phi_{0,k_2^0})(\tilde{\phi}_{1,m_0^0} - \frac{1}{2}\tilde{\phi}_{1,k_0^0} - \frac{1}{2}\tilde{\phi}_{1,k_1^0}) = 0.$$

The next step is to construct primary wavelets at level 0 which vanish moments across the corner. We impose the condition $A(j,m) = N(j,m)$, thus

$$\begin{bmatrix} \int_S P_0 \psi^{old}_{j,m_0^0}(\vec{x}) \\ \int_S P_1 \psi^{old}_{j,m_0^0}(\vec{x}) \\ \int_S P_2 \psi^{old}_{j,m_0^0}(\vec{x}) \end{bmatrix} = \begin{bmatrix} \int_S P_0 \phi_{j,k_0^0} & \int_S P_0 \phi_{j,k_1^0} & \int_S P_0 \phi_{j,k_2^0} \\ \int_S P_1 \phi_{j,k_0^0} & \int_S P_1 \phi_{j,k_1^0} & \int_S P_1 \phi_{j,k_2^0} \\ \int_S P_2 \phi_{j,k_0^0} & \int_S P_2 \phi_{j,k_1^0} & \int_S P_2 \phi_{j,k_2^0} \end{bmatrix} \begin{bmatrix} \tilde{s}_{j,k_0^0,m_0^0} \\ \tilde{s}_{j,k_1^0,m_0^0} \\ \tilde{s}_{j,k_2^0,m_0^0} \end{bmatrix}.$$

Evaluating the matrix gives us

$$\begin{bmatrix} 1/2 \\ 1/4 \\ 0 \end{bmatrix} = \begin{bmatrix} 1/2 & 1 & 1/2 \\ 1/6 & 5/6 & 1/2 \\ 0 & 1/6 & 1/3 \end{bmatrix} \begin{bmatrix} \tilde{s}_{j,k_0^0,m_0^0} \\ \tilde{s}_{j,k_1^0,m_0^0} \\ \tilde{s}_{j,k_2^0,m_0^0} \end{bmatrix}.$$

Then, $\tilde{s}_{j,k_0^0,m_0^0} = 13/16$, $\tilde{s}_{j,k_1^0,m_0^0} = 1/8$ and $\tilde{s}_{j,k_2^0,m_0^0} = -1/16$. It is now a simple matter to show that the wavelet $\psi_{j,m_0^0}$ vanishes polynomials.

We may now build wavelet basis around more complex objects. In Figures 4-10 and 4-11 we present results of linear wavelet constructions which vanish polynomials of order one in $R^2$. Notice that even at very crude discretizations of the circle, as shown in Figure 4-10, the wavelets still vanish polynomials.

### 4.2.4 Surface Wavelets

We now concentrate on the class of interpolating scaling functions over flat surface elements in $R^3$. We shall first start with the construction of surface wavelets on the plane and then extend them to $R^3$. Let $S$ be a (not necessarily connected) surface embedded in $R^3$. Now, partition $S$ into a finite number of triangular elements.

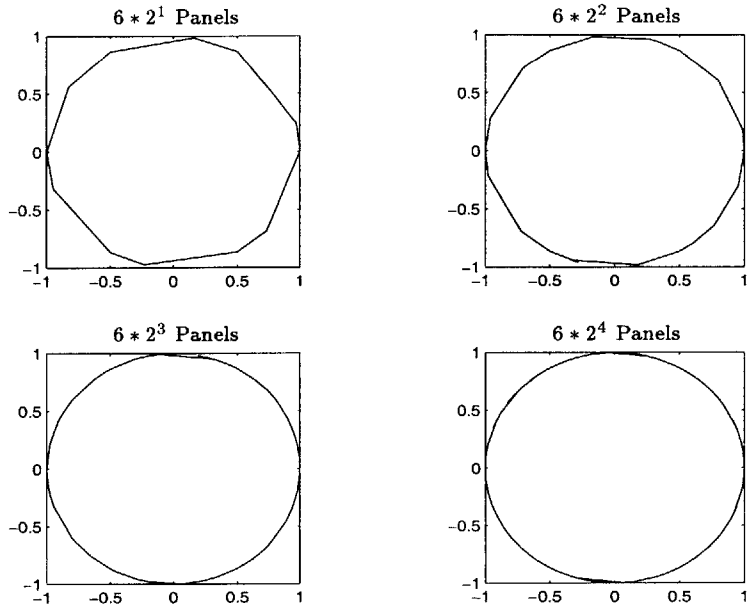


Figure 4-10: Multiple irregular discretizations of the circle with linear hats wavelets which vanish first order polynomials around corners.

Denote each individual triangle as $S_{0,v}$, where 0 refers to the level of resolution of the triangulation. The next step is to subdivide each triangle $S_{0,v}$ into 4 smaller triangles. Denote the refined triangles by $S_{1,v}$ at level 1 of resolution. This process is repeated for $n$ iterations. We denote the new refined triangles as $S_{j,v}$, where $j$ is the level of refinement that they belong to. Thus at any level of refinement $j$, $\bigcup_v S_{j,v} = S$. Let $\{P_i(\vec{x})\}$ be the set of polynomial functions over the surface element $S_{j,v}$. The polynomials are given by

$$P_i(\vec{x}) = x_1^a x_2^b,$$

where the indices $a$, $b$ and $c$ are chosen such that $P_i(\vec{x})$ represents all polynomial permutations over the partition $S_{j,k}$, up to the desired order, and $\{x_i \mid i = 1, 2\}$ are the global coordinates. The primary functions now take the form

$$\phi_{j,k}(\vec{x}) = \sum_{i=0}^{M-1} a_i P_i(\vec{x}) \tag{4.10}$$

over any partition $S_{j,v}$.

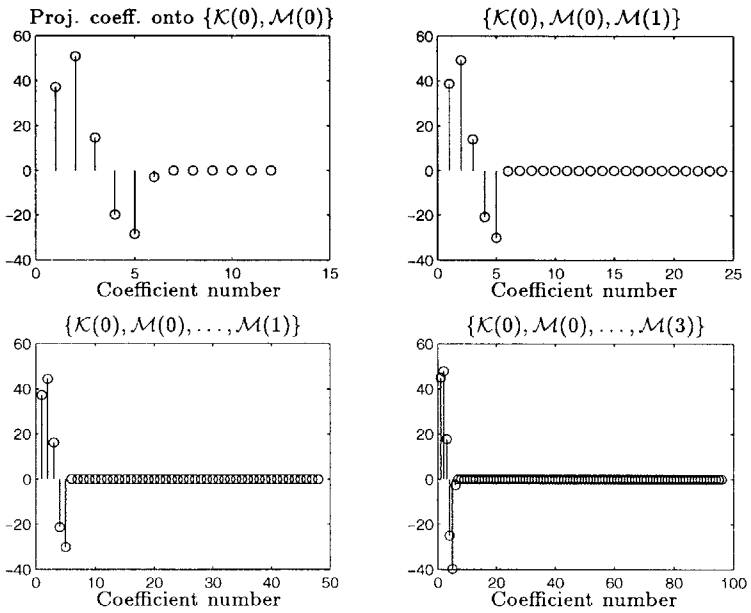


Figure 4-11: Compression of a first order polynomial $7 + 29x_1 + 23x_2$ using a wavelet basis. We project the polynomial onto the dual wavelet basis. The projection coefficients are obtained by integrating $\int (7 + 29x_1 + 23x_2)\phi_{j,k}$ for the dual scaling function and $\int (7 + 29x_1 + 23x_2)\psi_{j,k}$ for the dual wavelet. As seen in the graphs only the first six coefficients, which correspond to the projection coefficients of the dual scaling functions, integrate to a non zero number.

There are many ways to group the interpolating nodes $x_{j,k}$ at different scales of resolution to form a dense subset of nodes over any triangular element. However, it is desirable to have a fairly uniform density of scaling functions at every resolution level. We shall therefore take the following approach. Start with the triangle $S_{j,v}$ and let $S_{j+1,4v+l}$, $l = 0 \ldots 3$ be the refined triangulation of $S_{j,v}$. Pick $M$ nodes $x_k \in S_{j,v}, k \in \mathcal{K}(j)$. These $M$ nodes are used to construct values at interpolating nodes $x_m$ at the next level of refinement, where $x_m \in S_{j+1,4v+l}$ such that $m \in \mathcal{M}(j)$, for $l = 0 \ldots 3$. The refined nodes $x_m$ are chosen such that each refined triangle $S_{j,4v+l}$, $l = 0 \ldots 3$ contains exactly $M$ nodes and retains the original structure of the primary triangle.

We now divide the refined nodes into two categories: *interior* and *boundary* nodes. The neighborhood around any *interior* refined node $\vec{x}_m$ in $S_{j,v}$ is restricted such that

$$N(j,m) \subset \{k \in \mathcal{K}(j) \mid \vec{x}_k \in S_{j,v}\}.$$

which correspond to the nodes marked 4 in Figure 4-12. The neigborhood $N(j,m)$ corresponds to all the nodes marked $\times$.

The neighborhood around any *boundary* refined node $\vec{x}_m$ is chosen such that the nodes of $N(j,m)$ belong to the same triangle. However, for the other two edges the nodes $N(j,m)$ belong to the adjacent triangle. Notice that as long as we pick all the *boundary* nodes between two triangles to lie on a plane comming out of the surface, the new refined points will only depend on other boundary nodes in the same triangle, thus satisfying the requirements of Theorem 4.2.1. Another consequence is that the scaling functions will be $C^0(S)$ continuous across the boundary.

The primary wavelets may now be constructed by applying the lifting scheme and imposing vanishing moments over the surface $S$. For the interior nodes, the nodes of the neigborhood $A(j,m)$ are chosen from the same triangle. For the boundary nodes, at one edge, the nodes of $A(j,m)$ belong to the same triangle. For the other two edges the nodes of $A(j,m)$ belong to the adjacent triangle.

We now present a quadratic surface wavelet construction. In Figure 4-12 we have

an example of the nodes distribution to create quadratic wavelets on a flat surface. The first step is to create the scaling functions. For interior nodes marked as 4 we choose the the neigborhood $N(j,m)$ to be all six nodes marked $\times$. For the boundary nodes we choose $N(j,m)$ to be only the three nodes marked $\times$ on the same edge. This choice for the boundary nodes is sufficient since we only need three colinear points to define a quadratic exactly. In Figures 4-13 and 4-14 we have the support and shape of the quadratic scaling functions.

The next step is to impose vanishing moments on the wavelet. In this case the moments to vanish are $\{P_0,\ldots,P_5\} = \{1, x_1, x_2, x_1x_2, x_1^2, x_2^2\}$. We need in this case $A(j,m)$ to have cardinality six. From 4-1, all the nodes marked as $1, 4$, $A(j,m)$ to be equal to all six nodes marked $\times$. For nodes 2 and 3 we use all six nodes in $K(j)$ from the adjacent triangle. We then apply the lifting scheme to impose these vanishing moments.

The quadratic surface wavelets may now be extended to $R^3$ by mapping the scaling functions over each triangle in $R^2$, at the finest resolution, onto a mesh in 3D. The next step is to impose vanishing moments. However, the wavelet must vanish moments in the global domain directly over the mesh. In this case the polynomial moments are

$$P_i(\vec{x}) = x_1^a x_2^b x_3^c,$$

where $\{x_i \,|\, i = 1,2,3\}$ are the global domain coordinates. Thus if we want to kill the four moments $\{1, x_1, x_2, x_3\}$ we need at least four nodes in $A(j,m)$. We then proceed lift the wavelet , with the mapped scaling functions, to impose vanishing moments directly over the mesh.

Notice that the mapping will destroy the vanishing moment properties of the *dual* wavelet. For corners, we would have only one vanishing moment. However, we may avoid the *dual* wavelet altogether, if we solve a *Galerkin* formulation of a PDE, which relies only on the primary basis functions.

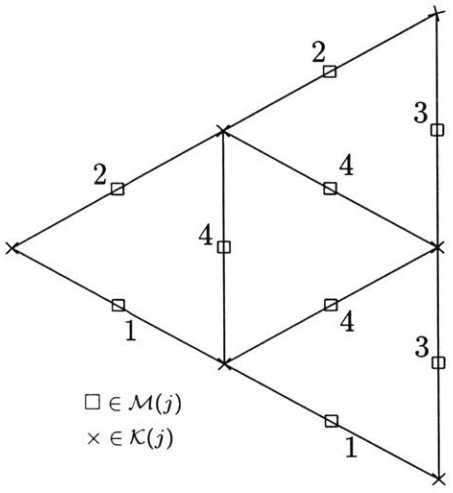


Figure 4-12: Example of the distribution of nodes for the construction of quadratic scaling functions and wavelets. For this example, $\{P_0, \ldots, P_5\} = \{1, x_1, x_2, x_1x_2, x_1^2, x_2^2\}$. For both the scaling function and wavelet, the nodes marked as 1 or 4 depend only from nodes, marked $\times$, in the principal triangle. The node numbers 2 and 3 depend from nodes in $K(j)$ from the adjacent triangle.

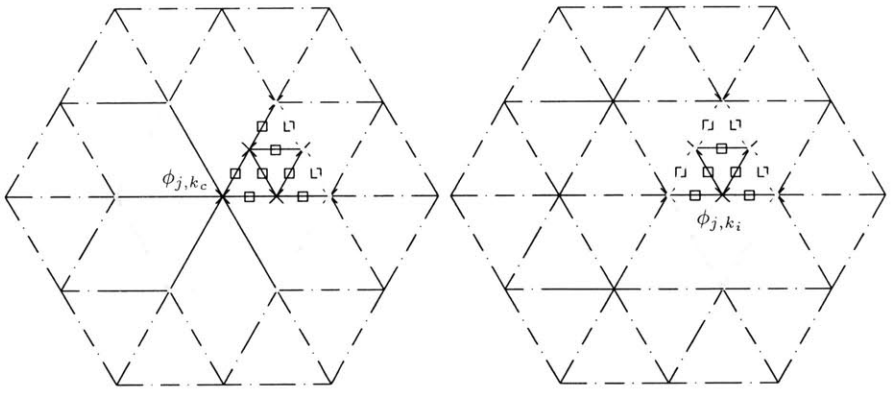


Figure 4-13: Support of the primary scaling functions over a triangulated surface domain in $R^3$ or $R^2$. The gray lines indicate the boundaries of the scaling functions. The $\times$ nodes belong to $\mathcal{K}(j)$ and the $\square$ nodes belong to $\mathcal{M}(j)$. As in the one dimensional case, we have two types of scaling functions. The left figure shows the support for scaling functions $\phi_{j,k_c}$ centered at the vertex of the triangular element $S_{j,v}$. In the right figure we have the support for $\phi_{j,k_i}$ which is centered at an interior node.

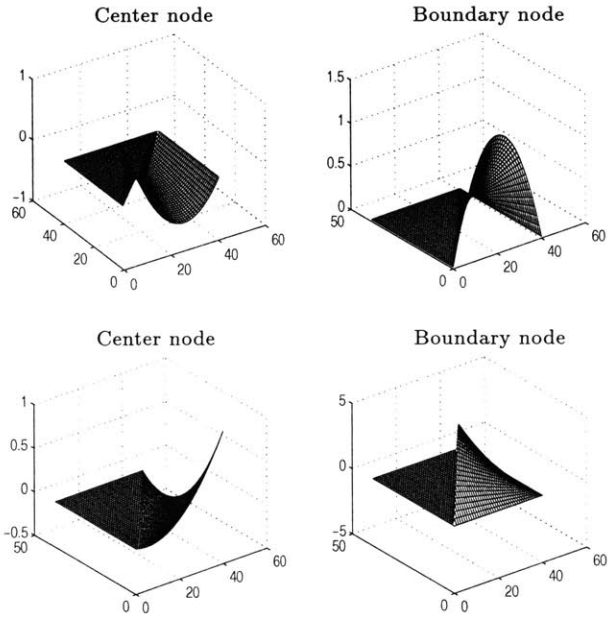


Figure 4-14: Example of four shape functions located at interior and exterior nodes. A scaling function is then constructed from all the neighboring triangles to the interpolating node.

# Chapter 5

# Applications of Wavelets on Curves and Surfaces in Computational Modeling

The multiwavelet for surfaces representations described in Chapters 3 and 4 provide a multilevel framework, which can support the study of 3D problems in computational mechanics in several ways. Essentially, the spatially adpative Multiwavelet, developed in the previous chapters, can be thought of as a tool for

(a) Represention of complex surfaces or functions on complex surfaces.

(b) Analysis of discrete data sampled at the nodes of an irregular mesh.

(c) Discretization of partial differential equations on arbitrary domains.

In this chapter we concentrate on applications to discretize PDEs in 3D. Moreover, we analyze the 3D integral formulation with linear surface wavelets introduced in Chapter 3 applied to Calderón-Zygmund integral operators. We derive a scheme based on a distance criterion between the source and the observation points. We show that it is only necessary to compute $\mathcal{O}\ (N(logN)^{7/2})$ entries of the stiffness matrix to achieve quadratic asymptotic convergence.

## 5.1 Discretization of partial differential equations

Traditional wavelet constructions have already been shown to be a useful tool for simulating the partial differential equations of physical processes. Examples of work involving differential forms can be found in Amaratunga et al. [5, 6, 7] and Qian et al. [39], while examples of work involving integral forms can be found in Beylkin et al. [8] and Dahmen et al. [15]. In all of these instances, the general approach is to use a traditional one-dimensional wavelet basis or a tensor product of such bases in a Galerkin procedure. This leads to fast, hierarchical and locally adaptive algorithms. The disadvantage of using a traditional wavelet basis is that it necessitates the discretization of the problem on a uniform grid. For 3D problems in particular, uniform grids can be unduly cumbersome. For example, Dahmen et al. [15] and von Petersdorff et al. [36] treat 3D problems by using a scalar or multiwavelet basis on a 2D uniform grid, which is then mapped to smooth 3D surface patches. However, no results from a practical implementation are presented in either case. In our work, we show how second-generation surface wavelets, which are *directly* constructed on a 3D mesh, can be used to simulate 3D problems, thereby extending their applicability beyond the domain of computer graphics. We analyze and implement our approach. Thus, we demonstrate that second-generation surface wavelets combine the advantages of traditional wavelets with a level of geometric flexibility similar to that associated with finite element techniques.

### 5.1.1 Differential Formulations

Although the focus of the present discussion has been on integral forms, it should be noted that the surface wavelet construction is also applicable to problems stated in differential form. Suppose now that we wish to solve the Laplace equation on a two dimensional domain, $S$. We may then consider expanding $u(\vec{x})$ as

$$u(\vec{x}) = \sum_{k \in K(n)} \lambda_{n,k}\, \phi_{n,k}(\vec{x}) \quad ; \quad \vec{x} \in S.$$

The Galerkin approach then yields the following system of equations

$$\sum_{k' \in K(n)} \lambda_{n,k'} \int_S \Delta\phi_{n,k'}(\vec{x})\tilde{\phi}_{n,k}(\vec{x})dS = 0 \quad ; \quad k \in K(n).$$

The inner products with respect to the operator,

$$\Omega^n_{k,k'} = \int_S \Delta\phi_{n,k'}(\vec{x})\tilde{\phi}_{n,k}(\vec{x})dS$$

are known as connection coefficients and they can be interpreted as the coefficients in an expansion of the form

$$\Delta\phi_{n,k'}(\vec{x}) = \sum_{k \in K(n)} \Omega^n_{k,k'}\, \phi_{n,k}(\vec{x}) \quad ; \quad \vec{x} \in S.$$

Once again, it is desirable to design the primary scaling function, $\phi_{n,k}(\vec{x})$, to have interpolating properties, since this allows the connection coefficients to be simply computed as $\Omega^n_{k,k'} = \Delta\phi_{n,k'}(\vec{x}_k)$. Note that this requires the scaling function to be twice differentiable with respect to the spatial dimensions. Subsequently, the multiscale representation can be obtained by performing a change of basis in a manner similar to that described for the integral form. One must also deal with the issue of boundary conditions, which can be enforced using techniques similar to those described in Amaratunga et al. [5, 6, 7] for traditional wavelet discretizations.

In general, the discretization of problems in differential form does not result in significant opportunities for compression, since the matrix is already sparse to start with. However, one can still realize significant performance benefits by using simple diagonal preconditioning to accelerate the solution of the multiscale system of equations [7].

### 5.1.2 Integral Formulations

Our methodology for solving integral equations using second generation surface wavelets is applicable to a wide class of engineering problems (for example, Laplace, Helmholtz and elasticity,) whose kernels exhibit decay of the form $1/r^{\alpha}$. Here, we develop the approach with reference to the Laplace equation on a closed 3D domain, noting that the procedure for other Calderon-Zygmund and pseudo-differential operators is similar.

Consider the model boundary value problem

$$\Delta u = 0, \quad u \in \Omega,$$

where $\Omega$ is a closed 3D domain of arbitrary shape. We prescribe a Dirichlet boundary condition

$$u = b, \quad u \in S,$$

where $S$ is the boundary of $\Omega$.

In order to use surface wavelets to efficiently discretize the problem, it must be first restated in boundary integral form. This can be done with the help of Green's theorem, which is commonly used to reduce the problem dimension (see e.g. Brebbia, [9]). We will restate the problem as a second-kind Fredholm integral equation[1]

$$\lambda(\vec{x})\mu(\vec{x}) + \int_S \mu(\vec{y})\, K(\vec{x},\vec{y})\, dS(\vec{y}) = b(\vec{x}) \quad ; \quad \vec{x} \in S \tag{5.1}$$

$K(\vec{x},\vec{y})$ is the kernel of the integral operator, which in this case is the normal derivative, $\partial/\partial n_y G(\vec{x},\vec{y})$, of the free space Green's function

$$G(\vec{x},\vec{y}) = \frac{1}{4\pi}\,\frac{1}{\|\vec{x}-\vec{y}\|}.$$

[1]The second-kind formulation is preferable to the first-kind formulation, since the latter generally leads to an ill-conditioned system of equations.

Here, the notation $||.||$ denotes the Euclidean vector norm. $\lambda(\vec{x})$ is a geometric parameter, which is equal to $1/2$ if the surface $S$ is smooth everywhere[2] . Eq. (5.1) must be solved for $\mu(\vec{x})$, after which the solution can be computed as the double layer potential

$$u(\vec{x}) = \int_S \mu(\vec{y})\, K(\vec{x},\vec{y})\, dS(\vec{y}) \quad ; \quad \vec{x} \in \Omega. \tag{5.2}$$

The general approach to discretization is to form a truncated wavelet expansion for the unknown quantity

$$\mu^{approx}(\vec{x}) = \sum_{k \in K(0)} \mu_k^{0,approx}\, \phi_{0,k}(\vec{x}) + \sum_{j=0}^{n-1} \sum_{m \in M(j)} \eta_m^{j,approx}\, \psi_{j,m}(\vec{x})$$

and then solve for the expansion coefficients $\mu_k^{0,approx}$ and $\eta_k^{j,approx}$ using a Galerkin or collocation scheme. Here, $n$ denotes the finest level in the multilevel mesh. When a Galerkin approach is used, one chooses the test functions (weighting functions) to be the dual wavelet basis

$$\left\{ \tilde{\phi}_{0,k}(\vec{x}), \tilde{\psi}_{j,m}(\vec{x}) | k \in K(0),\, m \in M(j),\; 0 \leq j < n \right\}$$

since the biorthogonality conditions permit some simplification of the resulting system of equations[3] . From an algebraic perspective, this system of equations is most easily developed if one proceeds as follows.

*Step 1: Form a single scale Galerkin system*

Start with an equivalent single scale expansion of the form

$$\mu^{approx}(\vec{x}) = \sum_{k \in K(n)} \mu_k^{n,approx}\, \phi_{n,k}(\vec{x}).$$

[2]If the surface is not smooth, $\lambda(\vec{x})$ can be determined using standard techniques outlined in Brebbia [9] .

[3]Strictly speaking, such a scheme is referred to as a Petrov-Galerkin scheme since the test functions differ from the trial functions.

Plug this into Eq. (5.1), weight with the dual scaling functions, $\tilde{\phi}_{n,k}(\vec{x})$ and integrate over $S$. This results in the system of equations

$$\lambda_k^n \mu_k^{n,approx} + \sum_{k' \in K(n)} K_{k,k'}^n \, \mu_{k'}^{n,approx} = b_k^n \quad ; \quad k \in K(n) \tag{5.3}$$

In this system, the right hand side is formally given by the integral

$$b_k^n = \int_S b(\vec{x}) \, \tilde{\phi}_{n,k}(\vec{x}) \, dS(\vec{x}) \tag{5.4}$$

but because of the interpolating property, this can be simply calculated as

$$b_k^n = b(\vec{x}_k)$$

Similarly, the matrix entries, $K_{k,k'}^n$, are given by

$$K_{k,k'}^n = \int_S \int_S K(\vec{x}, \vec{y}) \, \phi_{n,k'}(\vec{y}) \, dS(\vec{y}) \, \tilde{\phi}_{n,k}(\vec{x}) \, dS(\vec{x}) \tag{5.5}$$

and these can be calculated as

$$K_{k,k'}^n = \int_S K(\vec{x}_k, \vec{y}) \, \phi_{n,k'}(\vec{y}) \, dS(\vec{y}).$$

Since $\phi_{n,k'}(\vec{y})$ are simply linear interpolating functions, the $K_{k,k'}^n$ coefficients can be computed using standard Gaussian quadrature formulae similar to those commonly used in finite element modeling. Note that for computational tractability the kernel can be expressed as

$$K(\vec{x}, \vec{y}) = -\frac{1}{4\pi} \frac{(\vec{x} - \vec{y}) \cdot \vec{n}(\vec{y})}{\left\| \vec{x} - \vec{y} \right\|^3}, \tag{5.6}$$

where $\vec{n}(\vec{y})$ is the outward unit normal vector to the boundary at the point $\vec{y}$.

The coefficients $\lambda_k^n$ in Eq. (5.3) are samples of $\lambda(\vec{x})$ at the points $\vec{x}_k$ for the $n$th resolution mesh. In general, the $n$th resolution mesh will be a polyhedral approxi-

mation to the true surface geometry, which means that $\lambda(\vec{x})$ for the mesh will differ from $\lambda(\vec{x})$ for the true surface wherever there is an artificial discontinuity introduced by the geometric approximation. This typically occurs at element boundaries.

In matrix form, the single scale Galerkin equations may be written as

$$(\Lambda^n + K^n)\vec{\mu}^{n,approx} = \vec{b}^n$$

Here, $\vec{\mu}^{n,approx}$ is the vector of unknown coefficients $\mu_k^{n,approx}$, $\Lambda^n$ is a diagonal matrix with entries $\lambda_k^n$, $K^n$ is the stiffness matrix with entries $K_{k,k'}^n$, and $\vec{b}^n$ is the vector with entries $b_k^n$.

*Step 2: Perform a change of basis*

The second step is to decompose the level $n$ scaling functions, $\phi_{n,k}(\vec{x})$ and $\tilde{\phi}_{n,k}(\vec{x})$, into wavelets in Eq. (5.4) and (5.5). This is a recursive process, which can be performed by rearranging the scaling relations and the wavelet equations in the following form:

$$\phi_{j+1,k}(\vec{x}) = \phi_{j,k}(\vec{x}) - \sum_{m \in n(j,k)} h_{j,k,m}^0 \, \phi_{j+1,m}(\vec{x})$$

$$\phi_{j+1,m}(\vec{x}) = \psi_{j,m}(\vec{x}) + \sum_{k \in A(j,m)} h_{j,k,m}^1 \, \phi_{j,k}(\vec{x})$$

$$\tilde{\phi}_{j+1,k}(\vec{x}) = \tilde{\phi}_{j,k}(\vec{x}) - \sum_{m \in a(j,k)} h_{j,k,m}^1 \, \tilde{\psi}_{j,m}(\vec{x})$$

$$\tilde{\phi}_{j+1,m}(\vec{x}) = \tilde{\psi}_{j,m}(\vec{x}) + \sum_{k \in N(j,m)} h_{j,k,m}^0 \, \tilde{\phi}_{j+1,k}(\vec{x})$$

With some algebraic manipulation, it can be shown that this change of basis results in a system of equations of the form

$$W(\Lambda^n + K^n)\tilde{\psi}^T(W\vec{\mu}^{n,approx}) = W\vec{b}^n. \tag{5.7}$$

In this system, $W$ denotes the matrix that performs the DWT. For example, $W\vec{b}^n$ transforms $b_k^n$ according to the recursion

$$v_m^j = b_m^{j+1} - \sum_{k \in N(j,m)} h_{j,k,m}^0 \, b_k^{j+1}$$

$$b_k^j = b_k^{j+1} + \sum_{m \in a(j,k)} h_{j,k,m}^1 \, v_m^j$$

where

$$v_m^j = \int_S b(\vec{x}) \, \tilde{\psi}_{j,m}(\vec{x}) \, dS(\vec{x}).$$

Similarly, $\tilde{W}$ denotes the dual DWT matrix. The dual DWT operates on the rows of $\Lambda^n + K^n$ in Eq. (5.7), hence the transpose notation.

The matrix $\hat{K}^n = W(\Lambda^n + K^n)\tilde{W}^T$ is the realization of the integral operator in the wavelet basis. It is in fact the generalization to 3D triangular meshes of the standard form matrix, which was described by Beylkin et al. [8] for problems on uniform one-dimensional grids using traditional wavelets. Since $\hat{K}^n$ is the result of a boundary integral discretization, it is technically a densely populated matrix with $N^2$ entries, where $N$ is the total number of unknown coefficients in the wavelet expansion for $\mu(\vec{x})$. The entries of $\hat{K}^n$ are typically of the form

$$\beta_{m,m'}^{j,j'} = \int_S \int_S K(\vec{x}, \vec{y}) \, \tilde{\psi}_{j,m}(\vec{x}) \, dS(\vec{x}) \, \psi_{j',m'}(\vec{y}) \, dS(\vec{y}) \tag{5.8}$$

and they exhibit rapid decay as the distance $||\vec{x}_m - \vec{y}_{m'}||$ between the observation point $\vec{x}_m$ and the source point $\vec{y}_{m'}$ increases. This is considerably faster than the rate of decay of the entries in the single scale matrix, $K^n$. Consequently, one need only retain roughly $O((logN)^{\frac{7}{2}}N)$ of the most significant entries in $\hat{K}^n$ in order to compute the final solution with acceptable accuracy. In Section 5.2, we derive in the 3D case estimates for (a) the decay of the kernel coefficients, (b) the rate of convergence and (c) the number of entries that must be retained in the compressed matrix to match the rate of convergence that is obtained without compression.

## 5.2 Analysis of the 3D Integral Formulation

In section 5.1 we presented the application of the multiresolution linear surface wavelets to the Laplace equation

$$\Delta u = 0, \quad u \in \Omega,$$

where $\Omega$ is a closed 3D domain of arbitrary shape. We prescribed a Dirichlet boundary condition

$$u = b, \quad u \in S,$$

This PDE may be posed as an integral equation of the form

$$\lambda(\vec{x})\mu(\vec{x}) + \int_S \mu(\vec{y})\, K(\vec{x},\vec{y})\, dS(\vec{y}) = b(\vec{x}) \quad ; \quad \vec{x} \in S.$$

We will now obtain estimates for:

(a) the decay of the kernel expansion coefficients in the linear surface wavelet basis

(b) the rate of convergence of the numerical scheme when no matrix compression is performed, and

(c) the number of entries that must be retained in the compressed matrix, so that the rate of convergence under compression is of the same order as that which is obtained without compression.

Note that the following analysis is valid for the class of integral operators $T : L^2(S) \to L^2(S)$ of the form

$$T(\mu) = \int_S K_T(\vec{x},\vec{y})\mu(\vec{y})\ dS(\vec{y}) = b(\vec{x}).$$

The kernel $K_T(\vec{x},\vec{y})$ satisfies

$$|D_x^\alpha D_y^\beta K_T(\vec{x},\vec{y})| \leq \frac{C}{|x-y|^{2+|\alpha|+|\beta|}},$$

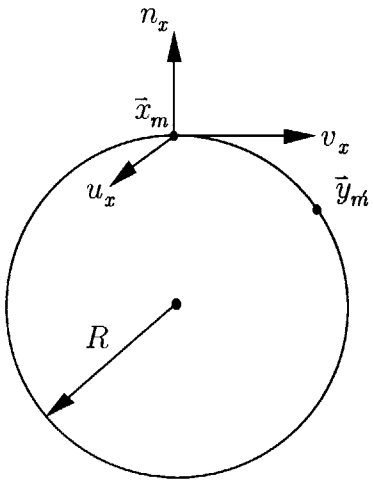


Figure 5-1: Local coordinate system for Taylor series expansion.

where $C$ is bounded and $D^\alpha$, $D^\beta$ are the cartesian derivatives in $R^3$ acting on a smooth extension of $K_T(\vec{x},\vec{y})$ to a tubular neighborhood of $S$. Furthermore we shall restrict $b(\vec{x}), \mu(\vec{x}) \in H_0^3(S)$.

### 5.2.1 Decay of the Kernel Coefficients in the Linear Surface Wavelet Basis

We now establish estimates for the decay of the kernel coefficients $\beta_{m,m'}^{j,j'}$ in the linear surface wavelet basis. Referring to Figure 5-1, we first expand the kernel in a three-dimensional Taylor series about $\vec{x} = \vec{x}_m$.

$$K(\vec{x},\vec{y}) = \sum_{p+q+r=0}^{M-1} \frac{u_x^p v_x^q n_x^r}{p!q!r!} \frac{\partial^{p+q+r} K}{\partial u_x^p \partial v_x^q \partial n_x^r}(\vec{x}_m,\vec{y}) \; + \sum_{p+q+r=M} \frac{u_x^p v_x^q n_x^r}{p!q!r!} \frac{\partial^M K}{\partial u_x^p \partial v_x^q \partial n_x^r}(\vec{\tau},\vec{y}). \tag{5.9}$$

Here, $u_x$, $v_x$ and $n_x$ denote a system of local coordinates such that directions

$u_x$ and $v_x$ lie in the tangent plane at the point $\vec{x}_m \in S$ and $n_x$ is the direction of the outward normal. $\vec{\tau}$ is a point such that $\vec{\tau} - \vec{x}_m \in [(0,0,0),(u_x,v_x,n_x)]$. The coordinates of any point $\vec{x} \in S$ in the neighborhood of $\vec{x}_m$ are constrained by the surface geometry. For example, in the case of the sphere of radius $R$ shown in Figure 5-1, we have

$$n_x = \left[R^2 - u_x^2 - v_x^2\right]^{1/2} - R = f(u_x, v_x).$$

Note that other smooth surfaces can be represented in a similar manner. We may expand $n_x$ in a two-dimensional McLaurin series as

$$n_x = \sum_{p+q=0}^{N-1} \frac{u_x^p v_x^q}{p!q!} \frac{\partial^{p+q} f}{\partial u_x^p \partial v_x^q}(0,0) \; + \sum_{p+q=N} \frac{u_x^p v_x^q}{p!q!} \frac{\partial^N f}{\partial u_x^p \partial v_x^q}(\xi_x, \eta_x), \tag{5.10}$$

where $(\xi_x, \eta_x) \in [(0,0),(u_x,v_x)]$. By combining Equations (5.9) and (5.10), we obtain a representation of the kernel in terms of $u_x$ and $v_x$ only.

We now consider the case of the linear surface wavelet basis described above. By their construction, the scaling functions $\phi_{j,k}(\vec{x})$, $k \in K(j)$, can reproduce linear functions of the form $c_0 + c_1 u_x + c_2 v_x$ in the neighborhood of $\vec{x}_m$. Since $\langle \phi_{j,k}(\vec{x}), \tilde{\psi}_{j,m}(\vec{x}) \rangle = 0$, we see that

$$\int_S \tilde{\psi}_{j,m}(\vec{x}) dS(\vec{x}) = 0, \tag{5.11}$$

$$\int_S u_x \tilde{\psi}_{j,m}(\vec{x}) dS(\vec{x}) = 0, \tag{5.12}$$

$$\int_S v_x \tilde{\psi}_{j,m}(\vec{x}) dS(\vec{x}) = 0. \tag{5.13}$$

Hence, if we expand the kernel with $M = 1$ and $N = 2$ in Equations. (5.9) and (5.10) respectively, we obtain from Equation (5.8) that

$$\beta_{m,m'}^{j,j'} = F(\xi_x, \eta_x) \int_S \frac{\partial K}{\partial n_x}(\vec{\tau}, \vec{y})\, \psi_{j',m'}(\vec{y})\, dS(\vec{y})\,, \tag{5.14}$$

where $\vec{\tau}$ lies within the support of $\tilde{\psi}_{j,m}(\vec{x})$ and

$$F(\xi_x, \eta_x) = \frac{1}{2}\frac{\partial^2 f}{\partial u_x^2}(\xi_x, \eta_x) \int_S u_x^2\, \tilde{\psi}_{j,m}(\vec{x}) dS(\vec{x}) + \frac{\partial^2 f}{\partial u_x \partial v_x}(\xi_x, \eta_x) \int_S u_x v_x\, \tilde{w}_{j,m}(\vec{x}) dS(\vec{x})$$

$$+\frac{1}{2}\frac{\partial^2 f}{\partial v_x^2}(\xi_x, \eta_x) \int_S v_x^2\, \tilde{\psi}_{j,m}(\vec{x}) dS(\vec{x}). \tag{5.15}$$

Using a similar Taylor series analysis, this time about $\vec{y} = \vec{y}_{m'}$ with $M = 1$ and $N = 1$, we find that $\int_S \frac{\partial K}{\partial n_x}(\vec{\tau}, \vec{y})\, \psi_{j',m'}(\vec{y})\, dS(\vec{y})$ is equal to

$$\left[\frac{\partial^2 K}{\partial u_y n_x}(\vec{\tau}, \vec{\nu}) + \frac{\partial f}{\partial u_y}(\xi_y, \eta_y)\, \frac{\partial^2 K}{\partial n_y n_x}(\vec{\tau}, \vec{\nu})\right] \int_S u_y\, \psi_{j',m'}(\vec{y})\, dS(\vec{y})$$

$$+ \left[\frac{\partial^2 K}{\partial v_y n_x}(\vec{\tau}, \vec{\nu}) + \frac{\partial f}{\partial v_y}(\xi_y, \eta_y)\, \frac{\partial^2 K}{\partial n_y n_x}(\vec{\tau}, \vec{\nu})\right] \int_S v_y\, \psi_{j',m'}(\vec{y})\, dS(\vec{y})$$

for some $\vec{\nu}$ lying within the support of $\psi_{j',m'}(\vec{y})$. From Equation (5.6), each of the terms $\partial^2 K(\vec{\tau}, \vec{\nu})/\partial u_y \partial n_x$, $\partial^2 K(\vec{\tau}, \vec{\nu})/\partial v_y \partial n_x$and $\partial^2 K(\vec{\tau}, \vec{\nu})/\partial n_y \partial n_x$ has the bound $C/\|\vec{\tau} - \vec{\nu}\|^4$. Hence we arrive at the estimate

$$\left|\beta_{m,m'}^{j,j'}\right| \leq \sup_{\vec{\tau} \in \tilde{A}_{j,m}} \sup_{\vec{\nu} \in A_{j',m'}} \frac{1}{\|\vec{\tau} - \vec{\nu}\|^4}(C_1 I_{j',m'}^{1,0} + C_2 I_{j',m'}^{0,1})(C_3 \tilde{I}_{j,m}^{2,0} + C_4 \tilde{I}_{j,m}^{1,1} + C_5 \tilde{I}_{j,m}^{0,2}), \tag{5.16}$$

where

$$I_{j',m'}^{p,q} = \int_{A_{j',m'}} u_y^p v_y^q\, \psi_{j',m'}(\vec{y}) dS(\vec{y}), \quad \tilde{I}_{j,m}^{p,q} = \int_{\tilde{A}_{j,m}} u_x^p v_x^q\, \tilde{\psi}_{j,m}(\vec{x}) dS(\vec{x})$$

and $A_{j',m'} = \text{support } \psi_{j',m'}(\vec{y})$, $\tilde{A}_{j,m} = \text{support } \tilde{\psi}_{j,m}(\vec{x})$. Using the Schwarz inequality

and Equation (3.27), we obtain

$$I^{p,q}_{j',m'} \leq \left\{ \int_{A_{j',m'}} \left| u_y^p v_y^q \right|^2 dS(\vec{y}) \right\}^{\frac{1}{2}} \left\{ \int_{A_{j',m'}} \left| \psi_{j',m'}(\vec{y}) \right|^2 dS(\vec{y}) \right\}^{\frac{1}{2}}$$

$$\leq C h_{j'}^{p+q+1}. \tag{5.17}$$

Similarly, we find that $\tilde{I}^{p,q}_{j,m} \leq C h_j^{p+q+1}$. Let $l^{j,j'}_{m,m'}$ denote the distance between the supports of $\tilde{\psi}_{j,m}(\vec{x})$ and $\psi_{j',m'}(\vec{y})$. We thus have

$$\left| \beta^{j,j'}_{m,m'} \right| \leq \frac{C h_j^3 h_{j'}^2}{(l^{j,j'}_{m,m'})^4}.$$

### 5.2.2 Convergence

Consider now the rate of convergence of the discrete approximation, in the case where no compression is performed on the operator matrix. This will represent the desired rate of convergence that we expect to match when compression is in fact performed.

Let $T\mu(\vec{x}) : L^2(S) \rightarrow L^2(S)$ be an integral operator, satisfying the following conditions of continuity and invertibility:

$$\|T\mu(\vec{x})\| \leq C\|\mu(\vec{x})\| \tag{5.18}$$

$$\|\mu(\vec{x})\| \leq C\|T\mu(\vec{x})\|.$$

Let the operator be discretized using a biorthogonal surface wavelet basis, which satisfies the Riesz stability criterion i.e.

$$A\|\mu(\vec{x})\|^2 \leq \|\vec{\mu}^n\|^2 + \sum_{j=n}^{\infty} \|\vec{\eta}^j\|^2 \leq B\|\mu(\vec{x})\|^2, \tag{5.19}$$

where $A$ and $B$ are constants independent of $n$ and $B \geq A > 0$. This will be true from Theorem 3.2.1 since $\mu(\vec{x}) \in H_0^3(S)$. We now expand $\mu(\vec{x})$ as

$$\mu(\vec{x}) = \sum_{k \in K(n)} \mu_k^n \, \phi_{n,k}(\vec{x}) + \sum_{j=n}^{\infty} \sum_{m \in M(j)} \eta_m^j \, \psi_{j,m}(\vec{x})$$

in the $L^2$ sense and the norms of the coefficient vectors, $\vec{\mu}^n$ and $\vec{\eta}^j$ are given by

$$\|\vec{\mu}^n\|^2 = \sum_{k \in K(n)} (\mu_k^n)^2, \quad \|\vec{\eta}^j\|^2 = \sum_{m \in M(j)} (\eta_m^j)^2 .$$

We are interested in understanding the behavior of the error $\|\mu^{exact}(\vec{x}) - \mu^{approx}(\vec{x})\|$, where $\mu^{exact}(\vec{x})$ is the exact solution to the integral equation

$$T\mu(\vec{x}) = b(\vec{x})$$

and $\mu^{approx}(\vec{x})$ is the approximate solution. From the Riesz criterion, we have

$$\|\mu^{exact}(\vec{x}) - \mu^{approx}(\vec{x})\| \leq C \left\{ \|\vec{\mu}^{n,exact} - \vec{\mu}^{n,approx}\|^2 + \sum_{j=n}^{\infty} \|\vec{\eta}^{j,exact}\|^2 \right\}^{\frac{1}{2}} . \quad (5.20)$$

In order to proceed, we must first show that the discrete operator matrix, $\Lambda^n + K^n$, satisfies the condition

$$\|\vec{\mu}^n\| \leq C \|(\Lambda^n + K^n)\vec{\mu}^n\| \quad \forall \vec{\mu}^n$$

for sufficiently large $n$. This ensures the invertibility of the matrix, because the minimum singular value then satisfies the condition

$$\sigma_{min}(\Lambda^n + K^n) = \min_{\vec{\mu}^n \neq 0} \frac{\|(\Lambda^n + K^n)\vec{\mu}^n\|}{\|\vec{\mu}^n\|} \geq C > 0. \quad (5.21)$$

Let $f(\vec{x})$ be a function in $H_0^3(S)$ with the expansion

$$f(\vec{x}) = \sum_{k \in K(n)} c_k^n \, \phi_{n,k}(\vec{x}) + \sum_{j=n}^{\infty} \sum_{m \in M(j)} d_m^j \, \psi_{j,m}(\vec{x})$$

and let its projection onto the subspace $V_n = \overline{span\{\phi_{n,k}(\vec{x}) | k \in K(n)\}}$ be $P_n f(\vec{x})$ i.e.

$$P_n f(\vec{x}) = \sum_{k \in K(n)} c_k^n \, \phi_{n,k}(\vec{x}).$$

From the Riesz condition (Theorem 3.2.1), we then have that

$$A\|f\|^2 \leq \|\vec{c}^{\,n}\|^2 + \sum_{j=n}^{\infty} \|\vec{d}^{\,j}\|^2 \tag{5.22}$$

and

$$\sum_{j=n}^{\infty} \|\vec{d}^{\,j}\|^2 \leq B\|f - P_n f\|^2.$$

Now since $\|f - P_n f\| \to 0$ as $n \to \infty$, we may find a positive constant $C_{n_0} < A/B$ such that, if $n_0$ is a sufficiently large integer and $n > n_0$,

$$\frac{\|f - P_n f\|^2}{\|f\|^2} \leq C_{n_0}.$$

This gives

$$\sum_{j=n}^{\infty} \|\vec{d}^{\,j}\|^2 \leq BC_{n_0}\|f\|^2$$

Hence, from Equation (5.22)

$$\|\vec{c}^{\,n}\|^2 \geq A\|f\|^2 - \sum_{j=n}^{\infty} \|\vec{d}^{\,j}\|^2$$

$$\geq (A - BC_{n_0})\|f\|^2$$

$$\geq C\|f\|^2$$

where $C > 0$. Now we set

$$f(\vec{x}) = TP_n\mu(\vec{x})$$

so that the coefficients of $P_nf$ and $P_n\mu$ are related by

$$\vec{c}^{\,n} = (\Lambda^n + K^n)\vec{\mu}^{\,n}.$$

We then have by the Riesz criterion

$$\|\vec{\mu}^{\,n}\| \leq C\|P_n\mu(\vec{x})\|,$$

by Equation (5.14)

$$\|\vec{\mu}^{\,n}\| \leq C\|TP_n\mu(\vec{x})\|,$$

by the Riesz criterion

$$\|\vec{\mu}^{\,n}\| \leq C\|\vec{c}^{\,n}\|,$$

and by Equation 5.21

$$\|\vec{\mu}^{\,n}\| \leq C\|(\Lambda^n + K^n)\vec{\mu}^{\,n}\|.$$

We may now relate the error in solving for the coefficients $\vec{\mu}^{\,n,exact}$ to the residual error, $\vec{r}^{\,n}$,

$$\begin{aligned}
\|\vec{\mu}^{\,n,exact} - \vec{\mu}^{\,n,approx}\| &\leq C\|(\Lambda^n + K^n)(\vec{\mu}^{\,n,exact} - \vec{\mu}^{\,n,approx})\| \\
&\leq C\|(\Lambda^n + K^n)\vec{\mu}^{\,n,exact} - \vec{b}^{\,n}\| \\
&\leq C\|\vec{r}^{\,n}\|. \qquad (5.23)
\end{aligned}$$

The residual error can be determined by inserting the exact solution, $\mu^{exact}(\vec{x})$, into the resolution $n$ Galerkin equations, which are formed from the boundary integral

equation by taking $\tilde{\phi}_{n,k}(\vec{x})$ as test functions. Thus, we obtain

$$\vec{r}^{\,n} = (\Lambda^n + K^n)\vec{\mu}^{n,exact} - \vec{b}^{\,n}$$

$$= \sum_{j=n}^{\infty} \gamma^{n,j} \vec{\eta}^{j,exact}, \tag{5.24}$$

where $\gamma^{n,j}$ has entries

$$\gamma^{n,j}_{k,m} = \int_S \int_S K(\vec{x},\vec{y})\psi_{j,m}(\vec{y})dS(\vec{y})\tilde{\phi}_{n,k}(\vec{x})dS(\vec{x}); \quad k \in K(n), \quad m \in M(j),$$

and $\vec{\eta}^{j,exact}$ has entries

$$\eta^{j,exact}_m = \int_S \mu^{exacl}(\vec{x})\tilde{\psi}_{j,m}(\vec{x})dS(\vec{x}); \quad m \in M(j). \tag{5.25}$$

Next, we rewrite Equation (5.24) in the form

$$\vec{r}^{\,n} = R^n \vec{q}^{\,n}, \tag{5.26}$$

where

$$R^n = \begin{bmatrix} (\Lambda^n + K^n) & \gamma^{n,n} & \gamma^{n,n+1} & \dots \end{bmatrix}$$

and

$$\vec{q}^{\,n} = \begin{bmatrix} 0 \\ \vec{\eta}^{n,exact} \\ \vec{\eta}^{n+1,exact} \\ \vdots \end{bmatrix}.$$

We now show that $\|R^n\|$ is bounded. Let $f(\vec{x})$ be a function in $L^2(S)$ and let the expansion coefficients of $f(\vec{x})$ and $Tf(\vec{x})$ be respectively given by

$$\vec{f} = \begin{bmatrix} \vec{c}^{\,n} \\ \vec{d}^{\,n} \\ \vec{d}^{\,n+1} \\ \vdots \end{bmatrix}$$

and

$$\vec{t} = \begin{bmatrix} \vec{g}^{\,n} \\ \vec{z}^{\,n} \\ \vec{z}^{\,n+1} \\ \vdots \end{bmatrix}.$$

Then

$$\begin{aligned} \|R^n\| &= \max_{f \neq 0} \frac{\|R^n \vec{f}\|}{\|\vec{f}\|} \\ &= \max_{f \neq 0} \frac{\|\vec{g}^{\,n}\|}{\|\vec{f}\|}. \end{aligned}$$

But from Equation (5.19)

$$\|\vec{g}^{\,n}\| \leq C \|Tf(\vec{x})\|$$

and

$$\|\vec{f}\| \geq C \|f(\vec{x})\|.$$

Then, because of Equation (5.18), we have

$$\|R^n\| \leq C \max_{f \neq 0} \frac{\|Tf(\vec{x})\|}{\|f(\vec{x})\|} \leq C. \tag{5.27}$$

Next, we consider the behavior of $\|\vec{q}^{\,n}\|$. By expanding $\mu^{exact}(\vec{x})$ in a Taylor series

about $\vec{x} = \vec{x}_m$ in Equation (5.25), we find that

$$\|\vec{\eta}^{j,exact}\| \leq Ch_j^2$$

for the linear surface wavelet basis. (In general, we will have one order higher than the highest order polynomial that can be reproduced by the scaling functions.) Hence, we have

$$\begin{aligned} \sum_{j=n}^{\infty} \|\vec{\eta}^{j,exact}\|^2 &\leq C \sum_{j=n}^{\infty} h_j^4 \\ &\leq C \sum_{j=n}^{\infty} (\frac{h_n}{2^{j-n}})^4 \\ &\leq Ch_n^4. \end{aligned} \tag{5.28}$$

Here we have assumed that equal subdivision is used to generate those hypothetical meshes with resolution $j > n$. Note that this does not impose any additional restrictions on the actual mesh. Thus,

$$\|\vec{q}^n\| = \left\{ \sum_{j=n}^{\infty} \|\vec{\eta}^{j,exact}\|^2 \right\}^{\frac{1}{2}}$$

$$\leq Ch_n^2. \tag{5.29}$$

Combining Equations (5.23), (5.26), (5.27) and (5.29) we have

$$\begin{aligned} \|\vec{\mu}^{n,exact} - \vec{\mu}^{n,approx}\| &\leq C\|\vec{r}^n\| \\ &\leq C\|R^n\|\|\vec{q}^n\| \\ &\leq Ch_n^2. \end{aligned} \tag{5.30}$$

Finally, from Eqs (5.20), (5.28) and (5.30) we have

$$\|\mu^{exact}(\vec{x}) - \mu^{approx}(\vec{x})\| \leq Ch_n^2.$$

### 5.2.3 Convergence under compression

We now examine the trade-off between compression and solution error. In the case where matrix compression is performed, we solve a discrete system of the form

$$\hat{K}^{n,comp}(W\vec{\mu}^{n,comp}) = W\vec{b}^{n}.$$

Here, the compressed matrix is given by

$$\hat{K}^{n,comp} = \hat{K}^n - \Delta\hat{K}^n$$

where $\hat{K}^n$ is the standard form matrix described earlier and $\Delta\hat{K}^n$ represents the entries discarded during compression.

As a first step, we note that the discrete wavelet transform operator, $W$, and its inverse are bounded because of the Riesz criterion. To see this, consider the projection of a function, $P_n\mu(\vec{x}) \in V_n$, which has the equivalent single scale and multiscale expansions

$$P_n\mu(\vec{x}) = \sum_{k\in K(n)} \mu_k^n \, \phi_{n,k}(\vec{x})$$

$$= \sum_{k\in K(0)} \mu_k^0 \, \phi_{0,k}(\vec{x}) + \sum_{j=0}^{n-1} \sum_{m\in M(j)} \eta_m^j \, \psi_{j,m}(\vec{x}).$$

Then, from Equation (5.19), we have

$$A\|P_n\mu(\vec{x})\|^2 \leq \|\vec{\mu}^n\|^2 \leq B\|P_n\mu(\vec{x})\|^2$$

$$A\|P_n\mu(\vec{x})\|^2 \leq \|W\vec{\mu}^n\|^2 \leq B\|P_n\mu(\vec{x})\|^2$$

for the single scale expansion and the multiscale expansion respectively. This gives

$$\sqrt{\frac{A}{B}}\|\vec{\mu}^n\| \leq \|W\vec{\mu}^n\| \leq \sqrt{\frac{B}{A}}\|\vec{\mu}^n\|.$$

The error in solving the boundary integral equation when the matrix is compressed is

$$\|\mu^{exact}(\vec{x}) - \mu^{comp}(\vec{x})\| \leq C\left\{\|\vec{\mu}^{n,exact} - \vec{\mu}^{n,comp}\|^2 + \sum_{j=n}^{\infty}\|\vec{\eta}^{j,exact}\|^2\right\}^{\frac{1}{2}}.$$

Now,

$$\begin{aligned}
\|\vec{\mu}^{n,exact} - \vec{\mu}^{n,comp}\| &\leq C\|(\Lambda^n + K^n)(\vec{\mu}^{n,exact} - \vec{\mu}^{n,comp})\| \\
&\leq C\|(\Lambda^n + K^n)\vec{\mu}^{n,exact} - \tilde{W}^T(\hat{K}^{n,comp} + \Delta\hat{K}^n)W\vec{\mu}^{n,comp}\| \\
&\leq C\|(\Lambda^n + K^n)\vec{\mu}^{n,exact} - \vec{b}^n - \tilde{W}^T\Delta\hat{K}^nW\vec{\mu}^{n,comp}\| \\
&\leq C\|\vec{r}^n - \tilde{W}^T\Delta\hat{K}^nW\vec{\mu}^{n,comp}\| \\
&\leq C\left\{\|\vec{r}^n\| + \|\tilde{W}^T\Delta\hat{K}^nW\vec{\mu}^{n,comp}\|\right\}. \qquad (5.31)
\end{aligned}$$

But

$$\begin{aligned}
\|\tilde{W}^T\Delta\hat{K}^nW\vec{\mu}^{n,comp}\| &\leq \sqrt{\frac{B}{A}}\|\Delta\hat{K}^nW\vec{\mu}^{n,comp}\| \\
&\leq \sqrt{\frac{B}{A}}\|\Delta\hat{K}^nW\vec{\mu}^{n,exact} - \Delta\hat{K}^nW(\vec{\mu}^{n,exact} - \vec{\mu}^{n,comp})\| \\
&\leq \sqrt{\frac{B}{A}}\|\Delta\hat{K}^nW\vec{\mu}^{n,exact}\| + \sqrt{\frac{B}{A}}\|\Delta\hat{K}^nW(\vec{\mu}^{n,exact} - \vec{\mu}^{n,comp})\|
\end{aligned}$$

$$\leq \sqrt{\frac{B}{A}}\|\Delta\hat{K}^n W\vec{\mu}^{n,exact}\| + \frac{B}{A}\|\Delta\hat{K}^n\|\|\vec{\mu}^{n,exact} - \vec{\mu}^{n,comp}\|. \tag{5.32}$$

Given that we must satisfy the basic requirement that $\|\Delta\hat{K}^n\|$ decreases monotonically with increasing $n$, we may combine Equations (5.31) and (5.32) to obtain

$$\|\vec{\mu}^{n,exact} - \vec{\mu}^{n,comp}\| \leq C\frac{\|\vec{r}^n\| + \sqrt{\frac{B}{A}}\|\Delta\hat{K}^n W\vec{\mu}^{n,exact}\|}{1 - C\frac{B}{A}\|\Delta\hat{K}^{n_0}\|}$$

for $n > n_0$, where $n_0$ is sufficiently big to make the denominator positive. Then, for the rate of convergence to remain unchanged as a result of compression, we see that the compression threshold must be controlled so that the term $\|\Delta\hat{K}^n W\vec{\mu}^{n,exact}\|$ exhibits behavior similar to $\|\vec{r}^n\|$ i.e.

$$\|\Delta\hat{K}^n W\vec{\mu}^{n,exact}\| \leq Ch_n^2.$$

Let us now examine the term $\Delta\hat{K}^n W\vec{\mu}^{n,exact}$ in detail. The uncompressed matrix, $\hat{K}^n$, is of the form

$$\hat{K}^n = \begin{bmatrix} K^0 & \gamma^{0,0} & \gamma^{0,1} & \cdots & \gamma^{0,n-1} \\ \alpha^{0,0} & \beta^{0,0} & \beta^{0,1} & \cdots & \beta^{0,n-1} \\ \alpha^{1,0} & \beta^{1,0} & \beta^{1,1} & \cdots & \beta^{1,n-1} \\ \vdots & \vdots & \vdots & & \vdots \\ \alpha^{n-1,0} & \beta^{n-1,0} & \beta^{n-1,1} & \cdots & \beta^{n-1,n-1} \end{bmatrix}$$

where the submatrices $K^0$, $\gamma^{0,j'}$, $\alpha^{j,0}$ and $\beta^{j,j'}$ respectively have entries of the form

$$K^0_{k,k'} = \int_S \int_S K(\vec{x},\vec{y})\,\tilde{\phi}_{0,k}(\vec{x})\,\phi_{0,k'}(\vec{y})\,dS(\vec{x})dS(\vec{y}) \quad ; \quad k \in K(0), k' \in K(0)$$

$$\gamma^{0,j'}_{k,m'} = \int_S \int_S K(\vec{x},\vec{y})\,\tilde{\phi}_{0,k}(\vec{x})\,\psi_{j',m'}(\vec{y})\,dS(\vec{x})dS(\vec{y}) \quad ; \quad k \in K(0), m' \in M(j')$$

$$\alpha_{m,k'}^{j,0} = \int_S \int_S K(\vec{x},\vec{y})\,\tilde{\psi}_{j,m}(\vec{x})\,\phi_{0,k'}(\vec{y})\,dS(\vec{x})\,dS(\vec{y}) \quad ; \quad m \in M(j), k' \in K(0)$$

$$\beta_{m,m'}^{j,j'} = \int_S \int_S K(\vec{x},\vec{y})\,\tilde{\psi}_{j,m}(\vec{x})\,\psi_{j',m'}(\vec{y})\,dS(\vec{x})\,dS(\vec{y}) \quad ; \quad m \in M(j), m' \in M(j').$$

Since the blocks $K^0$, $\gamma^{0,j'}$ and $\alpha^{j,0}$ represent only $CN$ out of the total of $N^2$ entries, we will suppose that the compression operation is restricted to the blocks $\beta^{j,j'}$. Then the only nonzero blocks in $\Delta\hat{K}^n$ are the submatrices, $\Delta\beta^{j,j'}$, which represent those portions of $\beta^{j,j'}$ that are discarded during compression.

Now recall that $W\vec{\mu}^{n,exact}$ has blocks of wavelet coefficients, which behave as

$$\|\vec{\eta}^{j,exact}\| \leq Ch_j^2.$$

We take advantage of this fact by absorbing the $h_j^2$ term into the submatrices, so that

$$\Delta\hat{K}^n W\vec{\mu}^{n,exact} = \mathrm{K}\,\vec{f},$$

where

$$\mathrm{K} = n^{\frac{1}{2}} h_n^{-2} \begin{bmatrix} 0 & 0 & 0 & \cdots & 0 \\ 0 & h_0^2\Delta\beta^{0,0} & h_1^2\Delta\beta^{0,1} & \cdots & h_{n-1}^2\Delta\beta^{0,n-1} \\ 0 & h_0^2\Delta\beta^{1,0} & h_1^2\Delta\beta^{1,1} & \cdots & h_{n-1}^2\Delta\beta^{1,n-1} \\ \vdots & \vdots & \vdots & & \vdots \\ 0 & h_0^2\Delta\beta^{n-1,0} & h_1^2\Delta\beta^{n-1,1} & \cdots & h_{n-1}^2\Delta\beta^{n-1,n-1} \end{bmatrix}$$

and

$$\vec{f}^{n} = n^{-\frac{1}{2}} h_n^2 \begin{bmatrix} 0 \\ h_0^{-2}\vec{\eta}^{0,exact} \\ h_1^{-2}\vec{\eta}^{1,exact} \\ \\ h_{n-1}^{-2}\vec{\eta}^{n-1,exact} \end{bmatrix} \tag{5.33}$$

with $n > 0$. The rescaled vector, $\vec{f}_n$, then behaves as

$$\|\vec{f}^{n}\| \leq C n^{-\frac{1}{2}} h_n^2 \left(\sum_{j=0}^{n-1} h_j^{-4} \|\vec{\eta}^{j,exact}\|^2\right)^{\frac{1}{2}}$$

$$\leq C h_n^2.$$

We must therefore control the submatrices $\Delta\beta^{j,j'}$ such that

$$\|\mathrm{K}\| \leq C. \tag{5.34}$$

Using Schur's Lemma [28], Equation (5.34) will be satisfied if there exists a sequence of positive real numbers, $\omega_k$, such that

$$\sum_{k'} |\mathrm{K}_{k,k'}|\, \omega_{k'} \leq C\omega_k \quad \forall k$$

$$\sum_{k} |\mathrm{K}_{k,k'}|\, \omega_{k} \leq C\omega_{k'} \quad \forall k'.$$

Consider a set of weights of the form $h_j^s$, where the exponent $s$ is to be selected subsequently. The boundedness of K can then be ensured by the conditions

$$n^{\frac{1}{2}} h_n^{-2} \sum_{j'=0}^{n-1} h_{j'}^2 \|\Delta\beta^{j,j'}\|_\infty h_{j'}^s \leq C h_j^s \quad ; \quad j = 0, 1, \cdots, n-1 \tag{5.35}$$

$$n^{\frac{1}{2}} h_n^{-2} \sum_{j=0}^{n-1} h_{j'}^2 \|\Delta\beta^{j,j'}\|_1 h_j^s \leq C h_{j'}^s \quad ; \quad j' = 0, 1, \cdots, n-1. \tag{5.36}$$

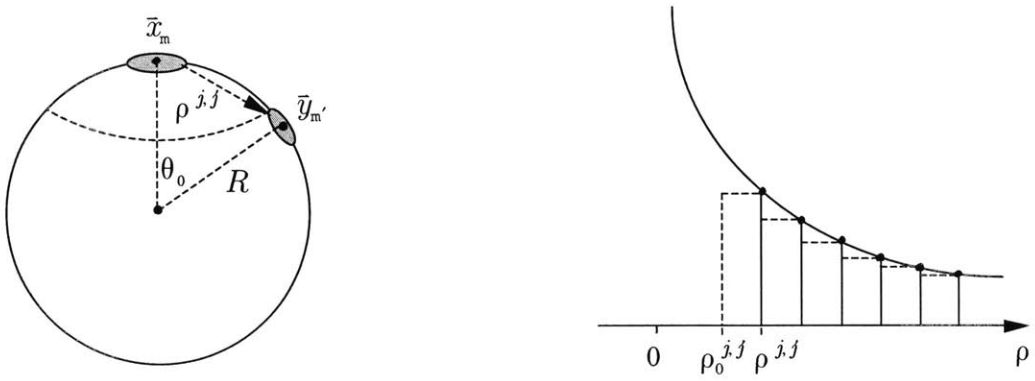


(a) (b)

Figure 5-2: (a) Compression of submatrices by discarding those entries for which the distance between basis functions exceeds $\rho^{j,j'}$ (b) Bounding the discrete sum by an integral.

Recall from subsection 5.2 that the submatrix $\beta^{j,j'}$ has entries of the form

$$\left|\beta^{j,j'}_{m,m'}\right| \leq \frac{Ch_j^p h_{j'}^q}{(l^{j,j'}_{m,m'})^r}.$$

Let us therefore consider the effect of compressing $\beta^{j,j'}$ by discarding all entries for which $l^{j,j'}_{m,m'}$ exceeds some prescribed value, $\rho^{j,j'}$ (Figure 5-2a). Then

$$\|\Delta\beta^{j,j'}\|_\infty = \sup_{m\in M(j)} \sum_{m'\in M(j')} \left|\Delta\beta^{j,j'}_{m,m'}\right|$$

$$\leq \frac{Ch_j^p h_{j'}^q}{\Delta S^{j'}} \sup_{m\in M(j)} \sum_{\substack{m'\in M(j') \\ l^{j,j'}_{m,m'} > \rho^{j,j'}}} \frac{\Delta S^{j'}}{(l^{j,j'}_{m,m'})^r}.$$

where $\Delta S^{j'}$ denotes an elemental area of resolution $j'$. The terms in the above sum decrease monotonically with increasing distance, $l_{m,m'}^{j,j'}$, between the supports of $\tilde{\psi}_{j,m}(\vec{x})$ and $\psi_{j',m'}(\vec{y})$. Hence, the sum can be bounded by an integral, as illustrated in Figure 5-2b [36]. This integral has a lower limit, $\rho_0^{j,j'}$, which differs from $\rho^{j,j'}$ by one mesh width, $h_{j'}$, i.e. $\rho^{j,j'} \geq \rho_0^{j,j'} + h_{j'}$. Imposing the added restriction, $\rho_0^{j,j'} \geq Ch_j$, so that $\rho + Ch_j \leq C\rho$ for $\rho > \rho_0^{j,j'}$, we have

$$\begin{aligned}
\|\Delta\beta^{j,j'}\|_\infty &\leq Ch_j^p h_{j'}^{q-2} \sup_{m\in M(j)} \int_{\substack{S \\ \rho > \rho_0^{j,j'}}} \frac{dS}{\rho^r} \\
&\leq Ch_j^p h_{j'}^{q-2} \sup_{m\in M(j)} \int_{\rho>\rho_0^{j,j'}} \frac{2\pi(\rho + Ch_j)d\rho}{\rho^r} \\
&\leq \frac{Ch_j^p h_{j'}^{q-2}}{(\rho_0^{j,j'})^{r-2}} \quad (r > 2). \qquad (5.37)
\end{aligned}$$

A similar process gives

$$\begin{aligned}
\|\Delta\beta^{j,j'}\|_1 &= \sup_{m'\in M(j')} \sum_{m\in M(j)} \left|\Delta\beta_{m,m'}^{j,j'}\right| \\
&\leq \frac{Ch_j^{p-2} h_{j'}^{q}}{(\rho_0^{j,j'})^{r-2}}. \qquad (5.38)
\end{aligned}$$

Comparing Equation (5.35) with Equation (5.37), we obtain the condition

$$n^{\frac{1}{2}} h_n^{-2} \sum_{j'=0}^{n-1} \frac{h_j^p h_{j'}^{q+s}}{(\rho_0^{j,j'})^{r-2}} \leq Ch_j^s \quad ; \quad j = 0, 1, \cdots, n-1.$$

To satisfy this condition, we require that

$$\frac{h_j^p h_{j'}^{q+s}}{(\rho_0^{j,j'})^{r-2}} \leq Cn^{-\frac{3}{2}} h_n^2 h_j^s$$

i.e.

$$\rho_0^{j,j'} \geq C(n^{\frac{3}{2}} h_n^{-2} h_j^{p-s} h_{j'}^{q+s})^{\frac{1}{r-2}}. \tag{5.39}$$

Similarly, by comparing Equation (5.36) with Equation (5.38), we obtain the concurrent requirement that

$$\rho_0^{j,j'} \geq C(n^{\frac{3}{2}} h_n^{-2} h_j^{p+s-2} h_{j'}^{q-s+2})^{\frac{1}{r-2}}. \tag{5.40}$$

Equations (5.39) and (5.40) can now be reduced to a single condition, by choosing $s = 1$. Then, since we also have $\rho_0^{j,j'} \geq Ch_j$ and $\rho^{j,j'} \geq \rho_0^{j,j'} + h_{j'}$, we obtain

$$\rho^{j,j'} \geq Cmax\left\{(n^{\frac{3}{2}} h_n^{-2} h_j^{p-1} h_{j'}^{q+1})^{\frac{1}{r-2}}, h_j\right\} + h_{j'}. \tag{5.41}$$

This is the condition for compressing the matrix such that the overall convergence rate for the numerical scheme matches the convergence rate that is obtained when no compression is performed.

We focus now on the case where

$$\frac{2}{r-2} \leq 1, \quad \frac{p-1}{r-2} \geq 1 \text{ and } \frac{q+1}{r-2} \geq 1.$$

Note that these conditions are satisfied for the values $p = 3$, $q = 2$ and $r = 4$, which were obtained in subsection 5.2. We may then satisfy Equation (5.41) by choosing

$$\rho^{j,j'} \geq Cn^{\frac{3}{4}} h_n^{-1} h_j h_{j'} \tag{5.42}$$

with $C > 1$.

Finally, we consider the minimum number of nonzero entries required in the compressed matrix, $\hat{K}^{n,comp}$, by letting the equality hold in Equation (5.42). Let $J$ be the number of rows in the block $\beta^{j,j'}$. Then the minimum number of entries, $\nu_{min}^{j,j'}$, that must be retained in the compressed version of $\beta^{j,j'}$ is

$$\nu_{min}^{j,j'} \approx \frac{\pi(\rho_{min}^{j,j'} + Ch_j)^2}{\Delta S^{j'}} J$$

$$\leq C(n^{\frac{3}{4}} h_n^{-1} h_j h_{j'})^2 h_j^{-2} h_{j'}^{-2}$$

$$\leq C n^{\frac{3}{2}} h_n^{-2}.$$

Thus, the minimum number of entries, $\nu_{min}$, that must be retained in $\hat{K}^{n,comp}$ is

$$\nu_{min} = \sum_{j=0}^{n-1} \sum_{j'=0}^{n-1} \nu_{min}^{j,j'}$$

$$\leq C n^{\frac{7}{2}} h_n^{-2}$$

$$\leq C(logN)^{\frac{7}{2}} N. \tag{5.43}$$

Equation (5.43) shows that we can make $\|\mu^{exact}(\vec{x}) - \mu^{comp}(\vec{x})\|$ exhibit similar behavior to $\|\mu^{exact}(\vec{x}) - \mu^{approx}(\vec{x})\|$ by retaining as few as $C(logN)^{\frac{7}{2}} N$ entries in the compressed matrix. Thus, because of the boundedness of the operator in Equation (5.2), we ensure that

$$\|u^{exact}(\vec{x}) - u^{comp}(\vec{x})\| = \|T(\mu^{exact}(\vec{x}) - \mu^{comp}(\vec{x}))\|$$

$$\leq C\|\mu^{exact}(\vec{x}) - \mu^{comp}(\vec{x})\|$$

$$\leq C h_n^2.$$

The analysis developed in this chapter may be readily generalized to higher accuracy, higher vanishing moments and in particular, to the *Galerkin* formulation.

# Chapter 6

# Implementation and Numerical Results

In this chapter we apply the 2-D and 3-D constructions developed in Chapters 3 and 4 to solve electrostatic problem posed as a second kind integral equation. We demostrate the advantages of using the multiscale wavelet bases for sparsification of the stiffness matrix.

## 6.1 Numerical Results for 3-D Computational Problems

We have implemented our approach for using second generation surface wavelets to solve integral equations in 3D and verified the theoretical results obtained in Chapter 5 for the spherical mesh shown in Figure 3-5. Our implementation uses a linear interpolating surface wavelet basis, as described in Chapter 3, with data structures that support input meshes of general shape. A description of these data structures may be found in our previous experimental work [3]. In the present implementation, however, we compress the matrix according to the theoretically derived, level-dependent, truncation condition, Eq. (5.42), or using a global compression threshold on the coefficients $\beta_{m,m'}^{j,j'}$. Eq. (5.42) provides an a-priori method to determine the entries that

are required in the sparse matrix.

Figures 6-1 (a) and (b) show corresponding compression and convergence results, which were obtained when our code was validated on a spherical mesh similar to the one shown in Figure 3-5. Figure 6-1a illustrates the number of entries retained in the compressed matrix, as a function of $N$. The figure also shows a curve of the form $C(logN)^{\frac{7}{2}}N$, from which we see that the observed results agree well with the theory. Now consider the effect of compression on the final computed solution, $u^{comp}(\vec{x})$, which is given by

$$u^{comp}(\vec{x}) = \sum_{k' \in K(n)} \mu_{k'}^{n,comp} \int_S K(\vec{x},\vec{y})\, \phi_{n,k'}(\vec{y})\, dS(\vec{y}) \quad ; \quad \vec{x} \in \Omega$$

Figure 6-1 (b) illustrates the behavior of the relative error

$$\varepsilon = \left| \frac{u^{exact}(\vec{x}) - u^{comp}(\vec{x})}{u^{exact}(\vec{x})} \right|$$

for a typical interior point, as a function of $N$. Again, we find that the observed results are in are in excellent agreement with the theoretical $O(h_n^2)$ convergence rate.

Figure 6-2 illustrates the sparsity patterns of the compressed matrices, which were obtained in the preceding experiments. Note that the symmetry of these patterns represents the symmetry of the truncation strategy. The matrix coefficients themselves are non-symmetric because the basis is biorthogonal rather than orthogonal. We have therefore used a generalized conjugate gradient method to iteratively solve the non-symmetric system of equations. As expected for second-kind integral equations the matrices were well conditioned, with condition numbers practically independent of $N$. The Krylov subspace iteration therefore converges in only a few iterations.

We now try a more complex mesh, as shown in Figure 6-3, and apply the level dependent distance criterion developed in Chapter 5. The results for this case are mixed. Since the course mesh has many corners, then we expect the compression to

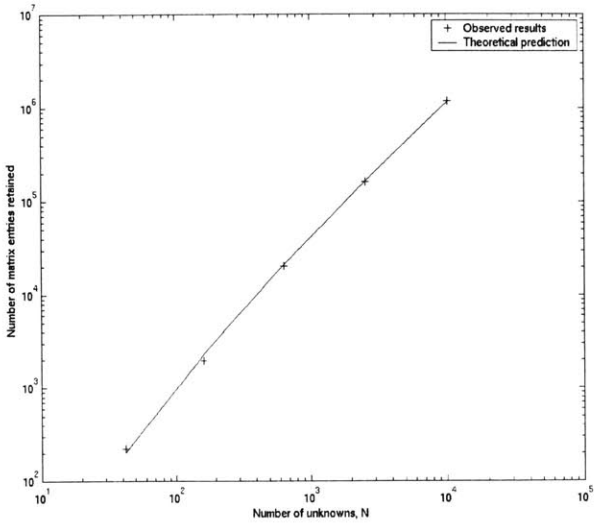


(a)

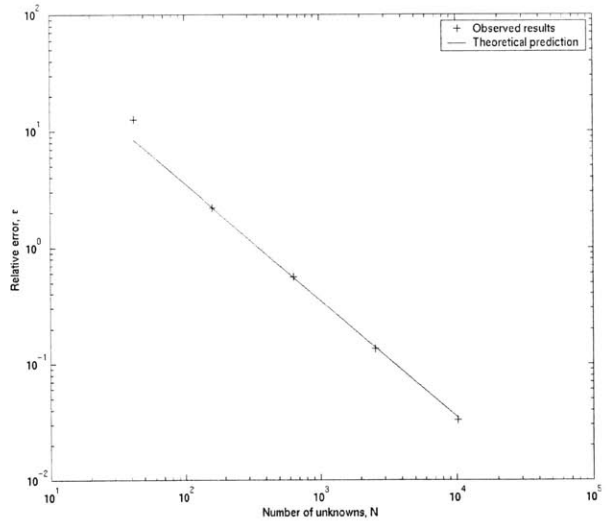


(b)

Figure 6-1: Compression of matrix such that the optimal rate of convergence is obtained. (a) Comparison of actual number of entries retained with $\mathcal{O}(logN)^{7/2}N)$ prediction. (b) Comparison of actual convergence rate with $\mathcal{O}(h_n^2)$.

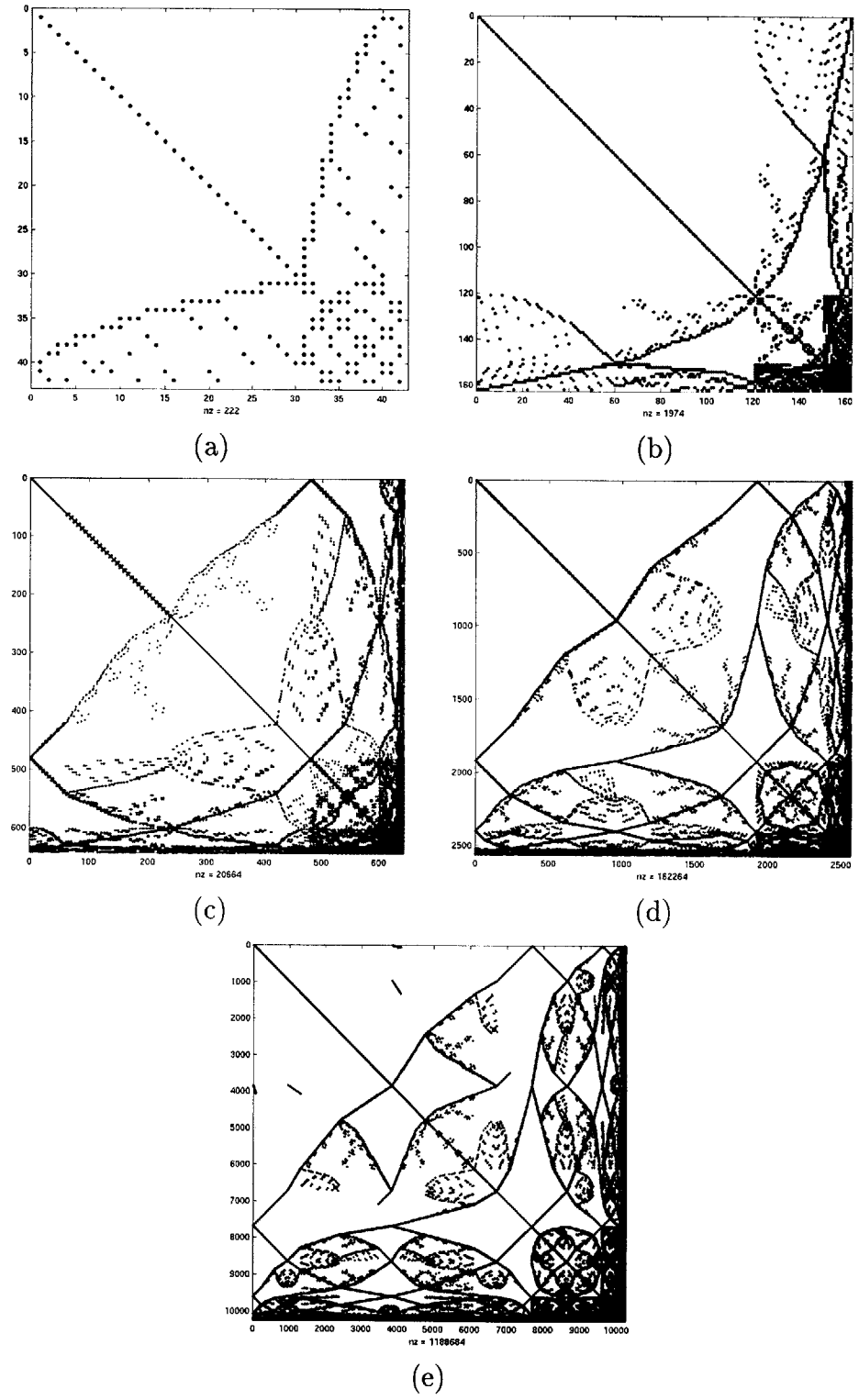


Figure 6-2: Examples of matrices compressed to achieve the optimal convergence rate. (a) $N = 42$ (b) $N = 162$ (c) $N = 642$ (d) $N = 2562$ (e) $N = 10242$.

be low at a small level of discretization. As we increase the number of nodes, the accuracy is nearly $\mathcal{O}(h^2)$ and the compression of the wavelet method increases to about 1:100. Most of the bottleneck for compression is located at the low levels of the mesh ($M(0)$ and $K(0)$). However, as we increase the order of disretization, the level dependent distance criterion tends to keep all the entries located at $M(0)$. See the sparsity patterns in Figure 6-2. In the current implementation, the primary and dual wavelets only vanish one moment across corners. Compression may be significantly improved by imposing more vanishing moments across corners. In section 6.2 we apply wavelets which vanish polynomial on corners.

We now have several options for assembling the stiffness matrix. One option involves computing the single scale formulation at level $V_n$ and applying the wavelet transform is the stiffness matrix. This leads to $N^2$ for memory storage and $\mathcal{O}(N^2)$ operations.

Another option is to compute the $\mathcal{O}((logN)^{\frac{7}{2}}N)$ entries directly. The primary wavelets are computed from a closed form expression. However, to obtain the duals we have to apply the recursive wavelet approach described in Chapter 5. This approach leads to $\mathcal{O}((logN)^{\frac{7}{2}}N)$ memory storage, but more than $\mathcal{O}(N^2)$ computations.

Another alternative is to use only the primary scaling functions to compute the entries of the stiffness matrix. Thus we form a set of *Galerkin* equations, with the test functions belonging to the primary wavelet spaces. This formulation allows computing the integrals directly because the primary functions have a closed form expression. We may then use a high order quadrature scheme to compute the entries of the stiffness matrix. This approach leads to $\mathcal{O}((logN)^{\frac{7}{2}}N)$ for memory storage. The computational cost varies on the complexity of the mesh, ranging from $\mathcal{O}((logN)^{\frac{7}{2}}N)$ or higher.

## 6.2 2D Galerkin Implementation

We test the linear wavelets introduced in Section 4.2.3 for a 2D problem integral equation. However, in this case, we form a set of *Galerkin* equations. This implies

Distributor Cap

Triangularized Cap

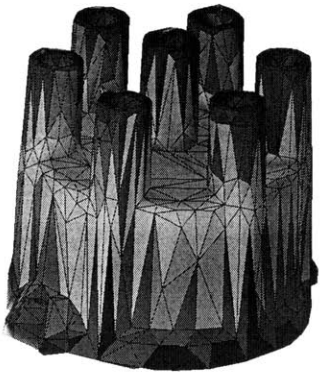

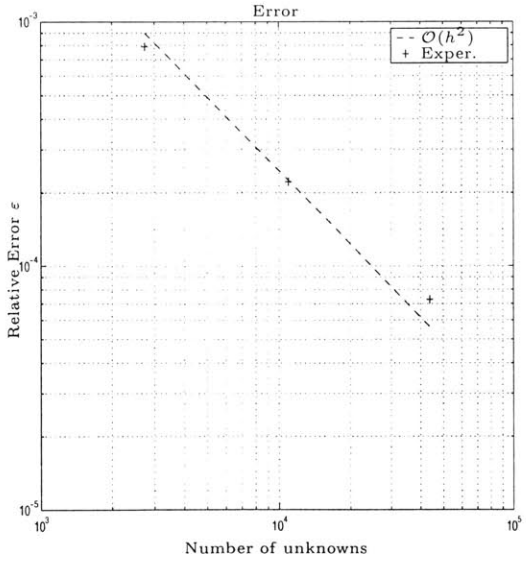


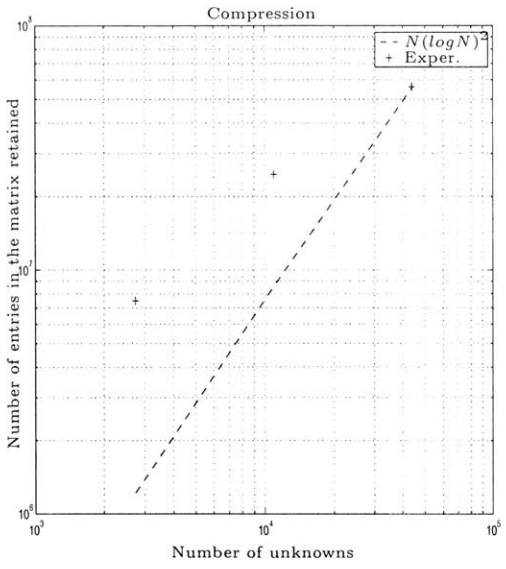


Figure 6-3: Laplace equation over a *semi*-regular distributor cap mesh [23]. The course mesh is highly irregular, but the subdivisions are regular. The figure on the left is the actual error vs number of unknowns. On the right we have a compression plot. Notice that as N becomes larger, the compression improves. In particular, for 44,000 nodes we achieve a 1:100 compression. However, due to the presence of corners in the mesh, compression vs accuracy is not very good at low levels of discretization.

the test functions belong to the primary wavelet spaces and we avoid altogether the dual scaling functions. This step will allow us to compute the integrals of the stiffness matrix directly. More precisely we solve the integral equation

$$\lambda(\vec{x})\mu(\vec{x}) + \int_{\Gamma} \mu(\vec{y})\, K(\vec{x},\vec{y})\, d\Gamma(\vec{y}) = b(\vec{x}) \quad ; \quad \vec{x} \in \Gamma$$

where $\Gamma$ is a curvilinear domain in $R^2$ and $K(\vec{x},\vec{y}) = \frac{1}{2\pi}\frac{\partial}{\partial n_y}\frac{1}{\|\vec{x}-\vec{y}\|}$. Since $\lambda(\vec{x}) = \frac{1}{2}$ almost everywhere, then we simply replace $\lambda(\vec{x})$ with $\frac{1}{2}$. Thus the discretized equations are:

$$\begin{aligned}
\int_{\Gamma} & \left( \frac{1}{2}\sum_{j=0}^{n-1}\sum_{k\in M(j)} \gamma_{j,k} w_{j,k}(\vec{x}) + \frac{1}{2}\sum_{k\in K(0)} \lambda_{0,k}\phi_{0,k}(\vec{x}) \right. \\
& + \left. \int_{\Gamma} K(\vec{x},\vec{y}) \sum_{j=0}^{n-1}\sum_{k\in M(j)} \gamma_{j,k} w_{j,k}(\vec{y}) + \sum_{k\in K(0)} \lambda_{0,k}\phi_{0,k}(\vec{y}) \right) \phi_{0,l}(\vec{x})\ d\Gamma(\vec{y}) d\Gamma(\vec{x}) \\
& = \int_{\Gamma} b(\vec{x})\phi_{o,l}(\vec{x})\ d\Gamma(\vec{x}) \quad \forall l \in M(0), \\
\int_{\Gamma} & \left( \frac{1}{2}\sum_{j=0}^{n-1}\sum_{k\in M(j)} \gamma_{j,k} w_{j,k}(\vec{x}) + \frac{1}{2}\sum_{k\in K(0)} \lambda_{0,k}\phi_{0,k}(\vec{x}) \right. \\
& + \left. \int_{\Gamma} K(\vec{x},\vec{y}) \sum_{j=0}^{n-1}\sum_{k\in M(j)} \gamma_{j,k} w_{j,k}(\vec{y}) + \sum_{k\in K(0)} \lambda_{0,k}\phi_{0,k}(\vec{y}) \right) w_{z,l}(\vec{x})\ d\Gamma(\vec{y}) d\Gamma(\vec{x}) \\
& = \int_{\Gamma} b(\vec{x}) w_{z,l}(\vec{x})\ d\Gamma(\vec{x}) \quad \forall l \in M(z), \\
& z = 0 \ldots n-1.
\end{aligned}$$

We apply the 2-D multiscale Galerkin method on a discretization of the circle at several levels of resolution, as shown in Figure 6-4. The asymptotic convergence for the full BEM matrix is of quadratic order, as expected. However, we do not need to compute the entire matrix. We apply a similar level dependent distance criterion as for the 3D case

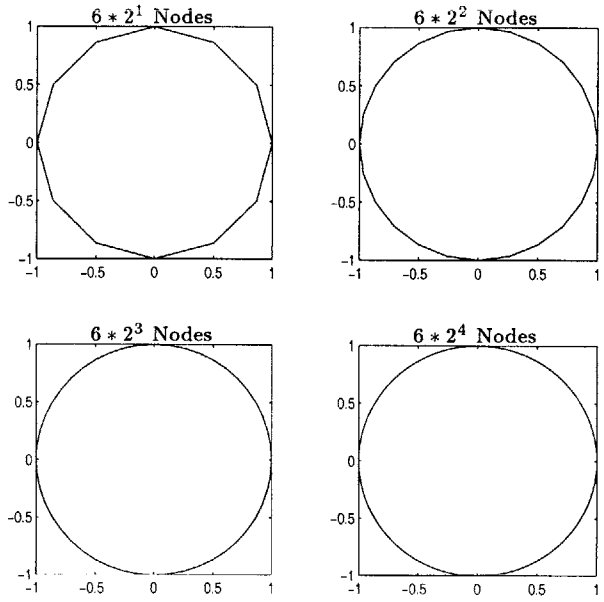


Figure 6-4: Multiple regular discretizations of the circle with linear hats wavelets which vanish first order polynomials around corners.

$$\rho^{j,j'} \geq Cn^{\frac{3}{4}} h_n^{-1} h_j h_{j'},$$

where $h_j$ is the characteristic mesh width. We only calculate the stiffness matrix entries which lie inside the distance threshold to obtain a very sparse matrix, see Figure 6-5. In particular, we retain only $\mathcal{O}(Nlog_2(N)^2)$ entries of stiffness matrix, but with asymptotic quadratic convergence, as shown in Figures 6-6 (a) and (b). Notice that for the 2D case, we have not yet proved that this criterion leads to asympotic convergence, altought it should be straightforward to prove it from the 3D analysis.

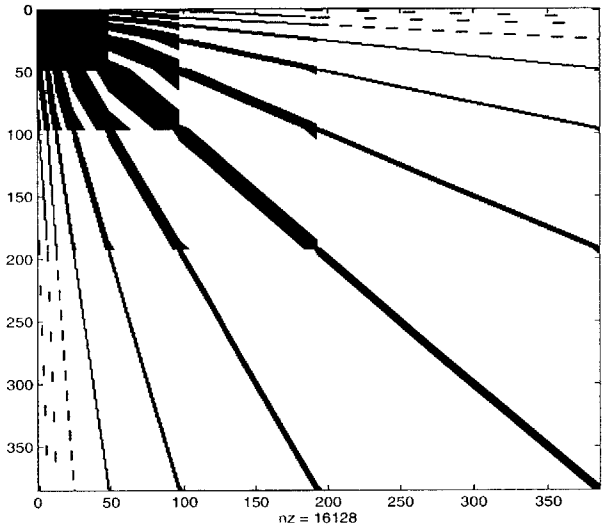


Figure 6-5: Sparsity Pattern for the stiffness matrix of size 384. As observed, after applying the distance criterion we obtain a very sparse matrix

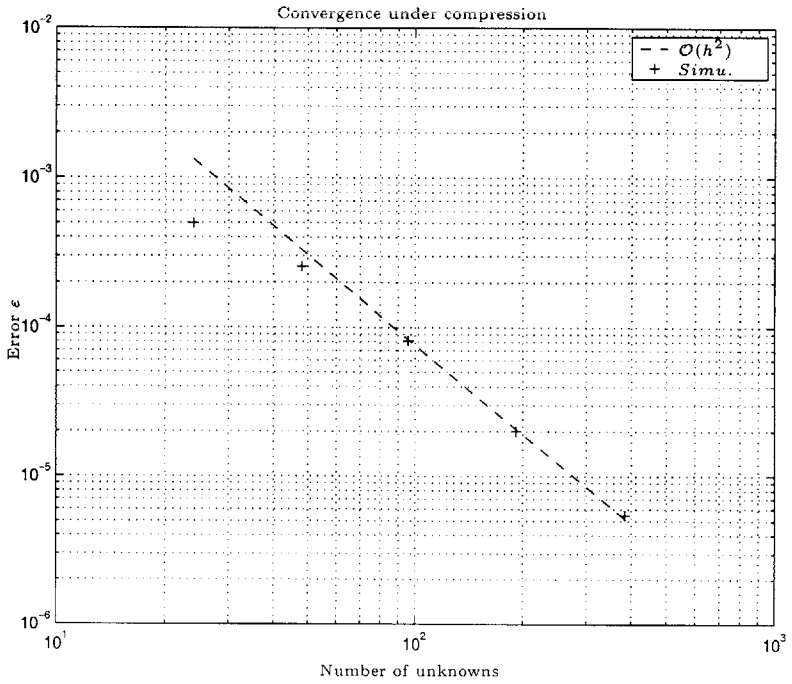


(a)

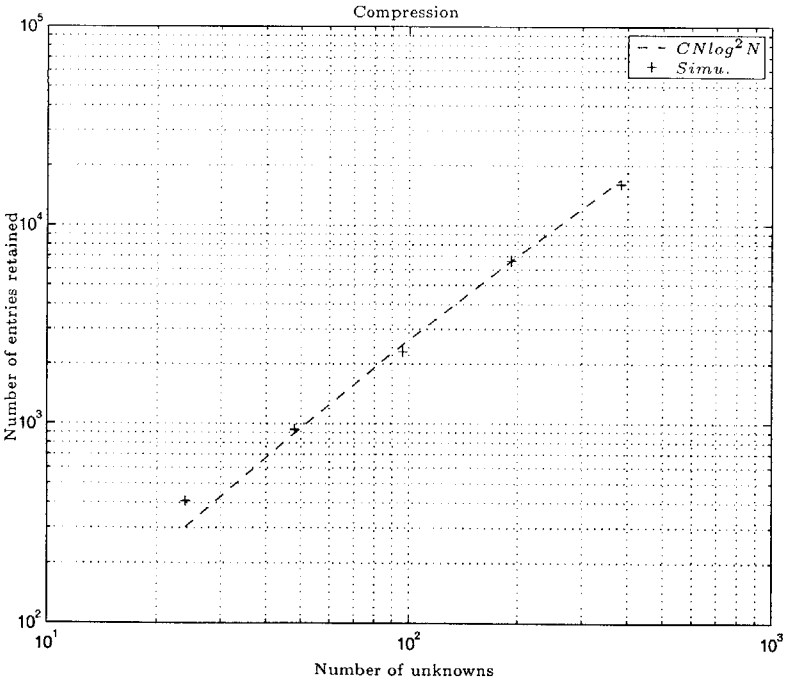


(b)

Figure 6-6: (a) Comparison of actual number of entries retained with $\mathcal{O}(N(log_2^2 N))$. (b) Comparison of actual convergence rate with $\mathcal{O}(h_n^2)$.

# Chapter 7

# Conclusions

In this chapter we summarize the thesis and give directions for future work.

## 7.1 Contributions and Discussion

In this thesis, we have demonstrated the existence of new wavelet constructions for complex surfaces and shown how their signal processing capabilities can be exploited in 3D computational modeling. The advantage of using these constructions is that they combine the multiresolution properties of traditional wavelets with a level of geometric flexibility similar to that of finite element methods. Thus, in addition to being a useful tool for geometric representation and solution post-processing in traditional numerical applications, our investigation has revealed that there are significant performance benefits to be realized when surface wavelets are applied to partial differential equations.

Our work is motivated by the construction of the linear hat wavelets, which where originally developed by the computer graphic community. However, these linear wavelets do not form a *Riesz* stable basis. The stability of the basis is important for solving PDEs since they relate the continuity and invertibility properties of the PDE operator to the singular values of the stiffness matrices. In the present work we show that that linear surface wavelets basis, under a rescaling and a min max condition on the mesh size $h_n$, is $H_0^3(S)$ stable, thus making them suitable for differential

equations.

We also prove the existence of a wide class of interpolating Multiwavelets over irregular grids in several dimensions with vanishing moments around corners. Although we explicitly derive 1D and 2D irregular wavelets, it is possible to generalize these constructions to higher dimensions, in particular volumetric discretizations.

We have shown how to discretize PDEs, both in integral and differential forms. A detailed analysis and implementation for a model 3D integral equation has revealed that it is possible to devise numerical schemes where only $\mathcal{O}((logN)^p N)$ entries of the matrix have to be computed with respect to the number of unknowns, $N$. For smooth surfaces, the accuracy of the numerical schemes is determined by the number of vanishing moments of the wavelet basis, in the tangential coordinate directions of the surface. A surface wavelet construction with linear interpolating properties (i.e. first order vanishing moments for the dual wavelet and at least zeroth order for the primary wavelet) was shown to produce a scheme with $O(h_n^2)$ accuracy for the characteristic mesh size $h_n$, both in theory and in practice. In principle, the theoretical proof extends to wavelets with higher order approximation.

We have shown that a wide class of Calderón-Zygmund integral operators may be solved with this scheme. This makes it potentially competitive with other methods, where the expansion must be tailored to the particular operator under consideration. The wavelet framework also has the advantage that schemes with higher order of accuracy and coefficient decay can be designed by replacing the wavelet basis with one that has additional vanishing moments.

The wavelet compression scheme has several limitations, in particular, the Petrov galerkin formulation with the dual wavelets as test functions. As pointed out in Chapter 6 forming the single scale matrix and then applying the wavelet transform still requires $\mathcal{O}(N^2)$ cost. This problem is mitigated by applying the Galerkin formulation described in Chapter 6 with the test functions as primary wavelets and calculating the compressed entries of the matrices directly. This allows a $\mathcal{O}((logN)^p N)$ algorithm for fairly irregular surfaces, but not completely irregular.

For completely irregular meshes, the bottleneck lies in the computation of the

coefficients. This motivates the development of new quadrature schemes which are operator dependent (cf. Multipole methods). This would lead to new fast schemes where the wavelet basis increases the rate of decay of the projection coefficients.

It is pointed out that a parallel development to the work in this thesis by *Tausch* and *White* [33] has been in existence. This method combines a polynomial multiscale basis with multipole expansions. This approach is well suited for solving integral equations of the first kind over complex geometries in 3D. Similar to the sparsification approach used in this thesis, this method constructs a multiscale basis with vanishing moments in 3D which leads to coefficients with fast decay. The multipole expansions are the used to compute the entries of the stiffness matrix. We briefly describe these new multiscale constructions.

Let $S$ be the surface of the finite element space $X_h$ which consists of piecewise constant functions $\chi_1, \ldots, \chi_N$ over flat panels $\pi_1, \ldots, \pi_N$, thus

$$\chi_i(x) = \begin{cases} \frac{1}{\sqrt{\pi_i}} & x \in \pi_i, \\ 0 & else. \end{cases}$$

Now embed the surface $S$ in a cube $\mathcal{C}_0$ at level 0. Divide the cube into eight cubes at level 1, and so forth. Denote all the cubes which contain part of the surface as $\mathcal{C}_l = 0, \ldots, L$ and for any cube $\nu \in C_l$ let $\mathcal{K}_\nu$ be the non-empty children cubes. With this formulation the scaling functions and wavelet functions at the bottom level $L$ may be constructed as

$$\begin{aligned} \Phi_{\nu,i} &= \sum_j q_{i,j}\chi_{\nu,j}, \quad i = 1, \ldots, v_\nu \\ \Psi_{\nu,i} &= \sum_j q_{i+v_\nu,j}\chi_{\nu,j}, \; i = 1, \ldots, w_\nu. \end{aligned}$$

The coefficients $q_{i,j}$ are obtained from the matrix $Q_\nu$, which in turn is obtained by the Singular Value Decomposition (SVD) of the multipole moment matrix $M_\nu$, i.e. $M_\nu = U_\nu^* \Sigma_\nu Q_v$. At higher levels, $\mathcal{C}_l$, the basis is constructed from the children

functions as

$$\begin{aligned}\Phi_{\nu,i} &= \sum_{j,\alpha} q_{i,(\alpha,j)}\Phi_{\alpha,j}, \quad i = 1,\ldots,v_\nu \\ \Psi_{\nu,i} &= \sum_{j,\alpha} q_{i+v_\nu,(\alpha,j)}\chi_{\alpha,j}, \; i = 1,\ldots,w_\nu.\end{aligned}$$

where the coefficients $q_{i,(\alpha,\beta)}$ are similarly obtained from the SVD of the moment matrix $M_\nu$ which contains the multipole moments of the functions $\Phi_\alpha, \alpha \in \mathcal{K}_\nu$.

The stiffness matrix is then computed by replacing the finite element space $X_h$ with the multiscale basis in the non-standard form representation [8]. The entries of the stiffness matrix are efficiently computed by multipole expansions [31]. This method leads to a sparse representation by only computing the entries of the matrix inside cubes $C_l$ which are "close". In particular, for some practical problems, this algorithm is near $\mathcal{O}(N)$ in cost and storage.

This method is very well suited for solving integral equations of the first kind, it may be used as an alternative to the method developed in this thesis for more general kernels by replacing the entries of the moment matrix $M_\nu$ with polynomial moments. However, in general, new strategies for compression would need to be developed, which are directly related to the kernel.

The basis formed in this approach also consists of polynomial functions. However, in contrast to the basis constructed in this thesis, they are not refinable functions i.e. the general shape of the scaling functions are different at every single scale of resolution. In addition, they do not have a simple analytical expression and the complexity of the functions grows with the number of levels. Moreover, an SVD has to be solved to compute the wavelet basis, which is more expensive than a matrix inversion.

We summarize the contributions of this thesis:

- The construction of a class of interpolating irregular Multiwavelets in $R^n$ which combine the fast transform, decorrelation and localization properties of wavelets with the flexibility of finite elements on irregular meshes. These constructions

may represent polynomials of arbitrary polynomial order. Moreover, we explicitly construct irregular Multiwavelets over curves and surfaces with vanishing moments around corners. In essence these novel constructions allow practical multiresolution decompositions over irregular meshes.

- Application of interpolating irregular Multiwavelets to solve Calderón-Zygmund integral operators. We derive theoretical estimates of convergence under compression in $R^3$, more explicity, we show that we may achieve the asymptotic convergence of the full stiffness matrix with only $\mathcal{O}(N(logN)^{7/2})$ entries.

- Implementation of a 3D linear surface Multiwavelet with one vanishing moment to solve a second kind integral equation over an irregular mesh.

- Implementation of a 2D linear surface Multiwavelet which vanishes global linear functions around corners to solve a second kind integral equation.

## 7.2 Future Research

In this thesis we have only explored the surface for the construction and application of surface wavelets for irregular grids. Future work in this area include the implementation of higher order wavelets, detailed error analysis of complex geometries and the development of the variational wavelet finite element approach to solving PDEs.

*Implementation of 3D Galerkin Integral Equations.* Extension of the 2D code to 3D for practical applications. In principle, wavelet constructions over multiply connected domains is possible. However, we have not show an application in this thesis.

*Quadrature Schemes.* For Calderón-Zygmund integral operators, with decaying singular kernels, we may use expansions of the charge density function (cf. Multipole Expansions [33]) with close and ffar field effects. This would lead to numerical algorithms which are tailor made for the operator. However, we would have control on the number of vanishing moments and thus control the rate of decay of the coefficients.

*Construction and analysis of new wavelets.* We may further explore the construction of new wavelets. In particular, the convergence analysis of the cascade algorithm for the dual scaling functions. This is a better approach than using the dual recursive wavelet idea used in this paper. These wavelets are useful for wave type problems where an explicit expression of the primary and dual scaling functions is needed.

*Convergence analysis under compression.* Analysis of convergence for the Galerkin formulation for higher order wavelets may give new strategies for higher compression.

*Data and graphical compression* Wavelets with higher vanishing moments may achieve greater compression of data. Applications of the surface wavelets developed in this thesis include data compression over irregular meshes, for example, topographical data for a terrain, or compression of the mesh itself.

*Wavelets applied to finite element variational approach for solving PDEs.* Wavelet transforms on finite element problems do not lead to greater sparsity, in contrast to boundary element problems, since the stiffness matrix is sparse to begin with. However, wavelets have been shown to be useful for many finite element problems, including local refinements and diagonal preconditioning [7]. Due to the adaptive nature of the wavelet constructions we envision the development of adaptive refinement schemes.

Finite element stiffness matrices become ill conditioned as the number of variables increase leading to a cost of $\mathcal{O}(N^2)$ to invert. The wavelet transform inherently separates operators into different scales of resolution, creating a stiffness matrix which is diagonally dominant. We may use the wavelet transform to our advantage by applying a diagonal preconditioner to redistribute the eigenvalues and make them approximately equal. This has the effect of significantly reducing the condition number of the stiffness matrix. The whole cost of this algorithm would be near $\mathcal{O}(N)$.

# Bibliography


[1] B. K. Alpert, 'A Class of Bases in $L^2$ for the Sparse Representation of Integral Operators', *SIAM J. Math. Anal.*, **24** (1993), 1, 246-262

[2] B. K. Alpert, G. Beylkin, R. Coifman, V. Rokhlin, 'Waveletlike Bases for the Fast Solution of Second Kind Integral Equations', *SIAM J. Sci. Comp.*, **14**, *(1993), 159-184*

[3] K. Amaratunga, 'A Wavelet-Based Approach for Compressing Kernel Data in Large-Scale Simulations of 3D Integral Problems', *IEEE Computing in Science and Engineering*, **2**, 4, 34-45 (2000).

[4] K. Amaratunga and J. E. Castrillón-Candás, 'Surface Wavelets: A Multiresolution Signal Processing Tool for 3D Computational Modeling', To appear in *International Journal of Numerical Methods in Engineering.*

[5] K. Amaratunga and J. R. Williams, 'Wavelet Based Green's Function Approach to 2D PDEs', *Engineering Computations*, **10**, 4, 349-367 (1993).

[6] K. Amaratunga, J. R. Williams, S. Qian and J. Weiss, 'Wavelet-Galerkin Solutions for One Dimensional Partial Differential Equations', *Int. J. Num. Mthds. Eng.*, **37**, 2703-2716 (1994).

[7] K. Amaratunga and J. R. Williams, 'Wavelet-Galerkin Solution of Boundary Value Problems', *Archives of Computational Methods in Engineering*, 4, 3, 243-285 (1997).

[8] G. Beylkin, R. Coifman and V. Rokhlin, 'Fast Wavelet Transforms and Numerical Algorithms I', *Comm. Pure Appl. Math.*, **44**, 141-183 (1991).

[9] C. A. Brebbia, J. C. F. Telles and L. C. Wrobel, 'Boundary Element Techniques: Theory and Applications in Engineering', Springer-Verlag, Berlin, 1984.

[10] J.W. Carnicer, W. Dahmen, and J.M. Peña, 'Local decomposition of refinable spaces, *Apply. Comp. Harm. Anal.* 3, 127-153, 1996.

[11] A. Cohen, 'Wavelet methods in Numerical Analysis', *Handbook of Numerical Analysis VIII* to appear in P.G. Ciarlet and J.L. Lions, Elsvier North Holland, Amsterdam.

[12] C. Canuto, A. Tabacco, and K. Urban. 'The Wavelet Element Method, part I: Construction and Analysis'. *Appl. Harm. Anal.*, 6:1-52, 1999.

[13] W. Dahmen, 'Wavelet and Multiscale Methods for Operator Equations', *Acta Numerica*, Cambridge University Press, 55-228, 1997

[14] W. Dahmen, W. Dahmen, A Kurdila, and P. Oswald, editors, *Multiscale methods for PDEs*, pages 287-346, San Diego, 1997. Academic Press.

[15] W. Dahmen, A. Kunoth and R. Schneider, 'Operator Equations, Multiscale Concepts and Complexity', *Lectures in Applied Mathematics*, **32**, 225-261 (1996).

[16] W. Dahmen, S. Prössdorf, R. Schneider, 'Wavelet Approximation Methods for Periodic Pseudodifferential Equations. Part 2 - Fast solution and matrix compression' *Advances in Computational Mathematics* **1** (1993), pp. 259-335.

[17] W. Dahmen, S. Prössdorf, R. Schneider, 'Multiscale methods for pseudodifferential equations', L.L. Schumaker, G. Webb (eds.), *Wavelet Analysis and its Applications* **3** Academic Press (1993), 191-235.

[18] W. Dahmen, S. Prössdorf, R. Schneider, 'Multiscale Methods for Pseudodifferential Equations on Manifolds', *Wavelet Analysis and its Applications* **5** Academic Press (1995), 385-424.

[19] W. Dahmen, E. Schneider, 'Composite Wavelet Bases for Operator Equations', *Math. Comp.*, **68**, 1533-1567, 1999.

[20] W. Dahmen, R. Schneider, 'Composite Wavelet Bases for Operator Equations', *Math. Comp.*, **68**, 1533-1567, 1999.

[21] I. Daubechies, 'Orthonormal Bases of Compactly Supported Wavelets', *Comm. Pure Appl. Math.*, **41**, 909-996 (1988).

[22] L. C. Evans, 'Partial Differential Equations', *Graduate Studies in Mathematics, vol 19, American Mathematical Society*, 1998.

[23] H. Hoppe *Modified 3-D Distributor Cap.* Courtesy mesh from Huges Hoppe.

[24] S. Jaffard. 'Wavelet Methods for Fast Resolution of Elliptic Equations'. *SIAM J. Numerical Analysis*, 29:965-986, 1992.

[25] J. Geronimo, D. Hardin, P.R. Massopust, and G. Donovan, 'Construction of Orthogonal Wavelets using Fractal Interpolation functions', *SIAM J. Math. Anal (1996)*

[26] L. Greengard and V. Rokhlin, 'A Fast Algorithm for Particle Simulations', *J. Comp. Phys.*, **73**, 325-348 (1987).

[27] A. Grossmann, and J. Morlet, 'Decomposition of Hardy Functions into Square-Integral Wavelets of Constant Shape', *SIAM J. Math. Anal.*, **15**, 723-736, (1984).

[28] Y. Meyer and R. Coifman, 'Wavelets - Calderon-Zygmund and Multilinear Operators', Cambridge University Press, 1997.

[29] J. Morlet, 'Sampling Theory and Wave Propagation', *Nato ASI Series, Issues in Acoustic Signal/Image Processing and Recognition*, **Vol. I**, C.H. Chen ed., Springer-Verlag, Berlin, 233-261, (1982).

[30] J. Morlet, G. Arens, I. Fourgeau, and D. Giard, 'Wave Propagation and Sampling Theory', *Geophysics*, **47**, 203-236, (1982).

[31] K. Nabors, F. T. Korsmeyer, F. T. Leighton and J. White, 'Preconditioned, Adaptive, Multipole-Accelerated Iterative Methods for Three-Dimensional First-Kind Integral Equations of Potential Theory', *SIAM J. Sci. Comput.*, **15**, 3, 713-735 (1994).

[32] A.V. Oppenheim and R. W. Schafer, 'Discrete-Time Signal Processing', Prentice-Hall, Englewood Cliffs, New Jersey, 1989.

[33] J. Tausch , and J. White, 'Multiscale Bases for the Sparse Representation of Boundary Integral Operators on Complex Geometry', *SMU Math Report 2000-01*, Department of Mathematics, Southern Methodist University.

[34] T. von Petersdorff, and C. Schwab, 'Wavelet Approximation for First Kind Integral Equations on Polygons', *Numeri. Math.*, **74**, 479-516, 1996.

[35] T. von Petersdorff, and C. Schwab, 'Fully Discrete Multiscale Galerkin Bem.', W. Dahmen, A Kurdila, and P. Oswald, editors, *Multiscale methods for PDEs*, pages 287-346, San Diego, 1997. Academic Press.

[36] T. von Petersdorff, C. Schwab and R. Schneider, 'Multiwavelets for Second-Kind Integral Equations', *SIAM J. Numer. Anal.*, **34**, 6, 2212-2227 (1997).

[37] A. Rathsfeld, 'A Wavelet Algorithm for the Boundary Element Solution of a Geodetic Boundary Value Problem', *Comput. Methods Appl. Mech. Engrg.*, Vol 157, 1998, pp 267-287.

[38] A. Rathsfeld, 'A Wavelet Algorithm for the Solution of the Double Layer Potential Equation over Polygonal Boundaries.', *Journal of Integral Equations and Applications*, **7**, 1995, 47-97.

[39] S. Qian and J. Weiss, 'Wavelets and the Numerical Solution of Partial Differential Equations', *J. Comp. Phys.*, **106**, 1, 155-175 (1993).

[40] W. Sweldens, 'The Lifting Scheme: A Custom-Design Construction of Biorthogonal Wavelets', *Appl. Comput. Harmon. Anal.*, **3**, 2, 186-200 (1996).

[41] W. Sweldens, 'The Lifting Scheme: A Construction of Second Generation Wavelets', SIAM J. MATH. ANAL., Vol. 29, No.2, pp. 511-546, March 1998

[42] P. Schroder and W. Sweldens, 'Spherical Wavelets: Texture Processing', In P. Hanrahan and W. Purgathofer, editors, Rendering Techniques '95, pp. 252-263, Springer Verlag, Wien, New York, 1995,

[43] P. Schröder and W. Sweldens, 'Spherical Wavelets: Efficiently Representing Functions on the Sphere', Computer Graphics Proceedings, SIGGRAPH 95, pp. 161-172, 1995.

[44] G. Strang and T. Nguyen, 'Wavelets and Filter Banks', Wellesley-Cambridge Press, Wellesley, MA, 1996.

[45] G. Strang and V. Strela, 'Short Wavelets and Matrix Dilation Equations', *IEEE Trans. Signal Proc.*, **43**, 1, 108-115, (1995).

[46] P. Steffen, P. N. Heller, R. A. Gopinath and C. S. Burrus , 'Theory of Regular M-band Wavelet Bases', *IEEE Trans. Signal. Proc.*, Special Issue on Wavelets and Signal Processing, **41**, 12, 3497-3511, (1993).

[47] J. R. Williams and K. Amaratunga, 'Introduction to Wavelets in Engineering', *Int. J. Num. Mthds. Eng.*, **37**, 2365-2388 (1994).

[48] P. P. Vaidyanathan, 'Multirate Systems and Filter Banks', Prentice-Hall, Englewood Cliffs, New Jersey, 1993.

[49] H. Yserentant, 'On the Multi-level Splitting of Finite Element Spaces', Numer. Math., 49:379-412,